University of Latvia
Faculty of Physics and Mathematics

Studies of Quantum Chaos and Phase Transitions in Nuclear Models

Jevgenijs Proskurins

Dissertation

Work performed
in the Nuclear Reaction Laboratory
Institute of Solid State Physics
University of Latvia

Scientific advisor
Dr.phys. Tamara Krasta

Riga, 2010

Abstract

Presented physics doctor dissertation is devoted to the use of quantum phase transition and chaos conceptions in algebraic and geometrical nuclear structure models. In the frameworks of algebraic approach of the standard Interacting Boson model (IBM-1), nuclear shape phase transitions are studied employing corresponding classical energy functional expressions, depending on nuclear quadrupole deformation parameters β and γ. Model parameter values, corresponding to phase transition critical lines and points, are obtained via a precise solution of equations for minima conditions. The results are compared with those obtained using the Landau method of the energy functional expansion in Taylor series. The above analysis of nuclear shape phase transitions is performed in the case of simplified Casten's version of IBM-1, in the case of $O(6)$-limit IBM-1 Hamiltonian including three-boson interaction terms, and in the case of complete IBM-1 Hamiltonian. Behaviour of quantum chaos statistical criteria - the nearest level energy spacing distribution $P(s)$, and dynamical criteria - the entropy of perturbed Hamiltonian H state wave functions $W(\Psi_i)$, and the fragmentation width of unperturbed Hamiltonian H_0 state basis functions $\kappa(\Phi_k)$, is studied in dependence from nuclear shape parameters in the frameworks of algebraic (simplified Casten's version of IBM-1) and geometrical (rigid triaxial rotator) models. Especial attention is given to the model parameter ranges in the vicinity of nuclear shape phase transition critical lines and points. The developed methods are applied for the analysis of critical phenomena experimentally observed in the structure of tungsten, osmium and platinum even-even nuclei with $184 \leq A \leq 194$ belonging to the $A \sim 190$ region.

The results of dissertation have been published in three refereed journal papers and one paper in international conference proceedings book; additional two journal papers are submitted for publication. One journal paper has been published in the local scientific journal. The results of dissertation have been reported in eight oral and two poster presentations both at international and local scientific conferences. The Bibliography of this dissertation includes 63 titles.

To the memory of the initial scientific advisor of this work, Dr.habil.phys. Juris Tambergs (1942-2008), who inspired and prompted these studies.

Acknowledgements

Most of the results presented in this doctor dissertation have been obtained as a part of Latvian Science Council research projects No. 05.1707 and No. 09.1194. Also, the financial support of the European Social Fund, which gave me a possibility to bring this work to its logical conclusion, is highly appreciated.

I would like to thank all physicists of the LU ISSP Nuclear Reaction Laboratory with whom I have had a pleasure to communicate and work together since 2005, during my Master Course and Doctor Course Studies. I am greatly indebted to former engineers of the Nuclear Reaction Laboratory Mag.phys. Andrejs Andrejevs and Leonids Neiburgs, as well as two students: Aleksandrs Dzalbs and Konstantins Bavrins for their assistance in some aspects of computer programming and numerical calculations. Especial thanks to my present scientific advisor Dr.phys. Tamara Krasta, who overtook the task to supervise and guide this doctoral work after a sudden demise of my previous teacher and advisor Dr.habil.phys. Juris Tambergs.

And last but not least, I would like to express my love and appreciation to my wife and children for their great patience and understanding, which enables me to devote a considerable part of my time to physics.

Contents

List of Figures

List of Tables

Abbreviations and Symbols

List of used abbreviations

BM	-	the collective Bohr-Mottelson model;
GOE	-	the Gauss orthogonal ensemble;
IBFM	-	the Interaction Boson-Fermion model;
IBM	-	the Interacting Boson model;
IBM-1	-	the standard IBM involving s and d-type bosons;
QPT	-	a quantum phase transition;

List of used symbols

A	-	a nuclear mass number $A = Z + N$, where Z - a number of protons, and N - a number of neutrons;
R	-	a radius of the deformed nuclear core in the laboratory reference system: $R = R(\theta, \phi, t)$;
R_0	-	a radius of the nuclear matter sphere with equivalent volume: for heavy nuclei, $R_0 \approx 1.25A^{1/3}$;
a_μ	-	nuclear collective variables $a_{\lambda\mu}$ in an internal reference frame, in the case of quadrupole deformation ($\lambda = 2$); μ assumes $2\lambda + 1$ values;
β	-	a quadrupole deformation parameter of the nuclear core; β_0 denotes a deformation at which corresponding theoretical nuclear energy has a minimal value;
γ	-	an asymmetry parameter (angle) of the deformed nuclear core;
θ_j	-	three Euler angles ($j = 1, 2, 3$), determining orientation of the nuclear internal reference frame in space ($a_{\lambda\mu} = \sum_j D^\lambda_{\nu\mu}(\theta_j)\alpha_{\lambda\nu}$), where $\alpha_{\lambda\nu}$ are collective coordinates in a laboratory reference system, and $D^\lambda_{\nu\mu}$ - denotes an irreducible representation (irrep) of group $SO(3)$;
$\mathbf{L}$	-	an angular momentum operator of the nuclear core;
$\mathbf{Q}$	-	a quadrupole moment operator of the nuclear core;
E_i^{exp}	-	an experimental energy of the i-th nuclear level;
I^π	-	a spin (total angular momentum) and a parity of the nuclear level; for even-even nuclei $I = L$;
K	-	a projection of I on the nuclear symmetry axis;
Φ^I_{MK}	-	basis functions of the collective nuclear model;

$Q(I,K)$	-	a quadrupole moment of nuclear collective state;
$B(E2)$	-	a reduced probability of E2 transition between two levels ($I_i \to I_f$);
l	-	an angular momentum of the nucleon pair forming a boson: $l = 0$ for s-bosons, and $l = 2$ for d-bosons; m denotes l projection in the $O(3)$ representation;
N_b	-	a total number of bosons: $N_b = n_s + n_d$;
$\mathbf{b}^+_{lm}, \mathbf{b}_{lm}$	-	creation and annihilation operators of boson state with angular momentum l and its projection m; $\mathbf{b}_{00} \equiv \mathbf{s}$, and $\mathbf{b}_{2m} \equiv \mathbf{d}_m$;
e_i	-	a boson energy; e_0 – a constant energy of nucleons that are not included in boson pairs (a doubly magic "core");
E_{cl}	-	a classical energy limit expression of IBM Hamiltonian (at $N_b \to \infty$);
H_0	-	a Hamiltonian of the unperturbed (regular) system;
ε_k	-	an energy of the k-th basis state of the unperturbed system's Hamiltonian H_0;
Φ_k	-	a k-th basis state wave function of the unperturbed system's Hamiltonian H_0;
H	-	a Hamiltonian of the perturbed (irregular) system;
n	-	a rank of diagonalized Hamiltonian matrix;
E_i	-	an i-th eigenvalue (level energy) of the perturbed system's Hamiltonian H;
S	-	a nearest level energy spacing $S = E_{i-1} - E_i$;
$P(S)$	-	a nearest level spacing distribution (a statistical quantum chaos criterion);
Ψ_i	-	an i-th state wave function of the perturbed system's Hamiltonian H;
c_{ik}	-	a mixing amplitude of the perturbed system's Hamiltonian H state wave function in the basis of the unperturbed system's Hamiltonian H_0 states : $\Psi_i = \sum c_{ik}\Phi_k$;
$W(\Psi_i)$	-	a wave function entropy of perturbed system's Hamiltonian H states (a dynamical quantum chaos criterion): $W(\Psi_i) = -\sum c^2_{ik} \cdot \ln(c^2_{ik})$;
$\Gamma_{spr}(k)$	-	a fragmentation width (energy spacing) of the unperturbed system's Hamiltonian H_0 basis state Φ_k over the states Ψ_i of the perturbed system's Hamiltonian H;
D_0	-	an average spacing between energies of the unperturbed system's Hamiltonian H_0: $D_0 = \varepsilon_{max} - \varepsilon_{min}/(n-1)$;
$\kappa(\Phi_k)$	-	a fragmentation of basis states (dynamical quantum chaos criterion): $\kappa(\Phi_k) = \Gamma_{spr}(k)/D_0$;

Chapter 1

Introduction

Progress in the development of experimental techniques allowing to study nuclei far from stability region and at high spin values, as well as extensive use of nuclear models based on group theory approach, spurted, especially during last two decades, an interest in the study of critical phenomena in nuclear structure. Scientific literature on nuclear physics includes a great number of papers devoted to various aspects of quantum phase transitions (QPT) and quantum chaos (see, e.g., a most extensive review article of P.Cejnar and J.Jolie [1], and references therein). In these studies, nuclear theoreticians apply conceptions and methods developed for other physical systems: so, for the study of QPT in nuclei, the classical thermodynamics approach is used, including the Landau theory of phase transitions.

However, there always is a possibility that some previously uncleared details, both theoretical and experimental, would lead to a deeper understanding of certain phenomena. Therefore, we have undertaken a study in the field seemingly well-covered by publications - the QPT and quantum chaos in algebraic (IBM-1) and geometrical (rigid triaxial rotator) nuclear models. Nevertheless, there still are some unanswered questions, that we shall try to answer. One of these questions is the extent to which a use of thermodynamics methods is justified in the case of nuclear theory, when the number of constituent particles is limited. Therefore, we shall consider an approach alternative to the ordinarily used Landau theory of phase transitions. When studying quantum chaos, the usually considered criteria are the energy level spacing distribution and the wave function entropy. We shall try to show that the fragmentation width of basis states [2], which is widely used in reaction theory, can be successfully applied as a quantum chaos cri-

terion for nuclear structure models. Developed theoretical methods of QPT and quantum chaos studies will be applied for the analysis of experimentally observed critical phenomena in the structure of even-even nuclei belonging to the transitional deformation region at $A \sim 190$, studied by the physicists of the LU ISSP Nuclear Reaction Laboratory.

Also, the understanding of such fundamental concepts as the quantum system's phase transitions, and the relationship between system's symmetries and quantum chaos, as well as the use of these conceptions for the study of a complex physical object - an atomic nucleus, have a considerable methodological and educational value. Therefore, the presented physics doctor dissertation serves also as a personal training ground and a basis for further studies of more complex and actual problems of nuclear physics or any other quantum system's theory.

Structure of the dissertation is as follows. In Section 1.1, we give a short review of basic conceptions and formulas used in the study of nuclear shape phase transitions and quantum chaos. Section 1.2 is devoted to the overview and characterization of the main up-to-date published results of other authors in the scope of studied theme. Problems, which have been considered in present study, as well as the methods chosen to resolve them are outlined in Section 1.3. Chapters 2-4 present detailed results of our studies of QPT and quantum chaos in the case of chosen algebraic and geometrical models of even-even nuclei. In Chapter 5, the theoretical methods developed in previous chapters are applied for the study of nuclear shape phase transition in the $A \sim 190$ region. Chapter 6 provides a summary of main results obtained in this dissertation, gives the account of their approbation in journal publications, and international and local scientific conferences, as well as indicates directions of possible future studies. The attached list of author's works includes 7 journal papers, of which 4 are already published in refereed editions, and 10 international and local conference abstracts. The Bibliography of this dissertation includes 63 titles.

1.1 Basic conceptions about nuclear shape phase transitions and quantum chaos

1.1.1 Geometrical (collective) and algebraic models of even-even atomic nuclei

Atomic nuclei are composite systems of nucleons – protons and neutrons, localized in space and bound by means of strong nucleon-nucleon interaction. In the framework of the non-relativistic quantum mechanics, a Schrödinger equation for a nucleus containing A nucleons (Z protons and N neutrons), if one considers only stationary properties of the nucleus, has the form

$$H\Psi\left(E \mid \vec{r}_1, \vec{r}_2, \ldots, \vec{r}_A; M\right) = E\Psi\left(E \mid \vec{r}_1, \vec{r}_2, \ldots, \vec{r}_A; M\right), \qquad (1.1)$$

where $\vec{r}_i$ denotes a coordinate of the i-th nucleon, $M \equiv (\vec{\sigma}_1\vec{\tau}_1, \vec{\sigma}_2\vec{\tau}_2, \ldots, \vec{\sigma}_A\vec{\tau}_A)$ – a set of A nucleon spin and isospin variables, Ψ – a wave function of the system, and E - it's energy. The general microscopic nuclear Hamiltonian H, depending on all $3A$ orbital and $4A$ spin-isospin variables, has the following structure

$$H = H_{kin} + H_e + H_p, \qquad (1.2)$$

where H_{kin} is a kinetic energy, H_e - a Coulomb interaction term, and H_p - a nucleon-nucleon interaction term.

Although the progress in calculation techniques made it possible to perform the *ab initio* many-particle Schrödinger equation calculations with realistic nucleon-nucleon interaction potentials (see, e.g., Ref.[3]), such solutions, as yet, have been obtained only in the case of lightest ($A \leq 16$) nuclei. In order to describe properties of heavier nuclei, one must develop phenomenological nuclear models employing various theoretical conjectures and approximations. The main assumption of the phenomenological approach is that one can regard a nucleus as a system consisting from a nuclear core plus a few valence nucleons (fermions). This concept has been developed mainly in two directions:

1) a unified model (geometrical) approach, introduced by O.Bohr and B.Mottelson in 1950s (see, e.g., [4, 5]);

2) an interacting boson (algebraic) approach, developing since the pioneering work of A.Arima and F.Iachello [6], and evolving to the Interacting Boson Model (IBM) and the Interacting Boson Fermion Model (IBFM) (see, e.g., [7, 8, 9]).

In the frameworks of the unified model approach, a nuclear core is described as a drop of incompressible "nuclear liquid". Valence nucleons are moving in the mean field formed by the core, that can have spherical or deformed shapes in the equilibrium ground state. Collective excitations of the core - rotation and vibrations, are the cause of dynamical deformation. These excitations are coupled with single-particle degrees of freedom of valence nucleons. The geometrical approach has been especially successful in the case of deformed even-even nuclei with mass numbers $140 < A < 200$.

One can describe collective excitations of the nuclear core employing collective variables $\alpha_{\lambda\mu}$, defined by the deviation of nuclear surface from the spherical equilibrium shape [5]:

$$R(\theta,\phi,t) = R_0\left[1 + \sum_{\lambda\mu}(-1)^{\mu}\alpha_{\lambda-\mu}(t)Y_{\lambda\mu}(\theta,\phi)\right], \tag{1.3}$$

where R_0 is the radius of the equivalent volume sphere. The nuclear surface, described by Eq. (1.3), is invariant under rotations and, therefore, $\alpha_{\lambda\mu}$ are the components of the irreducible tensor of rank λ, transforming according to the representations of group $SO(3)$:

$$a_{\lambda\mu} = \sum_{\nu} D^{\lambda}_{\nu\mu}(\theta_j)\alpha_{\lambda\nu}. \tag{1.4}$$

We shall limit our study of QPT and quantum chaos with models describing only quadrupole (λ=2) deformations of the even-even nuclear core. It can be shown (see, e.g., [5]) that, in such a case, one can introduce a new reference system, related with the principal symmetry axis of the nuclear core. In this internal reference system, collective variables $a_{2\mu} \equiv a_{\mu}$ can be replaced by new shape variables, introduced by O.Bohr and B.Mottelson [10]:

$$\begin{aligned} a_0 &= \beta\cos\gamma; \\ a_1 &= a_{-1} = 0; \\ a_2 &= a_{-2} = \frac{1}{\sqrt{2}}\beta\sin\gamma. \end{aligned} \tag{1.5}$$

Variables β and γ characterize the shape of the nucleus in the internal reference system, while three Euler angles $(\theta_1,\theta_2,\theta_3)$ describe the orientation of this internal reference system in space. The shape parameter β ($\beta^2 = \sum_{\nu} a_{\mu}^2 = a_0^2 + 2a_2^2$) defines a total quadrupole deformation of the

core: nuclear shape is prolate when $\beta > 0$, and oblate - when $\beta < 0$. The asymmetry parameter γ indicates a deviation of the nuclear core from the axial symmetry: when γ=0°, 60°,..., the core is axially-symmetric .

A standard collective Bohr-Mottelson (BM) model Hamiltonian [5] includes kinetic and potential energy terms, and depends on five collective variables (β, γ and three Euler angles θ_j $(j = 1, 2, 3)$):

$$\begin{aligned} & H^{BM} = H_{kin} + H_{pot} = \\ - \quad & \frac{\hbar^2}{2B_2}\left[\sum_{j=1,2,3}\frac{\mathbf{I}_j^2}{\mathcal{J}_j(\beta,\gamma)} + \frac{1}{\beta^4}\frac{\partial}{\partial\beta}\beta^4\frac{\partial}{\partial\beta} + \frac{1}{\beta^2}\frac{1}{\sin 3\gamma}\frac{\partial}{\partial\gamma}\sin 3\gamma\frac{\partial}{\partial\gamma}\right] + \frac{1}{2}C_2\beta^2, \end{aligned} \tag{1.6}$$

where

$$\mathcal{J}_j = 4\beta^2\sin^2\left(\gamma - j\frac{2}{3}\pi\right); \qquad (j = 1, 2, 3) \tag{1.7}$$

are nuclear moments of inertia along three internal axis, B_2 is a nuclear mass parameter, and C_2 is a stiffness parameter of quadrupole excitations.

The basis functions of BM are presented in the form:

$$\Phi^I_{MK} = \sqrt{\frac{2I+1}{16\pi^2(1+\delta_{K,0})}}\left(\chi_K D^I_{MK} + (-1)^{I+K}\chi_{-K}D^I_{M-K}\right), \tag{1.8}$$

where χ_K denotes an intrinsic wave function of the core, and D^I_{MK} – the rotational wave function; I is a total spin, and K - its projection on the nuclear symmetry axis. In the frameworks of collective BM model, the spectrum of even-even nucleus is described as a system of positive parity rotational bands, based on the axially-symmetric ground state, and the β- and γ-vibrations $(n_\beta, n_\gamma = 0, 1, 2, \ldots)$ of the core:

$$\begin{aligned} & K = 0, 2, 4, \ldots; \qquad && I = 0, 2, 4, \ldots \quad \text{for } K = 0; \\ & && I = K, K+1, K+2, \ldots \quad \text{for } K \neq 0. \end{aligned} \tag{1.9}$$

Another geometrical approach has been proposed in 1958 by A.S.Davydov and G.E.Filippov [11]. They assumed that there are nuclei having non-axial ground state deformation – rigid triaxial rotators. In such a case, collective coordinates a_0, a_2 Eq. (1.6) assume fixed non-zero values, and nuclear core has three different moments of inertia (1.7). The collective nuclear Hamiltonian of even-even nucleus in the case of rigid triaxial rotator model H^{3ax}

can be presented (see, e.g., [5]) as the Hamiltonian of the axially-symmetric rotator H_0^{ax} plus perturbation term, and the matrices of H^{3ax} are diagonalized in the basis of axially-symmetric rotator eigenfunctions Eq. (1.8) (with $\chi_K \equiv 1$). The nuclear triaxial rotator model is interesting for quantum chaos studies because of its relationship to the classical integrable system - the rigid asymmetric top (see, e.g., [12, 13]). We shall consider in Chapter 3 two versions of the nuclear rigid triaxial rotator model: a) Davydov's model [14], when nuclear core energies depend only on the asymmetry angle γ, and Bravin-Fedorov's model [15, 16], which includes the dependence both on γ and β.

Another phenomenological approach to the description of nuclear core is associated with interacting boson models (IBM) [7]. The main idea of IBM is that the nuclear core (consisting of even number of protons and even number of neutrons) is built from bosons – usually identified as the pairs of coupled nucleons, characterized by definite angular momentum value l. The number of bosons (N_b) usually is associated with the total number of nucleon pairs (particles or holes) outside the nearest closed proton and neutron shells for the given nucleus ((Z, N)=2,8,20,28,50,82,126). Nuclear collective Hamiltonian includes single boson excitation terms and two-boson interactions. Single-particle degrees of freedom of valence nucleons, included in the case of odd nuclei (the Interacting Boson-Fermion model (IBFM)) and odd-odd nuclei (the Interacting Boson-Fermion-Fermion model (IBFFM)), usually are the same ones as used in the unified model. The evaluation of interacting boson models is based on group theory approach, employing algebraic techniques of unitary groups and subgroups, characterizing a total number of bosonic and fermionic degrees of freedom.

In the simplest version of IBM - the IBM-1 model (or standard IBM), two types of bosons: one s-boson ($l = 0$) and five d-bosons ($l = 2$), are introduced in the form of $O(3)$-irreducible creation and annihilation operators:

$$\mathbf{b}^+_{lm} \equiv (\mathbf{s}^+_{00}, \mathbf{d}^+_{2m}); \qquad \mathbf{b}_{lm} \equiv (\mathbf{s}_{00}, \mathbf{d}_{2m}), \qquad \text{with} \quad \tilde{\mathbf{b}}_{lm} = (-1)^{l+m}\mathbf{b}_{l-m}, \tag{1.10}$$

which leads to six boson (collective) degrees of freedom, characterized by the symmetry of unitary group $U(6)$: 36 generators of this group form corresponding Lie algebra.

The most general nuclear Hamiltonian, conserving the total number of bosons $N_b = n_s + n_d$, consists from ($i = 1, 2, \ldots, N_b$) terms H^b_i with boson

energies e_i, and two-boson interaction terms V_{ij}:

$$H = H_{00} + \sum_{i=1}^{N} H_i^b + \sum_{i<j}^{N} V_{ij}, \tag{1.11}$$

where H_{00} denotes the doubly magic nuclear "core" Hamiltonian (energy constant e_0), which could be ignored if one considers excited level spectra of individual nuclei. In terms of boson creation and annihilation operators Eq. (1.10), the interacting boson Hamiltonian Eq. (1.11) can be presented as (see, e.g., [7, 9]):

$$\begin{aligned}
H^{IBM} &= \varepsilon_s(\mathbf{s}^+ \cdot \tilde{\mathbf{s}}) + \varepsilon_d(\mathbf{d}^+ \cdot \tilde{\mathbf{d}}) \\
&+\frac{1}{2}\sum_{J=0,2,4} C_J\sqrt{2J+1}\Big[\Big[\mathbf{d}^+ \times \hat{\mathbf{d}}^+\Big]^{(J)} \times \Big[\tilde{\mathbf{d}} \times \tilde{\mathbf{d}}\Big]^{(J)}\Big]^{(0)} \\
&+\frac{1}{\sqrt{2}}\, v_2 \left(\Big[\Big[\mathbf{d}^+ \times \mathbf{d}^+\Big]^{(2)} \times \Big[\tilde{\mathbf{d}} \times \tilde{\mathbf{s}}\Big]^{(2)}\Big]^{(0)} + \Big[\Big[\mathbf{s}^+ \times \mathbf{d}^+\Big]^{(2)} \times \Big[\tilde{\mathbf{d}} \times \tilde{\mathbf{d}}\Big]^{(2)}\Big]^{(0)}\right) \\
&+\frac{1}{2} v_0 \left(\Big[\Big[\mathbf{d}^+ \times \mathbf{d}^+\Big]^{(0)} \times \big[\tilde{\mathbf{s}} \times \tilde{\mathbf{s}}\big]^{(0)}\Big]^{(0)} + \Big[\Big[\mathbf{s}^+ \times \mathbf{s}^+\Big]^{(0)} \times \Big[\tilde{\mathbf{d}} \times \tilde{\mathbf{d}}\Big]^{(0)}\Big]^{(0)}\right) \\
&+u_2\Big[\Big[\mathbf{d}^+ \times \mathbf{s}^+\Big]^{(2)} \times \Big[\tilde{\mathbf{d}} \times \tilde{\mathbf{s}}\Big]^{(2)}\Big]^{(0)} + \frac{1}{2} u_0\Big[\Big[\mathbf{s}^+ \times \mathbf{s}^+\Big]^{(0)} \times \big[\mathbf{s} \times \mathbf{s}\big]^{(0)}\Big]^{(0)},
\end{aligned} \tag{1.12}$$

where ε_s and ε_d are energies of the s- and d-bosons and $C_0, C_2, C_4, v_0, v_2, u_0, u_2$ are constants of the seven two-boson interactions. Since the boson number N_b is a good quantum number, and we are not interested in nuclear binding energies, this basic IBM-1 Hamiltonian can be further simplified reducing the number of model parameters to six [7]:

$$\varepsilon, \quad C_0', \quad C_2', \quad C_4', \quad v_0, \quad \text{and} \quad v_2, \tag{1.13}$$

with $\varepsilon = \varepsilon_d - \varepsilon_s + (u_2/\sqrt{5} - u_0)(N_b - 1)$, and $C_J' = C_J + u_0 - 2u_2/\sqrt{5}$.

Wave functions of Hamiltonian Eq. (1.12) are classified according to the completely symmetric representations $[N_b]$ of group $U(6)$. Basis states for the diagonalization of IBM-1 Hamiltonian can be further labeled by quantum numbers of irreducible representations belonging to either of three subgroup chains [7, 9]:

$$U(6) \supset \begin{cases} U(5) \supset O(5) \supset O(3) \supset O(2) \\ O(6) \supset O(5) \supset O(3) \supset O(2) \\ SU(3) \supset O(3) \supset O(2) \end{cases} \tag{1.14}$$

Employing Casimir operators of corresponding subgroups, one can present the complete IBM-1 Hamiltonian in equivalent multipole expansion form proposed by Iachello and Arima [7, 17]:

$$\begin{aligned} H_{sd} &= \varepsilon' n_d + \frac{1}{2}\eta(\mathbf{L}\cdot\mathbf{L}) + \frac{1}{2}\kappa(\mathbf{Q}\cdot\mathbf{Q}) - 5\sqrt{7}\omega\left[[\mathbf{d}^+\times\tilde{\mathbf{d}}]^{(3)}\times[\mathbf{d}^+\times\tilde{\mathbf{d}}]^{(3)}\right]^{(0)} \\ &+ 15\xi\left[[\mathbf{d}^+\times\tilde{\mathbf{d}}]^{(4)}\times[\mathbf{d}^+\times\tilde{\mathbf{d}}]^{(4)}\right]^{(0)} \end{aligned} \tag{1.15}$$

where quadrupole moment operator $\mathbf{Q}$ is presented as [18]

$$\mathbf{Q}(\chi) = [\mathbf{d}^+\times\tilde{\mathbf{s}} + \mathbf{s}^+\times\tilde{\mathbf{d}}]^{(2)} + \chi[\mathbf{d}^+\times\tilde{\mathbf{d}}]^{(2)}, \tag{1.16}$$

and ε', η, κ, ω, ξ and χ are new model parameters. The expressions relating these parameters with those of the basic IBM-1 Hamiltonian Eq. (1.12) one can find, e.g., in [17].

Energies and wave functions of the complete IBM-1 Hamiltonian Eq. (1.15) are obtained by its diagonalization in the basis of eigenfunctions of either of three subgroup chains Eq. (1.14). All three reduction chains are equivalent and the rank n of the diagonalized matrix is determined by the total number of bosons N_b. Matrices are diagonalized at each spin I value allowed by the classification of basis states. The unperturbed Hamiltonians containing only the diagonal terms (Casimir invariants) of corresponding subgroup chain are known as the $U(5)$, $O(6)$, and $SU(3)$ limits of IBM-1, which are usually associated with the vibrational, asymmetric (γ-unstable) rotator, and axially-symmetric rotator nuclear core excitations [7, 9]. The most general and often used IBM-1 Hamiltonian diagonalization basis is that of the spherical $U(5)$ vibrational limit.

1.1.2 Description of nuclear shape phase transitions

A great attention during last decades has been devoted to the study of thermodynamic phase transitions in finite systems, such as Bose-Einstein condensates, atomic clusters, etc. The notion about quantum phase transitions (see, e.g., [1]), for the most part, is related to the study of critical phenomena of interacting quantum objects at zero temperature, when one observes a transition between two distinct types of the ground state wave function. This transition between $H(0)$ and $H(1)$ phases is described via the change

of perturbing interaction, which one can trace using a dimensionless control variable ρ that is usually normalized to fit into the range $\rho \in [0, 1]$:

$$H(\rho) = H_0 + \rho V = (1 - \rho)H(0) + \rho H(1). \tag{1.17}$$

The crossing of the critical point is usually studied in the infinite size limit when the number of particles $\mathcal{N} \to \infty$. At zero temperatures, the only possible cause of the onset of disorder are quantum fluctuations, therefore, such phenomenon is referred to as the quantum phase transition (QPT).

In the case of atomic nuclei, the classical thermodynamic phase transitions are studied at high excitation energies and/or high rotation frequencies. In the ground state and at low energy and spin values, one observes the change of the nuclear shape, which is represented by the minima of nuclear collective potential energy expression $V(\beta, \gamma)$ in the (β, γ) phase space diagram (see, e.g., [5]). Then one can study transitions between prolate ($\beta > 0$), oblate ($\beta < 0$) and spherical ($\beta = 0$) nuclear shapes. The analysis of the potential energy surface minima in dependence on specific nuclear model parameters allows to study the nuclear shape phase transitions employing either the Landau theory of phase transitions [19] or a catastrophe theory approach [20].

A classical thermodynamical potential $\Phi(P, T; \xi)$, depending on pressure P, temperature T and system's order parameter ξ, is a continuous function in the equilibrium state ξ_0. However, the derivatives of $\Phi(P, T; \xi)$ with respect to control parameter ξ may have discontinuities at ξ_0. One speaks about first order phase transition if there is a discontinuity in the first order derivative, and about second order phase transition if the discontinuity is observed for the second order derivative. According to the Landau theory of second order phase transitions [21], one can expand the precise thermodynamical potential expression in the vicinity of the critical point into Taylor series with respect to system's order parameter ξ

$$\Phi(P, T; \xi) = \Phi_0 + A(P, T)\xi^2 + B(P, T)\xi^3 + C(P, T)\xi^4 + \cdots, \tag{1.18}$$

and analyze the behaviour of obtained expansion coefficients in the (P, T) plane. The first order term in Eq. (1.18) is equal to zero when phases with $\xi_0 = 0$ and $\xi_0 \neq 0$ have different symmetries. If the coefficient $B(P, T)$ vanishes for all P and T, the first order phase transitions form continuous lines in the (P, T) plane. Second order phase transitions form either separate points or lines in the (P, T) plane: in the most simple case, when $A = 0$ and

$B = 0$, while $C > 0$, one obtains an isolated triple point ($P = P_c, T = T_c$) where three different phases meet.

The IBM-1, having a comparatively simple structure due to its algebraic symmetry properties, and including explicit dependence on N and Z via the total boson number N_b, provides a possibility to analyze these QPT in a wide range of nuclei. One can study these transitions considering the division of complete IBM-1 Hamiltonian into integrable Hamiltonians H_0 of limiting cases: $U(5)$, $O(6)$, and $SU(3)$, and the perturbation terms depending on chosen control parameter values. However, for the most part, the nuclear shape phase transitions are analyzed (see, e.g., [22]) employing a simplified model [23, 24], which is often called the Casten's version of IBM-1. The Hamiltonian of this version uses the self-consistent Q formalism [18] and depends only on two parameters (η, χ). The parameter space of this Hamiltonian usually is presented employing the so-called Casten's triangle. We shall consider the Casten's version of IBM-1 in detail in Section 2.1.

A deeper insight in the phenomenon of nuclear shape phase transitions one can obtain studying the classical energy functional expressions E_{cl} of corresponding algebraic models. One can obtain the classical energy expression of a model Hamiltonian H applying the time-dependent variational principle (see, e.g., [25])

$$\delta \int dt < \psi | i \frac{\partial}{\partial t} - H | \psi >= 0; \tag{1.19}$$

the trial functions $|\psi >$ are taken in the form of harmonic-oscillator coherent states $\alpha(t)$ for six types of bosons:

$$|\vec{\alpha} >= \exp(-|\vec{\alpha}|^2/2) \exp\left(\alpha_s \mathbf{s}^+ + \sum_{m=-2}^{2} \alpha_m \mathbf{d}_m^+ \right) |0> . \tag{1.20}$$

The projection of this coherent state on a subspace with N_b bosons has a form of boson condensate [26]. For $N_b \to \infty$ this procedure yields the classical limit of the model, depending both on the IBM-1 model parameters and on two intrinsic shape variables, which can be linked [27] with the BM model shape parameters β and γ. An alternative method for the evaluation of IBM Hamiltonian expectation value in the coherent state has been proposed in [28]. Once the classical energy functional expression E_{cl} of employed IBM-1 version is known, one can study its behaviour in the nuclear shape diagram (β, γ), linking this behaviour with three limiting cases of IBM-1 employing the notions about first and second order QPT (see [22]).

Nuclear QPT most often are studied only in dependence from the total quadrupole deformation parameter β (assuming $\gamma = 0$) since the nuclear potential energy $V(\beta, \gamma)$ minima do not depend on γ value in the case of quadrupole deformation (see, e.g., [5]), i.e., these minima are γ-soft (γ-unstable). In order to obtain stable non-axial minima, one should include additional interactions to the nuclear core Hamiltonian. In the case of IBM-1, the three-boson interaction terms should be added (see [7]) to the Eq. (1.12). Since the calculations employing complete obtained expressions are too complicated, one usually adopts some simplifications, i.e. considers the IBM-1 Hamiltonian in the γ-unstable $O(6)$-limit adding to it some cubic d-boson interaction terms (see, e.g., [29, 30]).

1.1.3 Quantum chaos and its criteria

The problem of chaos in quantum physics is still a theme of discussions (see, e.g., [31]). The views about this subject can be grouped as follows [2]: Most of authors support a moderate view stating that the term "quantum chaos" denotes the quantum limit of phenomena characteristic to chaotic systems of classical mechanics. The studies in this direction are based mostly on the use of quasi-classical approximations. However, since the quantum mechanics involves the classical one as its particular limiting case, it is impossible to define quantum chaos in a consistent way, from the point of view of classical mechanics. Therefore, the second, strictly negative opinion persists that there is no such thing as quantum chaos. The third group believes that the chaocitity displayed by quantum systems has a purely quantum origin, related with the symmetry properties of integrals of motion (dynamics) of corresponding quantum systems.

In the consideration of QPT, it has been already noted that the only possible cause of the onset of disorder at zero temperatures are quantum fluctuations. Therefore, the phenomena of QPT and quantum chaos are closely related, just as the starting points of their study, i.e., the division of non-integrable model Hamiltonian H into integrable (symmetric) part H_0 and perturbation term V. Solution of the Schrödinger equation for H is obtained via diagonalization of H matrix in the basis of H_0 eigenfunctions Φ_k ($k = 1, \ldots, n$), giving eigenvalues E_i and eigenfunctions Ψ_i, presented as

the superposition

$$\Psi_i = \sum_{k=1}^{n} c_{ik} \Phi_k, \tag{1.21}$$

where c_{ik} are mixing amplitudes.

One can say that quantum system is regular, if it is described by the integrable Hamiltonian H_0, i.e., the Hamiltonian consisting of Casimir invariants or integrals of motion of the corresponding symmetry group. If perturbation operator V is small with respect to H_0, then mixing amplitudes c_{ik} at $i \neq k$ would be small as well: the chaoticity of the perturbed system is low, i.e., one has a case of "weak chaos". If perturbation V is relatively large – quantum system approaches a "hard chaos" case, when one cannot distinguish the main component in the wave function superposition (1.21).

Chaos inherent to the quantum system can be characterized employing two different types of criteria – the statistical criteria, related with the H eigenvalue (energy) distributions, and the dynamical criteria, determined by the state vectors of the perturbed system in the chosen unperturbed system's basis. Since statistical quantum chaos criteria characterize the general chaoticity of the system, irrespectively of the choice of model diagonalization basis, one cannot relate them with QPT at zero temperatures. On the contrary, the dynamical quantum chaos criteria, due to the mode of their calculation, are useful indicators of QPT, especially in models describing low-lying states in nuclear spectroscopy. Also, the dynamical quantum chaos criteria are invariant under unitary transformations of system's basis functions. Because of growing interest about QPT studies, such dynamical quantum chaos criterion as the wave function entropy is now often analyzed in works, related with calculations in the frameworks of algebraic nuclear models (see, e.g., [32]).

The most popular statistical criterion of quantum chaos is a distribution $P(S)$ of nearest level spacings $S = E_{i-1} - E_i$. It has been proved [33] that, for regular, completely integrable quantum systems described by non-degenerate Hamiltonians, the level spacing distribution assumes a Poisson form

$$P_P(S) = \exp\left(-S\right). \tag{1.22}$$

On the contrary (see [34]), level spacings of the quantum analogue of the classically chaotic system (Sinai's billiard) obey Wigner distribution

$$P_W(S) = (\pi/2) \cdot S \cdot \exp\left(-\pi S^2/4\right), \tag{1.23}$$

which is consistent with the Gauss orthogonal ensembles (GOE) statistics of random matrices.

A transition from the regular (integrable) state of the system to the chaotic (non-integrable) one can analyze employing, e.g., the one-parameter Brody distribution [35]:

$$P_B(S) = aS^{\zeta} \exp\left(-bS^{\zeta+1}\right), \tag{1.24}$$

where $a = (\zeta+1)b$ and $b = \left\{\Gamma\left(\frac{\zeta+2}{\zeta+1}\right)\right\}^{\zeta+1}$. The form of distribution is determined by the value of Brody parameter ζ: when ζ=0, one obtains Poisson distribution Eq. (1.22); when ζ=1 - Wigner distribution Eq. (1.23).

The level spacing distribution is the most used statistical characteristic of quantum chaos. Another statistical quantum chaos criterion is, e.g., a spectral rigidity $\Delta_3(L)$, which has been applied for the energies of low-lying collective states of even-even nuclei in [36, 37]. Since we do not use this criterion in present work, we shall not consider it here.

The most popular dynamical quantum chaos criterion is a Shannon information entropy of the wave function defined as follows [38]:

$$W(\Psi_i) = -\sum_{k=1}^{n} |c_{ik}|^2 \cdot \ln\left(|c_{ik}|^2\right), \tag{1.25}$$

characterizing the admixture of the integrable (regular) Hamiltonian H_0 eigenfunctions Φ_k in the wave function Ψ_i of the perturbed Hamiltonian H. The minimal value of the wave function entropy $W(\Psi_i)^{min} = 0$ corresponds to the unmixed state, when the wave function coincides with one of H_0 eigenfunctions ($\Psi_i = \Phi_k$). The theoretically possible maximal entropy value $W(\Psi_i)^{max} = ln(n)$ corresponds to the case, when the perturbed Hamiltonian H wave function is uniformly spread (fragmented) over all regular Hamiltonian H_0 basis states, i.e., all mixing amplitudes are $|c_{ik}|^2 = 1/n$.

Another dynamical quantum chaos criterion, proposed by V.Bunakov [2], is the fragmentation of basis states $\kappa(\Phi_k)$. The value of this criterion for the k-th basis state Φ_k of some regular Hamiltonian H_0 is defined [2, 39] as the ratio of the Φ_k fragmentation width over the states Ψ_i of the perturbed Hamiltonian H ($\Gamma_{spr}(k)$) to the averaged spacing D_0 of the regular system's eigenvalues ε_k:

$$\kappa(\Phi_k) = \Gamma_{spr}(k)/D_0. \tag{1.26}$$

The detailed prescription for $\Gamma_{spr}(k)$ calculation one can find in [39], and in our work [R1]. The average distance D_0 between the energies of H_0 basis states $\varepsilon_1, \varepsilon_2, \ldots, \varepsilon_k, \ldots, \varepsilon_n$ one can calculate according to the formula

$$D_0 = \frac{|\varepsilon_{max} - \varepsilon_{min}|}{n-1}, \tag{1.27}$$

where ε_{max} and ε_{min} are the maximal and the minimal values from the set of eigenvalues $\varepsilon_1, \varepsilon_2, \ldots, \varepsilon_k, \ldots, \varepsilon_n$. Let us note, that one can calculate $\kappa(\Phi_k)$ values only in cases when the diagonal mixing amplitude fulfills the condition

$$|c_{i=k,k}|^2 < 0.5. \tag{1.28}$$

Employing criterion $\kappa(\Phi_k)$, one can distinguish three cases of quantum chaos:

1) when $\kappa(\Phi_k) = 0$, the quantum system is in the state of regular motion: corresponding Hamiltonian can be presented as a linear combination of Casimir invariants of system's symmetry groups, and there is no fragmentation over basis states ($\Gamma_{spr}(k) = 0$).

2) the $0 < \kappa(\Phi_k) < 1$ region is associated with the case of soft chaos, when one can identify after H diagonalization the k-th basis state due to the maximal value of its mixing amplitude c_{ik}. In this case $\Gamma_{spr} \neq 0$ and $\Gamma_{spr} < D_0$.

3) if $\kappa(\Phi_k) \geq 1$, then $\Gamma_{spr}(k) \geq D_0$: the system is in the state of hard chaos, when amplitudes of basis states are completely mixed, and one can not recognize their main components after the diagonalization of quantum Hamiltonian. In the case of hard chaos, the assignment of basis state quantum numbers to the states of perturbed Hamiltonian becomes ambiguous.

The fragmentation width of basis states in the classical limit is transformed [2] to the well-known classical characteristics of chaoticity – Lyapunov's exponent λ, which describes the exponential instability of classical trajectory with respect to small variations of initial conditions: the distance between two neighboring trajectories with time t grows as $\exp(\lambda t)$. That means that, in the case of hard chaos, when one cannot divide H into regular H_0 part and small perturbation V, the dynamical criteria are correlated with statistical ones.

1.2 The characterization of the main up-to-date studies of shape phase transitions and quantum chaos in algebraic and geometrical models of even-even nuclei

There is a great number of published papers devoted to all aspects of quantum phase transitions and quantum chaos. The number of publications constantly increases because of the growing interest in quantum methodology in later years. Problems related to QPT and quantum chaos are considered mainly in the frameworks of algebraic nuclear models, though there is a number of studies devoted to quantum chaos in shell model and geometrical collective model approaches (see, e.g., [40, 41, 42]). A good overview of the problem's state of art in the field of nuclear structure studies one can find in [1].

Algebraic models allow one to present system's Hamiltonian in terms of Casimir invariants belonging to some integrable (regular) system, enabling one to perform numerical analysis of phase transitions in terms of chosen critical variables. The most popular of these algebraic nuclear models is the standard interacting boson model IBM-1 and its simplified two-parametric Casten's version, employed for quantum chaos and QPT studies by most of authors. Further on we shall briefly characterize main results of these studies obtained in the case of low-lying states of even-even nuclei.

The classical energy E_{cl} expressions (when $N_b \to \infty$) of three IBM-1 limiting Hamiltonians have been first obtained and studied by Dieperink et al. [27]. P. Van Isacker and Jin-Quan Chen [28] have derived E_{cl} in the case of complete IBM-1 version as well as in the case of $O(6)$-limit Hamiltonian with three boson interaction terms. They also analyzed the properties of corresponding classical energy surfaces in the plane of BM parameters (β, γ) and shown that the classical limit of complete IBM-1 does not allow to reproduce stable triaxial deformation.

Historically first most important results about quantum chaos and QPT relationships in the frameworks of IBM-1 were published in papers by Y. Alhassid et al. [36, 24, 25, 37]. They studied chaos in the properties (energies and E2 transitions) of low-lying collective states of even-even nuclei introducing a simplified two-parametric IBM-1 Hamiltonian. The use of such approach allowed to study transitions between three limiting cases of IBM-1 via a change of one chosen variable. The theoretical $P(S)$ and spectral rigid-

ity distributions in dependence on these control variables were compared with GOE predictions. The classical limit of IBM-1, depending on five quadrupole shape parameters, has been obtained as well, and studied employing Monte Carlo techniques. The regular and transitional regions have been discovered in the parameter space of Casten's triangle. Similar results have been obtained by T. Mizusaki et al. [43], who studied the level statistics of a simplified IBM Hamiltonian diagonalized in the $U(5) \supset O(5)$ basis.

These studies were developed further by P. Cejnar, J. Jolie and co-workers in [38, 44, 45, 22, 19]. In [38], the information entropy of IBM-1 wave functions with respect to dynamical symmetry limits has been proposed as a measure of a symmetry breaking, i.e. a transition from one type of system's symmetry to another. The behaviour of $W(\Psi_i)$ in dependence on (η, χ) values in the space of extended Casten's triangle (which includes also "hidden" dynamical symmetries $\overline{SU(3)}$ and $\overline{(O(6))}$ has been studied. These studies have been continued in, e.g., [44, 45], where shape phase transitions and wave function entropy relationships have been analyzed employing the classical energy functional expression of simplified Casten's version of IBM-1. Singular behaviour of wave function entropy and six quadrupole shape invariants, proposed in [46], have been studied in relation to $U(5) - SU(3)$, $U(5) - O(6)$, and $SU(3) - O(6)$ phase transitions in [47].

The Landau theory of phase transitions has been applied for the analysis of phase transitions in IBM-1 Casten's version in [22, 19]. The expansion of corresponding classical energy expression in β orders (at $\gamma = 0^\circ$) has been used for the analysis of critical lines and points associated with first and second order nuclear shape phase transitions. In [45, 22], new types of IBM dynamical symmetries: $X(5)$ and $E(5)$, developed by F.Iachello in [48, 49], have been associated with critical points on the line separating spherical and deformed nuclei. The isolated second order phase transition point – the triple point between spherical and two deformed (oblate $\beta > 0$ and prolate $\beta < 0$) nuclear shapes, corresponding to $E(5)$ group symmetry, has been studied in [22]. This point is described as the meeting point of two phase transition critical lines: the first line $X(5) - E(5) - \overline{X(5)}$ is between higher and lower symmetries (spherical $U(5)$, and deformed $SU(3)$ and $O(6)$), while the second line $E(5) - O(6)$ - between symmetries, characterized by opposite signs of order parameter β (prolate $SU(3)$, when $\beta > 0$, and oblate $\overline{SU(3)}$, when $\beta < 0$).

A somewhat different approach to the analysis of QPT in the complete version of IBM-1, has been proposed by E. López-Moreno and O. Castaños

[20]. They employed the formalism of the catastrophe theory for the analysis of E_{cl} energy surfaces and shown that the equilibrium configurations in the most general case can be classified employing just two essential control variables (r_1, r_2) that are derived from the parameters of the complete IBM-1 Hamiltonian Eq. (1.12). The equations for critical lines and points in terms of (r_1, r_2) were obtained via the expansion of the classical energy expression $E_{cl}(\beta, \gamma = 0)$ in Taylor series with respect to nuclear quadrupole deformation β. The analysis of bifurcation and Maxwell sets of critical lines and points in the (r_1, r_2) plane was performed in relation to IBM-1 limiting symmetries $U(5)$, $O(6)$, and $SU(3)$.

The possibility to describe in the frameworks of IBM-1 a stable triaxial core deformation via the inclusion of three-boson interaction terms has been proposed by Heyde et al. [29]. Various cubic boson interaction terms have been added to the Hamiltonians of all three limiting cases, and the corresponding classical energy surfaces have been studied. The conclusion has been made that only $L = 3$ term is responsible for the stable minimum with $\gamma \neq 0^\circ$ or 60°. In [23], the proposed approach, employing the $O(6)$-limit IBM-1 Hamiltonian with the $L = 3$ three-boson interaction term, has been applied for the study of some Xe, Ba, and Pt isotopes, the low-lying spectra of which exhibit triaxiality. The inclusion of all $L = 0, 2, 3, 4, 6$ terms of the three-boson interaction in the $O(6)$ limit Hamiltonian has been analyzed in [50] where the energies and $B(E2)$ reduced transition probabilities of a number of $O(6)$-like nuclei were considered.

The prolate-oblate shape phase transition analysis, employing the $O(6)$-limit Hamiltonian with cubic terms $[\mathbf{QQQ}]^{(0)}$, where $\mathbf{Q}$ is an $O(6)$ quadrupole operator, has been performed in [30]. The energy spectra of this cubic term were considered earlier in [51], and it has been shown that they are similar to those of the BM rigid-rotator. It allows one to obtain $SU(3)$-like states in the $O(6)$-limit of IBM-1. Authors of [30] proposed two versions of the extended $O(6)$-limit Hamiltonian with cubic $[\mathbf{QQQ}]^{(0)}$ terms: the one with $O(6)$-invariant symmetry properties, and another - the $O(6)$-non-conserving. Classical energy minima and parameter space of proposed $O(6)$-invariant model have been studied and conditions were derived for critical lines and points, including a triple point where all three deformation types meet.

In studies of quantum chaos phenomena in nuclear spectroscopy, main attention until now has been paid to the statistical criteria, related with the distribution of energy spacings within the groups of levels with fixed spin and parity values I^π (see, e.g., [36, 37]). Considerably lesser attention has

been given to the study of dynamical criteria - the wave function entropy $W(\Psi_i)$ and the fragmentation of basis states $\kappa(\Phi_k)$. A thorough study of the behaviour of wave function entropy in the case of Casten's version of IBM-1 one can find in [38].

The fragmentation of basis states $\kappa(\Phi_k)$ has been proposed as a numerical criterion of quantum chaos by V. Bunakov in [2]. The behavior of this criterion and its classical limit have been studied in the case of Hénon-Heiles model in [39]. The use of $\kappa(\Phi_k)$ in the case of some nuclear models has been considered in preliminary calculations of J. Tambergs et al. [52]. The detailed analysis of this quantum chaos criterion, in the case of simplified Casten's version of IBM-1, has been performed for the first time in our work [R1], and, in the case of geometrical rigid triaxial rotator models, in [R4,R5].

The behaviour of statistical quantum chaos criteria in the case of geometrical collective BM and shell model has been analyzed in works of V.R. Manfredi and L. Salasnich [53, 54]. They have shown that ordered and chaotic states in nuclear models generally coexist. In the case of rigid triaxial rotator model [12, 13], it has been shown that, in spite of the fact that the asymmetric top is integrable in classical mechanics, the statistical criteria of quantum chaos (level spacing distribution $P(S)$ and spectral rigidity $\Delta_3(L)$) do not follow the Poisson statistics, as it should be for the quantum Hamiltonian of a classically integrable problem. This anomalous behaviour has been explained in [13] as due to the semi-classical quantization and diagonalization procedure. However, the analysis of terms of nuclear shape parameters β and γ was not performed.

Of numerous studies were some aspects of QPT and quantum chaos are considered in relation to properties of specific nuclei, we shall note the papers [55, 56], devoted to the transition between vibrational $U(5)$ and rotational $SU(3)$ type nuclei. In [55], the region of possible coexistence of two deformation phases along $0 \leq \eta \leq 1$ line (with $\chi = -\sqrt{7}/2$ is considered. Indications of such coexistence have been found in experimental low-lying spectra of even-even ^{150,152,154}Sm nuclei. The conditions for the values of simplified Casten's IBM-1 version parameters, characterizing nuclei belonging to the arc of regularity between $SU(3)$ and $U(5)$ limits, have been obtained in [56].

The transition between prolate and oblate nuclear shapes in the $A \sim$190 region, considered also in present dissertation, has been studied employing different theoretical approaches: the mean-field based calculation (see, e.g., [57, 58]), the Woods-Saxon-Strutinsky calculations [59, 60], and algebraic IBM-1 (see, e.g., [32]). The authors of all these model calculations have

analyzed and compared properties of low-lying and yrast states of various tungsten, osmium, and platinum isotopes drawing conclusions about deformation of specific nuclei in dependence on Z and N. In difference from our work, the authors of [32] have employed a simplified Casten's version of IBM-1 taking into account the dependence on only one model parameter χ.

1.3 The aims and methods of presented research work

The problems that are to be resolved in the scope of this dissertation can be defined as follows:

1) to obtain precise analytical expressions for the classical energy functional E_{cl} minima conditions in terms of nuclear quadrupole deformation parameter β, and to apply the obtained expressions for the analysis of nuclear shape phase transition critical lines and points in the case of several simplified IBM-1 versions, and in the case of complete IBM-1 Hamiltonian, comparing the results with those obtained employing the approach of the Landau theory of phase transitions, when the higher order terms of E_{cl} expansion are disregarded;

2) to analyze and compare the behaviour of statistical and dynamical quantum chaos criteria in terms of nuclear quadrupole deformation parameters and shape phase transitions in the frameworks of algebraic IBM-1 and geometric rigid triaxial rotator models of even-even nuclei;

3) to assess a possibility to employ the basis state fragmentation width $\kappa(\Phi_k)$ as a dynamical quantum chaos criterion in the case of algebraic (IBM-1) and geometrical (rigid triaxial rotator) nuclear structure models;

4) to apply the developed theoretical approach for the study of prolate-oblate shape phase transition, which is experimentally observed in the tungsten, osmium, and platinum isotope chains belonging to the $A \sim$190 region.

For the study of precise analytical solutions of the classical energy functional minima problem, and the comparison of obtained results with those obtained by other authors, following IBM-1 versions have been chosen:

a) the simplified two-parameter Casten's version;

b) the $O(6)$-limit Hamiltonian with included cubic d-boson interaction terms;

c) the $O(6)$-limit Hamiltonian with attached cubic quadrupole moment term $[\hat{Q}\hat{Q}\hat{Q}]^{(0)}$ in two variants: the one conserving the dynamical $O(6)$-symmetry, and the $O(6)$-symmetry non-conserving variant; one should note that, in the latter case, the E_{cl} minima problem has not been studied before;

d) the complete IBM-1 version.

For all model versions, precise analytical solutions for the E_{cl} minima condition equations in terms of nuclear quadrupole deformation parameter β (at $\gamma = 0$) have been obtained employing the computer program package Mathematica. The behaviour of these minima in dependence on IBM-1 parameter values have been analyzed in terms of QPT critical lines and points. The results of precise solution method have been compared with analogous results obtained using the Landau phase transition theory approach. The effects due to accounting of higher order terms of E_{cl} expansion have been assessed in the case of complete IBM-1 version.

The standard IBM-1 computer program package PHINT by O.Scholten [17] has been used for the diagonalization of IBM-1 model Hamiltonian in order to obtain eigenvalues and eigenfunctions for the evaluation of statistical ($P(S)$) and dynamical ($W(\Psi_i)$ and $\kappa(\Phi_k)$) quantum chaos criteria, as well as for the calculation of theoretical energy values in the case of $A \sim$190 region nuclei.

A specially written computer program has been used for the diagonalization of rigid triaxial rotator model Hamiltonian matrices at different nuclear spin I values. The model Hamiltonian matrices have been obtained in dependence on γ, in the case of Davydov's model, and γ and β, in the case of Bravin-Fedorov's model.

The behaviour of quantum chaos criteria has been studied in the frameworks of:

a) the algebraic simplified Casten's version of IBM-1; and

b) two geometric rigid triaxial (asymmetric) rotator models.

These models have a relatively simple structure and a small number of model parameters: one parameter γ - in the case of Davydov's model, and two parameters - in the case of Bravin-Fedorov's model and in the case of simplified Casten's version of IBM-1. The parameters of the Casten's version of IBM-1 (η, χ) are directly linked with the nuclear quadrupole deformation parameters via classical limit energy E_{cl} expressions. It provides an opportunity to compare the behaviour of quantum chaos criteria in the frameworks of both approaches: geometrical and algebraic.

Hamiltonian matrices of both models at each nuclear spin I value have

finite rank: $n = n(I)$, in the case of rigid triaxial rotator models, and $n = n(I, N_b)$, in the case of IBM-1. However, one should take into account that, while nuclear spin I values are unlimited in the frameworks of geometrical approach, in the case of IBM-1, a boson number N_b determines a cut-off value for the nuclear spin. The existence of an upper limit affects the observed mixing of IBM-1 states at higher spin values.

The developed methods are applied for the analysis of relationships between shape phase transitions and quantum chaos criteria in the case of specific transitional nuclei. For this purpose, we have chosen 15 even-even isotopes of tungsten ($Z = 74$), osmium ($Z = 76$), and platinum ($Z = 78$) with $184 \leq A \leq 194$, belonging to the transitional deformation region at $A \sim$190. Nuclei of these three elements are known to have shapes ranging from the stable prolate axial-symmetry (^{184}W) to the asymmetric γ-unstable (^{194}Pt) form.

This is one of regions where traditionally the prolate-oblate shape phase transition is studied; so, there is a possibility to compare our results both with experimental data and with the results of other model calculations. The confidently established experimental data about excited level energies and electromagnetic properties of considered nuclei have been taken from the ENSDF data compilations [61] with a deadline up to January 2010. Therefore, we use for our analysis experimental information which is more accurate than that available for the most of earlier studies.

We have limited our calculations with nuclei belonging to the $184 \leq A \leq 194$ region and having boson numbers N_b from 7 to 12, excluding experimentally well-known heavier platinum isotopes. Such choice was motivated: a) by the lack of confident experimental data about heavy tungsten and osmium isotopes in the ENSDF data base; b) by the fact that one needs a sufficient number of basis states for the calculation of quantum chaos criteria; c) by the circumstance that, at $A \geq 194$, when neutron number approaches the closed shell at $N = 126$, it is hard to distinguish which phase transition takes place - the prolate-to-oblate or the deformed-to-spherical.

Analysis of experimental data shows that the nuclear shape phase transition in the W-Os-Pt region has a very complex nature. In fact, two parallel transitions take place: the $SU(3) - O(6) - \overline{SU(3)}$ phase transition from the deformed prolate shape to the deformed oblate shape, and the deformed-to-spherical $O(6) - E(5) - U(5)$ transition. Besides, deformation of the nuclear ground state and that of higher excitations can be different, i.e, there is a possibility of shape coexistence.

Therefore, one must consider the variation of IBM-1 parameters in the entire model parameter space, not just along some selected phase transition critical line, i.e., to use the complete version of IBM-1 in multipole representation, which enables one to describe in a uniform way various nuclear shapes and to study the transition from one shape to another. The values of model parameter have been obtained via the fit of theoretical spectra to the experimental energies of low-lying collective states in the case of each of considered nuclei. In difference from the most of well-known prolate-oblate shape phase transition studies, we have considered in our analysis the entire low-lying spectrum of each nucleus. Usually, only a few lowest levels are taken into account (see, e.g., [32]).

The obtained results have been analyzed both in terms of the $SU(3) - O(6) - \overline{SU(3)}$ first order phase transition control variable χ, and employing the catastrophe theory essential control parameters (r_1, r_2), introduced in [20]. The behaviour of the statistical and dynamical quantum chaos criteria, calculated for each nucleus in the frameworks of algebraic complete IBM-1 version, has been studied both in dependence from the phase transition control parameters, and in dependence from nuclear spin I. A possibility to compare the results of algebraic IBM model with the ones obtained using geometrical rigid triaxial rotator approach has been considered.

Chapter 2

The studies of QPT and quantum chaos in the case of simplified IBM-1 versions

We have started our studies of nuclear shape quantum phase transitions and quantum chaos with the most simple algebraic model - the two-parametric Casten's version of IBM-1. The results of these studies have been published in two papers [R1,R2] and reported at the international conference in 2005 [A1].

These studies were continued by considering more complex partial versions of IBM-1, which are obtained when one attaches to the $O(6)$-limit Hamiltonian three-boson interaction terms. Such modification allows one to describe stable triaxial shapes in the frameworks of IBM-1. Phase transitions in the case of $O(6)$-limit Hamiltonians with attached cubic quadrupole moment operator, enabling one to describe rigid rotator $SU(3)$ states attached to the γ-soft core, have been considered as well. The results of our studies of classical energy minima conditions in the case of simple IBM-1 versions with three-boson interactions have been published in our paper [R3] and reported at the international [A3] and local [A2] scientific conferences in 2006.

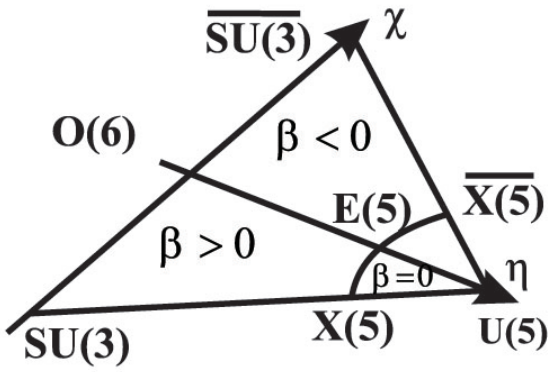

Figure 2.1: IBM-1 critical lines and points in the extended Casten's triangle.

2.1 Conditions for the classical energy minima in the case of the simplified Casten's version of IBM-1

In the frameworks of Casten's version, Hamiltonian of the standard IBM-1 is written in a following simplified form (see, e.g., [36, 38]):

$$H(N_b, \eta, \chi) = \eta \cdot \mathbf{n}_d + \frac{\eta - 1}{N_b} \mathbf{Q}(\chi) \cdot \mathbf{Q}(\chi), \tag{2.1}$$

depending from the total boson number N_b and two model parameters η and χ. In (2.1), $\mathbf{n}_d$ is the number operator of d-bosons; and the quadrupole operator $\mathbf{Q}(\chi)$ is defined as Eq. (1.16). This simplified version retains all dynamical symmetries of complete IBM-1 Hamiltonian [38]. Eq. (2.1) one can obtain from the multipole representation Hamiltonian Eq. (1.15) by letting $\varepsilon' = \omega = \xi = 0$. Parameters η and χ can assume values $0 \leq \eta \leq +1$, and $-\sqrt{7}/2 \leq \chi \leq +\sqrt{7}/2$, varying within the space of extended Casten's triangle (see Fig. 2.1). This triangle is formed by lines linking the vertex $\chi = 0$, $\eta = +1$, corresponding to spherical $U(5)$ dynamical symmetry limit of IBM-1, with the $\chi = -\sqrt{7}/2$, $\eta = 0$ and $\chi = +\sqrt{7}/2$, $\eta = 0$ vertexes, corresponding to deformed $SU(3)$- and $\overline{SU(3)}$-symmetric prolate and oblate shapes, respectively. The $\chi = \eta = 0$ point corresponds to the $O(6)$ dynamical symmetry of γ-soft (unstable) shape.

Geometric interpretation of the algebraic Hamiltonian Eq.(2.1) one can derive, e.g., employing the formalism of s- and d-boson condensate states (see [26]), depending from N_b, and the analogues of BM nuclear quadrupole deformation parameters β and γ. The classical energy functional $E_{cl}(N_b, \eta, \chi; \beta)$ of Hamiltonian Eq.(2.1) has the form [44, 22]:

$$E_{cl}(N_b, \eta, \chi; \beta) = \frac{1}{(1+\beta^2)^2}\left\{N_b \cdot \eta - A_0\left(\left[\frac{2N_b+5}{7}\right]\cdot\chi^2 - 4\right)\right\}\beta^4 +$$

$$\left\{4\sqrt{\frac{2}{7}}\cdot N_b \cdot A_0 \cdot \chi\right\}\beta^3 + \left\{N_b\cdot\eta - A_0\left([4N-8]+\chi^2\right)\right\}\beta^2 - 5A_0, \quad (2.2)$$

with $A_0 = (1-\eta)$. In Eq. (2.2), the asymmetry parameter γ has been excluded by means of substitution $\gamma_0 \to 0$, since the minima of IBM-1 classical energy expression (with $\beta = \beta_0$ and $\gamma = \gamma_0$) are attained at $\gamma = 0$ (when $\chi < 0$) and $\gamma = 60^\circ$ (when $\chi > 0$). It means also that one can replace β_0 with $-\beta_0$, assuming $\beta_0 > 0$ in the case of prolate ($\chi < 0$), and $\beta_0 < 0$ in the case of oblate ($\chi > 0$) shape.

The condition on the second order derivative of Eq.(2.2) (see, e.g., [62]):

$$\frac{d^2 E_{cl}(N_b, \eta, \chi; \beta)}{d\beta^2}\Big|_{\beta=0} = 0, \quad (2.3)$$

gives equation for the critical points separating spherical $\beta = 0$ and deformed $\beta \neq 0$ shapes:

$$2(N_b\eta - A_0(4N_b^2 + \chi^2 - 8)) = 0. \quad (2.4)$$

The solution of Eq. (2.4) with respect to parameter η:

$$\eta = (4N_b + \chi^2 - 8)/(5N_b + \chi^2 - 8), \quad (2.5)$$

defines the first order phase transition line $X(5) - E(5) - \overline{X(5)}$.

The solution of the equation system consisting from Eq. (2.5) and equation

$$\chi = \pm(\sqrt{7}/2)(\eta - 1) \quad (2.6)$$

allows one to obtain values $\eta_{X(5)}$, $\chi_{X(5)}$, describing the location of the critical point on the $U(5) - SU(3)$ line, characterized by the $X(5)$ dynamical symmetry [49] (analogously for the $\overline{X(5)}$ point, see Fig. 2.1).

The solution of Eq. (2.5) at $\chi = 0$ gives the position of an isolated triple point $\eta_{E(5)} = (4N_b - 8)/(5N_b - 8)$ where critical lines of the second order

phase transition between spherical and deformed shapes meets with first order phase transition line separating prolate ($\beta > 0$) and oblate ($\beta < 0$) deformations. This critical point is characterized by the $E(5)$ symmetry [48]. Therefore, the first order prolate-oblate phase transition line can be denoted as $E(5) - O(6)$.

Usually one applies for the study of nuclear shape phase transitions the approach proposed by Landau, as it has been done, e.g., in [19, 22]. One uses the expansion $(1+\beta^2)^{-2} = 1 - 2\beta^2 + 3\beta^4 - 4\beta^6 + \cdots$ and rewrites Eq.(2.2) in the form

$$E_{cl}(N_b, \eta, \chi; \beta) = E_0(\eta) + A_L(N_b, \eta, \chi)\beta^2 + B_L(N_b, \eta, \chi)\beta^3 + C_L(N_b, \eta, \chi)\beta^4 + \cdots . \tag{2.7}$$

However, it is possible to obtain a precise analytical solution for the energy minimum of Eq.(2.2), which follows from the extreme condition

$$\frac{\partial E_{cl}(N_b, \eta, \chi; \beta)}{\partial \beta} = 0 \tag{2.8}$$

yielding an equation (see [R1,R2])

$$\frac{2\left\{A\beta^4 + B\beta^3 + C\beta^2 + D\beta\right\}\beta}{7(1+\beta^2)^3} = 0 \tag{2.9}$$

with following coefficients:

$$\begin{aligned} A &= \eta\sqrt{14}N_b A_0 \chi, \\ B &= 3A_0\chi^2 - N_b(28 - 21\eta - 4A_0\chi^2), \\ C &= -6\sqrt{14}N_b A_0 \chi, \\ D &= -56A_0 - 7N_b(5\eta - 4) + 7A_0\chi^2. \end{aligned} \tag{2.10}$$

If one excludes a trivial solution by conditions $(1+\beta^2)^3 \neq 0$, and $\beta \neq 0$, one can reduce Eq. (2.9) to a cubic equation

$$A\beta^3 + B\beta^2 + C\beta + D = 0, \tag{2.11}$$

with coefficients A, B, C, D given by Eqs.(2.10).

Solutions of the cubic equation (2.11) give values of deformation parameter β at the minima of classical energy functional Eq.(2.2) as three roots β_{0i} $(i = 1, 2, 3)$, which are complicated and, in general, complex functions from the total boson number N_b and IBM-1 model parameters η, χ. So, we shall not give here the obtained explicit expressions.

2.2 Analysis of the classical energy surface of the Casten's IBM-1 version employing the precise solution of the minima equation

We have performed the detailed analysis (see [R1,R2]) of the behaviour of cubic equation Eq. (2.11) roots β_{0i} $(i = 1, 2, 3)$ in the space of parameters (η, χ) covering the entire extended Casten's triangle. A special attention has been given to the regions in the vicinity of first and second order phase transition lines. Similar analysis has been carried out also for corresponding classical energy minimum values $E_0^i = E_0^i(N_b, \chi, \eta; \beta_{0i})$, obtained by inserting deformation parameter values β_{0i} into Eq.(2.2).

Main features of roots β_{0i} $(i = 1, 2, 3)$ one can analyze considering the values of the discriminant of Eq. (2.11):

$$D_3 = \frac{B^2C^2 - 4B^3D + 18ABCD - A(4C^3 + 27AD^2)}{A^4}. \tag{2.12}$$

When $D_3 < 0$, we have one real root and two complex conjugated roots. At $D_3 > 0$ one has three real, unequal roots, while, at $D_3 = 0$, there are two real, equal roots, i.e. one observes a degeneracy. The values of these roots have opposite signs and mirror symmetric absolute values with respect to $U(5) - O(6)$ line at $\chi = 0$, separating the left and the right side of the extended Casten's triangle (see Fig. 2.2). While performing the numerical analysis, it has been found that the results have weak dependence from the total boson number N_b. Therefore, all results are presented at fixed value $N_b = 8$.

On Fig. 2.2, one can discern clearly the $O(6) - E(5)$ first order phase transition line, separating the left and right sides of extended Casten triangle (with $\beta_0 > 0$ and $\beta_0 < 0$), as well as the triple point $E(5)$. The roots $\beta_{01,03}$ are real below the $X(5) - E(5) - \overline{X(5)}$ arc line, while the root β_{02} is real in the entire space of Casten' triangle.

In the bottom, "deformed shape" part of Casten's triangle, below the $X(5) - E(5) - \overline{X(5)}$ arc line (when $0 \leq \eta \leq \eta(E(5))$), we have the $D_3 > 0$ case with three real, unequal roots. However, one of these roots (β_{02}) assumes nonphysically large values. In the top, "spherical shape" part of Casten's triangle, above the arc line $X(5) - E(5) - \overline{X(5)}$ (when $\eta(E(5)) < \eta < 1$), we

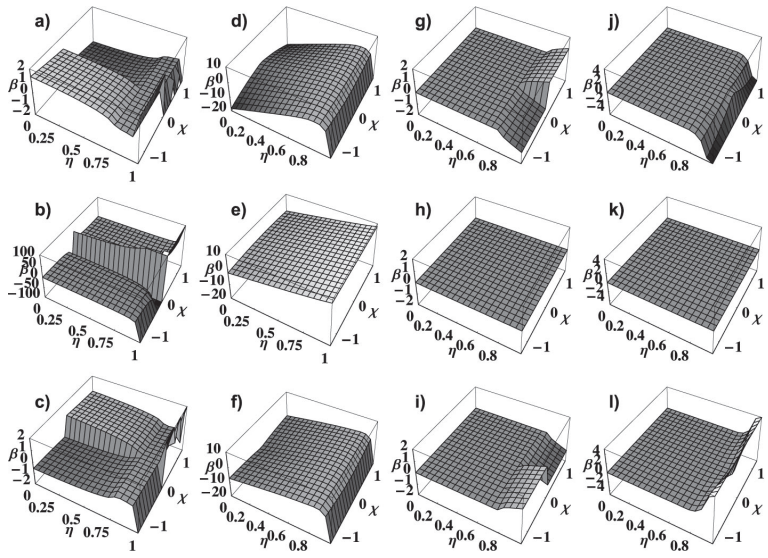

Figure 2.2: Real (a-c) (and imaginary (g-i)) parts of β_{0i} $(i = 1, 2, 3)$ and corresponding minimal energy values $E_{0i}(N_b, \eta, \chi; \beta_{0i})$ (d-f; and j-l).

have the $D_3 < 0$ case with one real root (β_{02}) assuming nonphysically large values and two complex conjugate roots (β_{01}, β_{03}), just as one can expect in the spherical shape region.

Now, let us consider the $\chi = 0$ case, corresponding to the $U(5) - O(6)$ line separating the left and right sides of extended Casten's triangle. From Eq. (2.10), it follows that in this case $A = C = 0$, and, instead of the cubic equation (2.11), one obtains a square equation:

$$B'\beta^2 + D' = 0, \tag{2.13}$$

with $B' = 7N_b(4 - 3\eta)$ and $D' = 56(1 - \eta) + 7N_b(5\eta - 4)$. Eq. (2.13) has two roots

$$\beta^s_{01,02} = \mp\sqrt{-\frac{D'}{B'}} = \mp\sqrt{\frac{8(\eta - 1) - N_b(5\eta - 4)}{N_b(4 - 3\eta)}}\ . \tag{2.14}$$

The values of roots $\beta^s_{01,02}$ on the $O(6) - E(5)$ line $(0 \leq \eta \leq \eta(E(5)))$ are real (see Fig. 2.3) and have opposite signs in the left and the right sides of the extended Casten's triangle, decreasing from the maximal value at the $O(6)$ critical point $(\eta = 0)$ to the value $\beta^s_{01,02} = 0$ at the triple point of $E(5)$

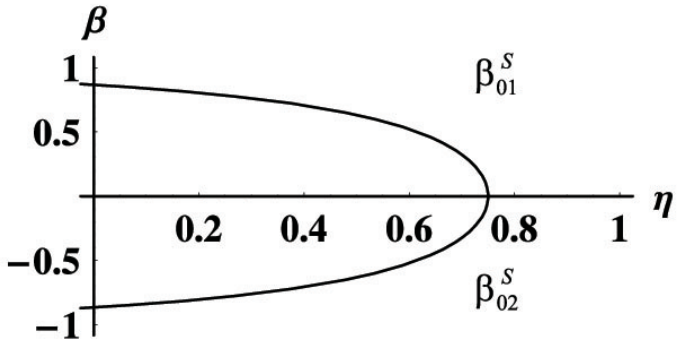

Figure 2.3: Dependence of Eq. (2.13) roots $\beta^s_{01,02}$ from the values of parameter η at $\chi = 0$ and $N_b = 8$ ($\eta(E(5)) = 0.75$).

dynamical symmetry. It demonstrates the $O(6) - E(5)$ line as the first order phase transition line between oblate ($\beta < 0$) and prolate ($\beta > 0$) nuclear shapes. In the $E(5)-U(5)$ region of the $\chi = 0$ line (when $\eta(E(5)) \leq \eta \leq +1$), $\beta^s_{01,02}$ assumes purely imaginary values increasing from zero up to $\beta^s_{01,02} = \pm i$.

The most interesting behaviour is observed along the $X(5) - E(5) - \overline{X(5)}$ arc line, defined by condition Eq. (2.5) and corresponding to the second order phase transition line between spherical ($\beta = 0$) and deformed ($\beta \neq 0$) nuclear shapes. Inserting Eq. (2.5) into expressions Eq. (2.10), one can reduce the solving of cubic equation Eq. (2.11) on this line to the trivial solution $\beta_0 = 0$ and to the solutions of the square equation:

$$B''\beta^2 + C''\beta + D'' = 0 \tag{2.15}$$

with coefficients $B'' = \sqrt{14}N_b\chi$, $C'' = 2(N_b-1)(\chi^2-14)$ and $D'' = -3\sqrt{14}N_b\chi$. Equation (2.15) has two roots:

$$\begin{aligned} \beta^{arc}_{01,02} &= \frac{1}{\sqrt{14}N_b\chi}\Bigg[(N_b-1)(\chi^2+14) \\ &\mp \frac{1}{2}\sqrt{168N_b^2\chi^2 + 4(N_b-1)^2(\chi^2-14)^2}\Bigg]. \end{aligned} \tag{2.16}$$

From Eq.(2.15), it follows that $\beta_0 = 0$ at the triple point $E(5)$, when $\chi = 0$ (see Fig. 2.4).

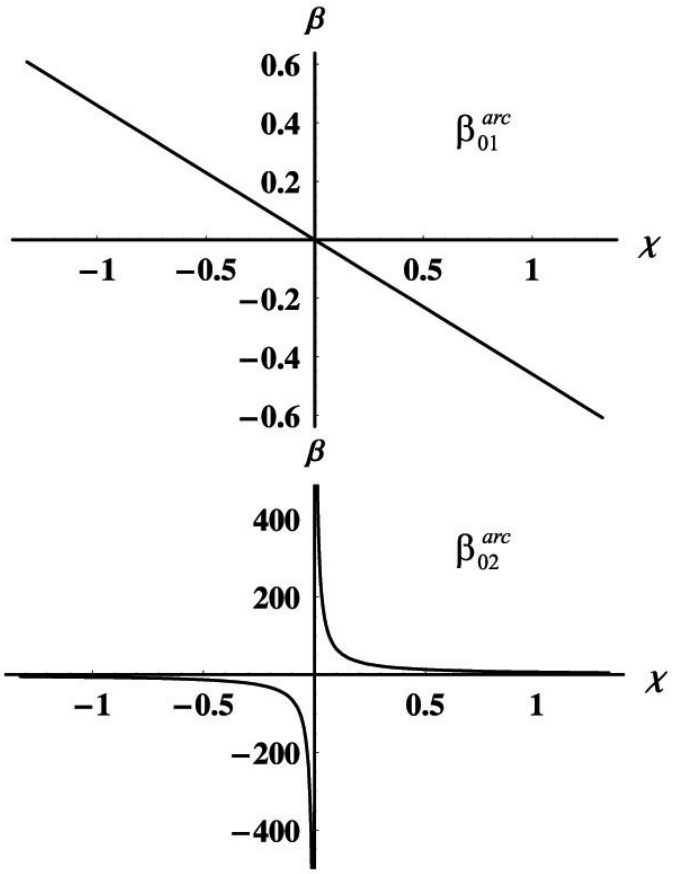

Figure 2.4: Dependence of Eq. (2.15) roots $\beta_{01,02}^{arc}$ from the values of parameter χ on the $X(5) - E(5) - \overline{X(5)}$ arc line at $N_b = 8$.

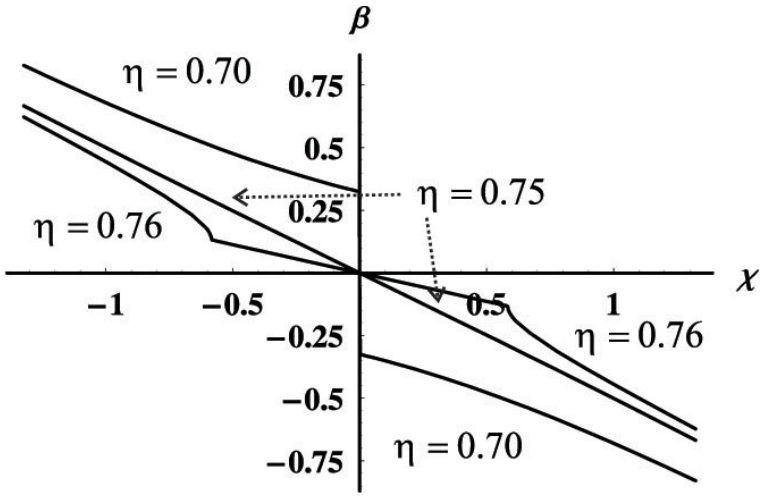

Figure 2.5: Values of β_{01} root of Eq. (2.11) in the vicinity of the triple point $E(5)$ at $N_b = 8$.

Comparison of roots $\beta^s_{01,02}$, and $\beta^{arc}_{01,02}$ of square equations (2.13), and (2.15) with three roots β_{0i} $(i = 1, 2, 3)$ of the original cubic equation (2.11) allows to establish following correspondences:

1) for the $O(6) - E(5)$ first order phase transition line (when $\chi = 0$ and $0 \leq \eta \leq \eta(E(5))$ – between roots $\beta^s_{01,02}$ of Eq.(2.13), and $\beta_{01,03}$ of Eq.(2.11), while the root $\beta_{02} \to \mp\infty$;

2) for the $X(5) - E(5) - \overline{X(5)}$ second order phase transition line – between root β^{arc}_{01} of Eq.(2.15) and roots $\beta_{01,03}$ of Eq.(2.11), as well as between root β^{arc}_{02} of Eq.(2.15) and root β_{02}.

The final choice between obtained values of deformation parameter β_0 one can make by considering the values of the classical energy functional $E_{cl}(N_b, \eta, \chi; \beta)$. If one inserts obtained root values β_{0i} $(i = 1, 2, 3)$ into Eq. (2.2), one obtains corresponding energy minimum surfaces (see Fig. 2.2). One can see that the first root β_{01} of Eq.(2.11) is preferable, since it gives deeper energy minimum values. The dependence of β_{01} from model parameters η, χ in the vicinity of the triple point $E(5)$ is shown on Fig. 2.5.

The results of our approach to the minimum problem of the classical energy functional of the simplified Casten version of IBM-1 allow one to obtain precise values of deformation parameter β at each (η, χ) point of Casten's triangle. These values are well suited for the analysis of phase transition

lines and critical points as well as for other studies involving the considered model. In general, the qualitative conclusions drawn in our analysis of phase transition critical lines and points in the frameworks of the simplified Casten's version of IBM-1 are similar to those obtained employing the Landau theory approach [44, 22]. However, the results of the analytical solution of the classical energy minimum problem allow to obtain more precise numerical values of β_0 and $E_{cl}(N_b, \eta, \chi; \beta_0)$.

2.3 Analysis of statistical and dynamical criteria of quantum chaos

Let us consider the results of the evaluation of statistical and dynamical quantum chaos criteria in the frameworks of simplified Casten's version of IBM-1. A special attention has been given to the behaviour of these criteria in the vicinity of shape phase transition critical lines and points. Quantum chaos criteria calculations have been performed at boson number $N_b = 8$ that has been used also for our analysis of shape phase transitions (see Sect. 2.2). This number belongs to the boson number range employed for nuclear structure calculations in the transitional deformation region at $A \sim$190. In the most of other theoretical studies devoted to statistical quantum chaos criteria in the frameworks of Casten's IBM-1 version (see, e.g., [36, 43], values $N_b \geq 20$ are used, which correspond to the middle of deformation region.

Values of statistical and dynamical quantum chaos criteria have been calculated in selected points within the (η, χ) parameter space represented by Casten's triangle (see Fig. 2.1). The number assigned to each point is given in column 1 of Table 2.1. Values of model parameters have been chosen in the range from below the $X(5) - E(5) - \overline{X(5)}$ second order phase transition line Eq. (2.5) separating spherical and deformed shapes to the $SU(3) - O(6) - \overline{SU(3)}$ line (at $\eta = 0$) corresponding to the maximal deformation. Calculations have been performed only for the prolate deformation part ($\chi < 0$) of the extended Casten's triangle, since the solutions of IBM-1 Hamiltonian are mirror symmetric with respect to parameter χ values.

The results of quantum chaos statistical criterion calculations show that the simplified Casten's version of IBM-1 at $N_b = 8$ is quite regular. The deviation of nearest level spacings distributions $P(S)$ (where $S = E_i - E_{i-1}$ have been normalized to their mean value $< S >$) from the Poisson form

Table 2.1: Results of quantum chaos criteria calculations in selected points of the Casten's triangle at $N_b = 8$.

Point	χ		η		ζ^a	$\kappa_{av}(\Phi_k)^b$	$W_{av}(\Psi_i)^b$	W_{av}/W^c_{max}
1	χ^d_{max}	-0.5788	$0.75 \cdot \eta^d_{E(5)}$	0.5625	0.157	5.367	1.423	0.618
2	$0.75 \cdot \chi_{max}$	-0.4341	-"-	-"-	-	5.501	1.436	0.624
3	$0.5 \cdot \chi_{max}$	-0.2894	-"-	-"-	0.182	3.028	1.266	0.550
4	$0.25 \cdot \chi_{max}$	-0.1447	-"-	-"-	-	2.765	0.932	0.405
5	$\chi = 0$	0	-"-	-"-	0.170	2.610	-	-
6	χ_{max}	-0.8268	$0.5 \cdot \eta_{E(5)}$	0.3750	0.127	6.516	1.550	0.673
7	$0.75 \cdot \chi_{max}$	-0.6201	-"-	-"-	-	6.137	1.557	0.676
8	$0.5 \cdot \chi_{max}$	-0.4134	-"-	-"-	0.094	7.639	1.562	0.678
9	$0.25 \cdot \chi_{max}$	-0.2067	-"-	-"-	-	4.525	1.276	0.554
10	$\chi = 0$	0	-"-	-"-	0.092	2.750	-	-
11	χ_{max}	-1.0748	$0.25 \cdot \eta_{E(5)}$	0.1875	0.105	7.898	1.786	0.776
12	$0.75 \cdot \chi_{max}$	-0.8061	-"-	-"-	-	6.343	1.712	0.744
13	$0.5 \cdot \chi_{max}$	-0.5374	-"-	-"-	0.124	7.206	1.482	
14	$0.25 \cdot \chi_{max}$	-0.2687	-"-	-"-	-	7.289	1.518	0.644
15	$\chi = 0$	0	-"-	-"-	0.093	1.396	-	-
16	$\chi(SU(3)) = -\sqrt{7}/2$	-1.3229	$\eta = 0$	0	0.061	7.903	1.878	0.816
17	$0.75 \cdot \chi(SU(3))$	-0.9922	-"-	-"-	-	8.806	1.759	0.764
18	$0.5 \cdot \chi(SU(3))$	-0.6614	-"-	-"-	0.115	7.193	1.756	0.763
19	$0.25 \cdot \chi(SU(3))$	-0.3307	-"-	-"-	-	7.649	1.654	0.718
20	$\chi(O(6)) = 0$	0	-"-	-"-	0.012	3.060	-	-

[a] - Brody coefficient value is fitted to $P(S)$ distribution of all n_{lev}=105 theoretical states with L from 0 to $L_{max} = 16$;

[b] - averaged values of dynamical quantum chaos criteria for $L = 0$ states ($n = 10$);

[c] - $W_{max}(\Psi_i) = \ln(10) = 2.302585$;

[d] - χ_{max} value is calculated on the $U(5) - SU(3)$ line as $\chi = -(\sqrt{7}/2)(\eta - 1)$;
$\eta_{E(5)}$ – according to expression $\eta_{E(5)} = (4N_b - 8)/(5N_b - 8)$.

Eq. (1.22), determined by the fit of Brody formula Eq. (1.24) to the spacing distributions of all $n_{lev} = 104$ states of unfolded theoretical spectrum ($L = 0$ to $L_{max} = 16$), is very slight even in the case of maximal mixing farther away from the vertexes of Casten's triangle (see Table 2.1). When boson number N_b increases, the relative role of mixing is reduced because of the increased number of boson states: $P(S)$ distribution form becomes more Poissonian (see Fig. 2.6). However, one should take into account that, at such relatively low boson numbers, $P(S)$ distribution is strongly influenced by the model basis cut-off which affects the energies of higher spin states.

Now, let us discuss the calculation of dynamical quantum chaos criteria: the wave function entropy $W(\Psi_i)$ and the fragmentation of basis states $\kappa(\Phi_k)$. Table 2.1 lists the averaged values of both criteria obtained for the $L = 0$ states at $N_b = 8$ in selected points of the Casten's triangle. The number of basis states for the diagonalization of IBM-1 model Hamiltonian in such a case is $n = 10$.

Regions near the $U(5)$ vertex ($\chi = 0, \eta = +1$) are characterized by relatively pure $U(5)$ basis state functions Φ_k entering in the mixed state wave functions Ψ_i. Therefore, a correct evaluation of quantum chaos criteria for (χ, η) points of this region is impossible: in the case of basis state fragmentation width $\kappa(\Phi_k)$, it is due to the violation of condition Eq.(1.28), while in the case of wave function entropy $W(\Psi_i)$, because some mixing amplitude values $c_{ik} = 0$ in Eq.(1.25). The area where one can regularly evaluate both $\kappa(\Phi_k)$ and $W(\Psi_i)$ values lies approximately from the bottom $SU(3) - O(6) - \overline{SU(3)}$ line of the extended Casten's triangle up to about the middle part ($0 < \eta \leq 0.75 \cdot \eta_{E(5)}$), but ending below the second order phase transition line $X(5) - E(5) - \overline{X(5)}$. In the case of $N_b = 8$, the triple point $E(5)$ has coordinates $\eta_{E(5)} = 0.75$ and $\chi = 0$. The behaviour of dynamical quantum chaos criteria along this phase transition line in shown on Fig. 2.7.

The need for separate consideration of quantum chaos criteria on the phase transition line is due to the scaling factor $(\eta - 1)/N_b$ at the second term of Eq.(2.1), which determines the strength of basis state mixing in the case of Casten's version of IBM-1. Since this scaling factor increases when the value of parameter η decreases moving away from the $U(5)$ vertex towards the bottom line $SU(3) - O(6) - \overline{SU(3)}$, the growth of $\kappa(\Phi_k)_{av}$ and $W(\Psi_i)_{av}$ values reflects the increasing degree of mixing of $U(5)$ basis states in this direction of the Casten's triangle. From the results presented in Table 2.1, one can see that, on the $U(5) - SU(3)$ line and in the area near it (with

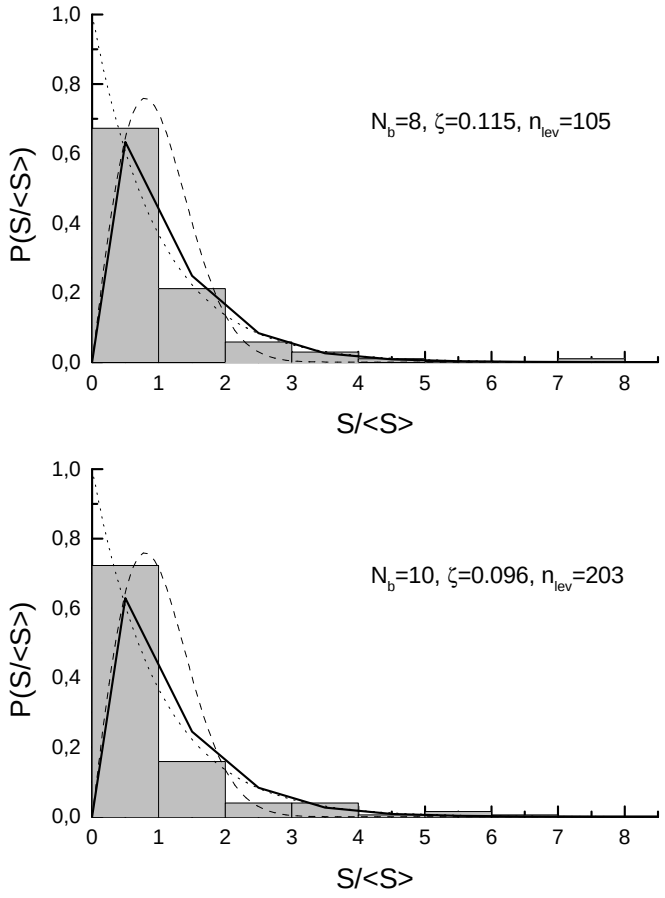

Figure 2.6: The nearest level energy spacing distributions $P(S/ < S >)$ at N_b=8 and 10 in the middle of $SU(3) - O(6)$ line of the Casten's triangle. Solid line represents the fitted Brody distribution curve, while dotted line corresponds to Poisson distribution and dashed line to Wigner distribution.

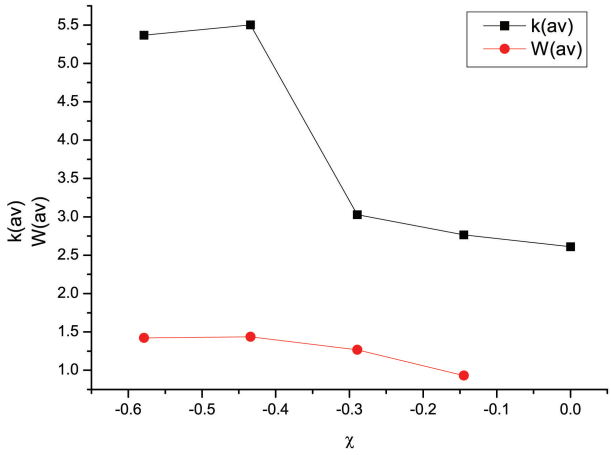

Figure 2.7: Behaviour of averaged dynamical quantum chaos criteria $\kappa(\Phi_k)_{av}$ and $W(\Psi_i)_{av}$ along the $X(5)-E(5)-\overline{X(5)}$ phase transition line at $N_b = 8$.

$\chi = 0.75 \cdot \chi_{max}$), the behaviour of $\kappa(\Phi_k)_{av}$ and $W(\Psi_i)_{av}$ values is correlated: increasing from the middle part (with $0.75 \cdot \eta_{E(5)} = 0.5625$) to the bottom line ($\eta = 0$). The correlation between $\kappa(\Phi_k)_{av}$ and $W(\Psi_i)_{av}$ values with respect to parameter χ value, when it changes in the direction from the $X(5)-SU(3)$ line towards the first order phase transition line $E(5)-O(6)$, is lost when mixing increases (see Table 2.1).

2.4 Analysis of shape phase transitions in the frameworks of simple IBM-1 versions including three-boson interactions

It has been shown already in [7] that, in order to obtain stable triaxial shape in the frameworks of IBM-1, one should include into the model Hamiltonian three-boson interaction terms. This idea has been further developed in [28, 29] where a cubic d-boson interaction operator H_{3d} has been attached to the

$O(6)$-limit Hamiltonian of IBM-1. This operator has the form

$$H_{3d} = \sum_{L'} \theta_{L'} \left[\mathbf{d}^{+}\mathbf{d}^{+}\mathbf{d}^{+}\right]^{(L')} \cdot \left[\tilde{\mathbf{d}}\tilde{\mathbf{d}}\tilde{\mathbf{d}}\right]^{(L')}, \tag{2.17}$$

where L' assumes values $L' = 0, 2, 3, 4, 6$, and $\theta_{L'}$ denotes interaction parameters for terms with different L' values. The $O(6)$-limit Hamiltonian in multipole form one can obtain from Eqs. (1.15), (1.16) letting $\varepsilon' = \chi = \xi = 0$.

The classical energy expression of the $O(6)$-limit IBM-1 Hamiltonian with attached cubic d-boson interaction operator (2.17) can be written as [28]:

$$E_{3d}(O(6)) = c_1 \frac{N_b\beta^2}{1+\beta^2} + c_2 N_b(N_b-1)\left[\frac{1-\beta^2}{1+\beta^2}\right]^2$$
$$+ \sum_{L'} \theta_{L'} N_b(N_b-1)(N_b-2)\frac{\beta^6}{(1+\beta^2)^3}\left(A_{L'} + B_{L'}\cos^2(3\gamma)\right), \tag{2.18}$$

where c_1 and c_2 are related with the parameters of the IBM-1 $O(6)$-limit Hamiltonian; and $A_{L'}$ and $B_{L'}$ are numerical constants (see Table 2.2).

Table 2.2: Values of coefficients $A_{L'}$, $B_{L'}$ for the terms of cubic d-boson interaction operator

L'	0	2	3	4	6
$A_{L'}$	0	1/5	-1/7	3/49	14/55
$B_{L'}$	2/35	0	1/7	3/35	-8/385

In order to study problems related with the description of stable triaxial shapes, we have analyzed minima of the classical energy expression Eq.(2.18) with respect to quadrupole deformation parameters β and γ employing conditions

$$\frac{\partial E_{3d}(O(6))}{\partial\beta} = \frac{\partial E_{3d}(O(6))}{\partial\gamma} = 0. \tag{2.19}$$

These conditions have been applied both in the case if one attaches the entire sum of L' terms in Eq.(2.17), as well as in the case if one attaches each $L' = 0, 2, 3, 4, 6$ term separately. In order to facilitate a comparison with the earlier results, we have used in Eq.(2.18) the c_1, c_2, and cubic d-boson interaction parameter θ_3 values of Ref.[29] (see comments of Table 2.3). Also, following the recommendation given in [50], we have adopted the same value

$\theta \equiv \theta_{L'} = \theta_3$ for all separate L' terms in Eq.(2.17) reducing the number of model parameters and simplifying calculations.

Non-zero equilibrium deformation minima of the classical energy expression (2.18) without cubic d-boson operator one can obtain at

$$\beta_0 = \sqrt{\frac{4c_2(N_b-1)-c_1}{4c_2(N_b-1)+c_1}}, \tag{2.20}$$

when a condition $c_1 < 4(N_b-1)c_2$ is fulfilled (see [28]). In the case of our adopted c_1, c_2 values, this condition determines a boson number limit $N_b^{min} = 5$: the energy minimum with $\beta_0 \neq 0$ can exist only when $N_b \geq N_b^{min}$. This N_b^{min} value has been taken as the initial boson number for our study of classical energy Eq. (2.18) minima in dependence on N_b, and on the choice of L' terms in Eq.(2.17). The condition (2.19) for the asymmetry parameter γ in all cases gives the classical energy minimum at $\gamma_0 = 30^\circ$, independently from β and N_b values. The results of our calculations are presented in Table 2.3 and on Fig. 2.8.

Analysis of the obtained results allows to make following conclusions:

1) the cubic d-boson interaction term with $L' = 0$ gives no contribution to the classical energy minimum value $E_{min} = E_{3d}(O(6), \beta_0, \gamma_0 = 30^\circ)$ because $A_0 = 0$ (see Table 2.2), and $B_0 \cos^2(3\gamma) = 0$ at $\gamma_0 = 30^\circ$. It means that the total classical energy minimum in this case coincides with that of the $O(6)$-limit of IBM-1 (see panel (a) in Fig. 2.8);

2) in the case of $L' = 2$ term, the coefficient $B_2 = 0$ (see Table 2.2), and, therefore, the classical energy contribution from the cubic d-boson interaction does not depend from the asymmetry parameter γ. Therefore, this term of operator (2.17), if considered alone, cannot be a cause of triaxial shape;

3) the remaining three separate cubic d-boson interaction terms with $L' = 3, 4, 6$ give energy minimum values for Eq. (2.18) at $\beta_0 \neq 0$ and $\gamma_0 = 30^\circ$ (see Table 2.3, and panels (b) and (c) in Fig 2.8). The same is true also for the case when one includes the sum of all operator (2.17) terms with $L' = 0, 2, 3, 4, 6$ (see the last two columns in Table 2.3 and panel (d) in Fig. 2.8).

The analysis of the equilibrium deformation β_0 values in dependence from the total boson number N_b, performed in the case of attached separate $L' = 0, 3, 4, 6$ terms, and in the case of attached sum of all terms in Eq.(2.17), disclosed following features:

Table 2.3: Equilibrium deformation values β_0 and corresponding classical energy minimum values $E_{min} = E_{3d}(O(6), \beta_0, \gamma_0 = 30°)$ (in MeV) of the $O(6)$-limit Hamiltonian with cubic d-boson interaction in dependence from the total boson number N_b for separate L' interaction terms of Eq. (2.17).

	$L'=0$		$L'=3$		$L'=4$		$L'=6$		$\sum_{L'=0,2,3,4,6}$	
N_b	β_0	E_{min}	β_0	E_{min}	β_0	E_{min}	β_0	E_{min}	β_0	E_{min}
5	0.310	0.485	0.316	0.484	0.307	0.485	0.300	0.485	0.297	0.486
8	0.599	1.009	0.766	0.926	0.569	1.029	0.509	1.073	0.486	1.091
20	0.839	3.013	-	-	0.678	4.165	0.528	5.543	0.487	5.955
50	0.935	7.972	-	-	0.610	25.917	0.445	38.286	0.407	41.277
100	0.967	16.225	-	-	0.532	122.824	0.380	172.276	0.346	182.030
150	0.978	24.476	-	-	0.486	307.522	0.345	412.367	0.314	434.110

Comment: The following parameter values have been used: $c_1 = 0.33$ MeV and $c_2 = 0.025$ MeV; the cubic d-boson interaction parameter $\theta = \theta_3 = 0.06$ MeV has been adopted for all L' terms.

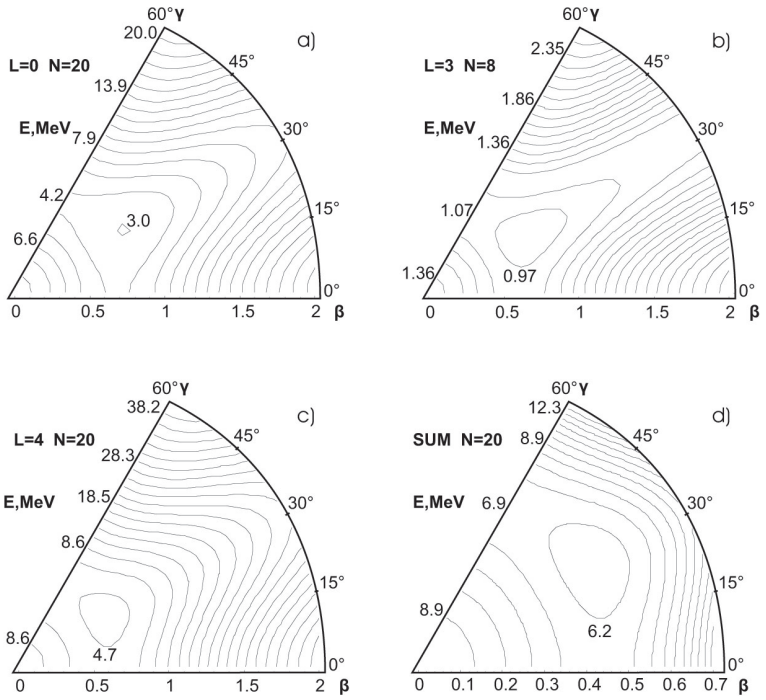

Figure 2.8: Classical energy surface of the IBM-1 $O(6)$-limit Hamiltonian with cubic d-boson interaction Eq. (2.17: a) with only $L' = 0$ term, at $N_b = 20$; b) with only $L' = 3$ term, at $N_b = 8$; c) with only $L' = 4$ term, at $N_b = 20$; d) with the sum of all $L' = 0, 2, 3, 4, 6$ terms, at $N_b = 20$.

1) in the case of $L' = 0$ term, β_0 values are increasing with growing N_b values: at $N_b \to \infty$, the total classical energy minimum is attained at $\beta_0 = 1$, i.e., one obtains the same result as in the case of pure γ-independent $O(6)$ limit of IBM-1 (see p.108 in [7]);

2) in the case of $L' = 3$ term, the value $N_b = 8$, considered in [29], turns out to be the maximal boson number, at which the energy minimum satisfying the conditions Eq.(2.19) is possible at used parameter values c_1, c_2, θ. There is no energy minimum for boson numbers $N_b > 8$.

3) in the case of $L' = 4, 6$ terms, and in the case of sum of all terms, β_0 values are increasing until some maximal β_0^{max} value (at $N_b^{max} = 18, 12, 11$, correspondingly) is reached, then β_0 decreases, i.e., $\beta_0 \to 0$, when $N_b \to \infty$ at $N_b > N_b^{max}$.

An important conclusion following from our calculations of the classical energy minima in the case of $O(6)$-limit Hamiltonian with cubic d-boson interaction is that, in order to study triaxial nuclear shapes, one should take into account not just the $L' = 3$ term of operator (2.17), the role of which has been stressed in the literature until now (see [29, 9]), but the $L' = 4, 6$ terms as well, i.e. one should take into account the entire sum of cubic d-boson operator Eq.(2.17) terms, as it has been pointed out also in [50].

Another significant conclusion is that triaxial equilibrium shape obtained in the case of considered cubic d-boson interaction Eq. (2.17) is the effect due to finite boson number. This conclusion is supported by the fact that if one applies conditions Eq. (2.19) to the reduced classical energy expression, obtained from Eq.(2.18) at $N_b \to \infty$ (see [R3]), one does not obtain minima with $\beta_0 \neq 0$ and $\gamma_0 \neq (0^\circ, 60^\circ)$.

Another approach to the accounting of three-body interactions in the frameworks of IBM-1 has been proposed in [30]. They have considered the $O(6)$-limit Hamiltonian with attached cubic $O(6)$ quadrupole operator interaction term $[\mathbf{QQQ}]^{(0)}$. Such model allows to describe the $SU(3)$-type rigid rotator states based on the $O(6)$-symmetric γ-soft core, and to study, e.g., triaxial nuclei with observed β-vibrational band. In [30], two simple IBM-1 Hamiltonians have been proposed: 1) the H_1, conserving the dynamical $O(6)$-symmetry of the original $O(6)$-limit Hamiltonian, and 2) the H_2, which includes the $[\mathbf{QQQ}]^{(0)}$ term in the form, which is $O(6)$-symmetry non-conserving.

At the $N_b \to \infty$ limit, the classical energy functionals E_{ir} (see [30]) of

both model Hamiltonians H_i $(i = 1, 2)$ can be presented via expression [R3]:

$$E_{ir}(\alpha\delta_{i,1} + \alpha'\delta_{i,2}, \vartheta; \beta, \gamma) = c_{i,1}\frac{\beta^2}{1+\beta^2} + c_{i,2}\frac{(1-\beta^2)^2\delta_{i,1} + \beta^2\delta_{i,2}}{(1+\beta^2)^2}$$

$$-4\vartheta\sqrt{\frac{8}{35}}\frac{\beta^3\cos(3\gamma)}{(1+\beta^2)^3}, \tag{2.21}$$

where $c_{i,1} = 4$ and $c_{i,2} = \alpha/4$, in the case of $i = 1$ model, and $c_{i,1} = 1$ and $c_{i,2} = 4\alpha'$, in the case of $i = 2$. Model parameters α and α' are related with those of the $O(6)$-limit of IBM-1 in the case of $O(6)$-invariant and the case of $O(6)$ non-conserving Hamiltonian, correspondingly; ϑ is a strength parameter of the cubic $[\mathbf{QQQ}]^{(0)}$ interaction.

It has been noted in [29, 28], that stable triaxial nuclear shapes one obtains if the corresponding classical energy expression of a chosen IBM-1 version includes terms proportional to $\cos^2(3\gamma)$. Since the classical energy expression Eq. (2.21) includes only the $\sim \cos(3\gamma)$ dependence, that means that the inclusion of $[\mathbf{QQQ}]^{(0)}$ terms allows one to obtain E_{ir} minima only at $\gamma_0 = 0^\circ$ or 60° asymmetry angles: either prolate ($\beta_0 > 0, \vartheta > 0$) or oblate ($\beta_0 < 0, \vartheta < 0$). These solutions are completely symmetric with respect to ϑ sign. (see [30]).

If one assumes in Eq.(2.21) asymmetry angle $\gamma_0 = 0^\circ$, then applying the energy minima condition Eq.(2.19) one obtains the following quartic equations for the quadrupole deformation parameter β:

$$A_i\beta^4 + B_i\beta^3 + C_i\beta^2 + D_i\beta + E_i = 0, \tag{2.22}$$

where the values of coefficients A_i, B_i, C_i, D_i, E_i for both model versions ($i = 1, 2$) are given in Table 2.4.

Table 2.4: Values of coefficients of the quartic equations (2.22) for the classical energy minima conditions in the case of two $O(6)$-limit Hamiltonians with included cubic $[\mathbf{QQQ}]^{(0)}$ interaction.

i	A_i	B_i	C_i	D_i	E_i
1	$4+\alpha$	$12\sqrt{\frac{2}{35}}\vartheta$	8	$-12\sqrt{\frac{2}{35}}\vartheta$	$4-\alpha$
2	$1-4\alpha'$	$12\sqrt{\frac{2}{35}}\vartheta$	2	$-12\sqrt{\frac{2}{35}}\vartheta$	$1+4\alpha'$

Solution of the equations (2.22) gives four roots β^i_{0j} $(j = 1, 2, 3, 4)$ for each variant $(i = 1, 2)$ of the classical energy expression Eq.(2.21). As it has been

pointed out in our analogous study in the case of extended Casten's triangle of IBM-1 [R1,R2] (see Sect. 2.2), only the real roots $Re(\beta^i_{0j}) \neq 0$ have physical meaning related to energy minima of prolate or oblate deformed nuclei in the (α, ϑ) parameter space; $\beta^i_{0j} = 0$ or complex values correspond to the case of spherical nuclei.

In order to find in the (α, ϑ) plane areas corresponding to real and complex values of β^i_{0j} roots, we have applied a method described in [63]. For this purpose Eq. (2.22) has been rewritten in a reduced form

$$x^4 + qx^2 + rx + s = 0, \tag{2.23}$$

obtained by means of a substitution $\beta = x - B_i/(4A_i)$. If one calculates discriminant D_4 of Eq.(2.23), then one can classify roots x_{0j} $(j = 1, 2, 3, 4)$ according to 13 groups [63] defined by simple relationships for quantities D_4, q, r, s. For instance, the case of only complex roots takes place in following three variants:

$$\begin{aligned}
&\text{a)} \quad D_4 > 0, \quad q \geq 0; \\
&\text{b)} \quad D_4 > 0, \quad q < 0, \quad s > \frac{q^2}{4}, \quad qs = s - \frac{q^2}{4} > 0; \\
&\text{c)} \quad D_4 = 0, \quad q > 0, \quad s = \frac{q^2}{4}, \quad qs = s - \frac{q^2}{4} = 0, \quad r = 0.
\end{aligned} \tag{2.24}$$

Employing this method, we have analyzed features of the roots β^i_{0j}, corresponding to minima of the classical energy functional Eq.(2.21) in the (α, ϑ) plane in the case of the H_1 model, and in the (α', ϑ) plane in the case of H_2 Hamiltonian. Main attention has been given to the determination of areas where Eq.(2.22) has only complex roots. These areas correspond to spherical nuclear shapes, and their boundaries define phase transition from the spherical shape to the deformed ones. The stages of such analysis performed using relationships Eqs.(2.24) are displayed on Fig. 2.9 in the case of both model versions $(i = 1, 2)$.

For both models, two real roots a_{01} and a_{02} of the sixth order equation for the discriminant D_4 of Eq.(2.22) determine the lines separating $D_4 > 0$ and $D_4 < 0$ areas in the (α, ϑ) plane. These lines form the sharp peaked ellipsoid like figure which intersects the ϑ axis at $\vartheta^1_0 = \mp 5.57773$ in the case of first model (when $\alpha = 0$), and at $\vartheta^2_0 = \mp 1.39443$ in the case of second model (when $\alpha' = 0$). Inside these ellipsoid like figures and in the areas between

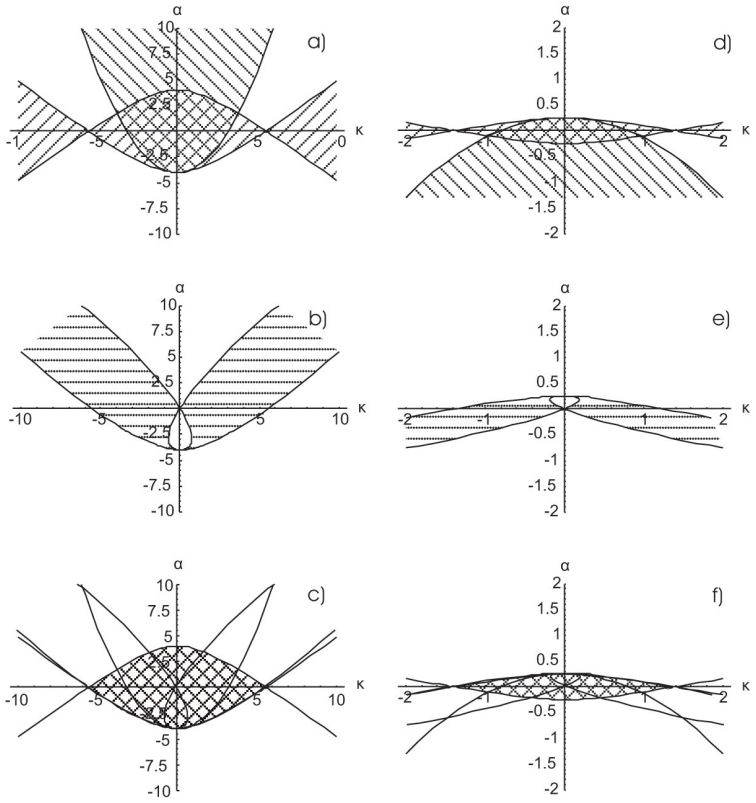

Figure 2.9: The region of only complex roots β_{0j}^{i} of Eq.(2.22) in the case of $O(6)$-symmetric model (a-c), and in the case of $O(6)$-non-conserving model (d-f). Panels (a) and (d) display the areas where the condition Eq. (2.24a) is fulfilled; (b) and (e) - where the condition Eq.(2.24b) is fulfilled; (c) and (f) - where either condition Eq.(2.24a) or (2.24b) is fulfilled.

a_{01}, a_{02} lines, behind the left (right) intersection points (when $|\vartheta| > |\vartheta_0^{1,2}|$), we have the $D_4 > 0$ area while in all remaining areas $D_4 < 0$.

The square equation for the coefficient q before the second order term of Eq.(2.23)

$$q(\alpha, \vartheta^2) = 0 \tag{2.25}$$

determines the parabolic line separating area with $q > 0$ (inside of parabola) from that with $q < 0$ (see panels (a) and (d) in Fig. 2.9). The common area, delimited by the ellipsoid like figure restricted by the $a_{01,02}(\alpha, \vartheta)$ lines and the $q > 0$ region, corresponds to the fulfillment of the first condition (see Eq.(2.24a)) for only complex roots β_{0j}^i.

The area in the (α, ϑ) plane where the second condition Eq.(2.24b) is fulfilled one can find by solving equation

$$qs = s - \frac{q^2}{4} = 0. \tag{2.26}$$

The line formed by the real roots of Eq.(2.26) determines the area (see panels (b) and (e) of Fig. 2.9) inside of which $qs > 0$. Now, if one draws the superposition of this area with the previous one, presented on panels (a) and (d) of Fig. 2.9, one obtains the entire area in the (α, ϑ) plane (see panels (c) and (f) in Fig. 2.9), where one has only complex values of roots β_{0j}^i.

Finally, additional analysis of the fulfillment of the third condition (see Eq.(2.24c)) for the existence of only complex roots β_{0j}^i on the $D_4 = 0$ line has been performed. The analysis has shown that this third condition can be satisfied only for a few isolated points on the $D_4 = 0$ line for both considered models.

Conditions for the prolate-oblate shape phase transitions, related with the sign conversion of parameter ϑ, one can analyze looking for relationships $\beta_{0l}(\alpha, \vartheta) = -\beta_{0m}(\alpha, -\vartheta)$ in the case of both models. Position of the triple point where spherical and prolate-oblate deformed nuclear shapes coexist is determined by the condition (see, e.g., [62]):

$$\left.\frac{d^2 E_{ir}(\alpha\delta_{i,1} + \alpha'\delta_{i,2}, \vartheta; \beta, \gamma = 0)}{d\beta^2}\right|_{\beta=0} = 0. \tag{2.27}$$

The solution of obtained equation gives triple point coordinates at $(\alpha = 4, \vartheta = 0)$ in the case of H_1 model $(i = 1)$ at $(\alpha' = -1/4, \vartheta = 0)$ in the case of H_2 model $(i = 2)$.

Comparison of our results obtained in the case of $O(6)$-symmetric model with cubic $[\mathbf{QQQ}]^{(0)}$ interaction with those of Ref. [30] shows some discrepancies. So, in our approach, the spherical shape region forms a closed ellipsoid like figure (see panel (c) of Fig. 2.9). Opposite to it, in [30] (see the text and Fig. 5 therein), the spherical shape region doesn't form a closed area. Phase transitions in the case of $O(6)$-symmetry non-conserving model with $[\mathbf{QQQ}]^{(0)}$ interaction were not considered in [30].

Chapter 3

The study of quantum chaos in the case of geometrical rigid triaxial rotator models

Because of their Hamiltonian structure geometrical nuclear models are rarely used for QPT studies at low energy and spin values. However, quantum chaos phenomena related to spectroscopic characteristics of various geometrical models, especially at high angular momenta of the nuclear core, have attracted notable attention during last decade. A considerable methodological interest for quantum chaos studies has the nuclear triaxial rotator model because its classical analogue is a well-known integrable system.

In our studies of quantum chaos criteria, we have considered two versions of the nuclear rigid triaxial rotator model: the Davydov's model and Bravin-Fedorov's model. Greatest attention has been given to the calculations and comparison of dynamical quantum chaos criteria - the wave function entropy $W(\Psi_i)$ and the fragmentation of basis states $\kappa(\Phi_k)$. The obtained results have been included in the journal paper manuscript [R4] and published in the proceedings of the international conference. The journal paper manuscript presently is revised and extended including data on quantum chaos statistical criteria calculations. Also, the results of our studies have been reported at the international [A5,A8] and local [A4,A6] scientific conferences in 2007 and 2008.

3.1 The description of nuclear level energies employing rigid triaxial rotator models

The Davidov's rigid triaxial rotator model (see, e.g., [14, 5]) is a simplest collective model which allows one to describe excited levels of even-even nucleus having a stable triaxial deformation with asymmetry angle $\gamma = \gamma_{eff} \neq 0$. In the case of rigid quadrupole deformation ($\beta = \beta_{eff}$, $\gamma = \gamma_{eff}$), one can present the collective nuclear core Hamiltonian Eq. (1.6) as

$$H_D = \frac{1}{2}\sum_{j=1}^{3}\frac{\mathbf{I}_j^2}{\sin^2(\gamma - j\frac{2\pi}{3})}, \tag{3.1}$$

where $\mathbf{I}_j$ are the projections of the total nuclear angular momentum operator $\mathbf{I} \equiv \mathbf{L}$ on Descartian axes coinciding with principal directions of the nuclear momentum of inertia. Nuclear level energy values are evaluated in $E_1 = \hbar^2[4B_2\beta_{eff}^2]^{-1}$ units.

Matrix elements of Hamiltonian Eq.(3.1) in the basis formed by the axially-symmetric rotator eigenfunctions Eq. (1.8), in which the intrinsic part $\chi_K \equiv 1$, have the form [14]:

$$< IK|H_D|IK' >= \delta_{K,K'}\left\{\frac{1}{4}(a+b)[I(I+1)-K^2] + \frac{1}{2}cK^2\right\} + \delta_{|K-K'|,2}\times$$

$$\left\{\frac{(a-b)[1+(-1)^I\delta_{0,K}]}{8\sqrt{1+\delta_{0,K}}}\sqrt{(I-K)(I-K-1)(I+K+1)(I+K+2)}\right\}, \tag{3.2}$$

where parameters a, b, and c, related to moments of inertia (1.7) along three internal axis , are expressed via the asymmetry angle γ as follows:

$$a^{-1} = \sin^2(\gamma - 2\pi/3); \qquad b^{-1} = \sin^2(\gamma + 2\pi/3); \qquad c^{-1} = \sin^2\gamma. \tag{3.3}$$

There is no mixing between odd and even K values. Therefore, it is useful to use a new basis system (see, e.g., [12]) formed by symmetric and antisymmetric combinations of eigenfunctions (1.8):

$$\begin{array}{l}\Phi_k^s(I,M,K) = \left(\Phi_k(I,M,K) + \Phi_k(I,M,-K)\right)/\sqrt{2};\\ \Phi_k^a(I,M,K) = \left(\Phi_k(I,M,K) - \Phi_k(I,M,-K)\right)/\sqrt{2}.\end{array} \tag{3.4}$$

A matrix of Hamiltonian Eq. (3.1) in the basis (3.5) consists of four submatrices, labeled by a parity of K and a wave function symmetry (s or a). States with even and odd spin values are considered separately. A rank $n_0(I)$ of the diagonalized matrix at each nuclear spin I value is finite: 1) for even spin values, $n_0(I_{even}) = (I_{even} + 2)/2$, and K assumes following $n_0(I_{even})$ values: $K = 0, 2, 4, \ldots, I_{even}$; 2) for odd spin values, $n_0(I_{odd}) = (I_{odd} - 1)/2$, and K assumes following $n_0(I_{odd})$ values: $K = 2, 4, 6, \ldots, I_{odd} - 1$. Wave functions of the rigid triaxial rotator model are obtained as a superposition

$$\Psi_i^{s,a}(I) = \sum_k c_{ik} \Phi_k^{s,a}(I, M, K), \tag{3.5}$$

where c_{ik} are mixing amplitudes.

In the frameworks of BM collective model, an equilibrium state of the collective nuclear surface (1.3) is spherical, and one describes small deviations from this spherical shape. If the equilibrium state of nuclear surface is deformed, one should employ a refined approach (see [15]) resulting in a more precise Hamiltonian expression in the case of rigid triaxial rotator model. The Hamiltonian proposed by Bravin and Fedorov includes the dependence from both nuclear quadrupole deformation parameters β and γ and is written as [15, 16]:

$$H_{BF} = \frac{1}{2} \sum_{j=1}^{3} \frac{\mathbf{I}_j^2}{\sin^2(\gamma - j\frac{2\pi}{3}) \Theta_j(\beta, \gamma)}, \tag{3.6}$$

where

$$\begin{aligned} \Theta_j(\beta, \gamma) &= 1 + \frac{45}{196\pi}\beta^2 - \frac{9\sqrt{5}}{14\sqrt{\pi}}\beta \cos\left(\gamma - j\frac{2\pi}{3}\right) \\ &- \frac{195\beta^2}{392\pi} \cos\left(2\left(\gamma - j\frac{2\pi}{3}\right)\right) \end{aligned} \tag{3.7}$$

Hamiltonian matrices of the triaxial rotator models defined by Eqs.(3.2) and (3.6) have been diagonalized for all even and odd spin values in the range $I = 2, 3, \ldots, 100, 101$, i.e., up to maximal ranks $n_0(I_{even} = 100) = 51$, and $n_0(I_{odd} = 101) = 50$, giving energies of 2600 theoretical states: $E_1(I), E_2(I), \ldots, E_{n_0}(I)$. The diagonalization procedure has been performed at $N_\gamma = 28$ asymmetry angle values $\gamma = 3^\circ, 4^\circ, \ldots, 30^\circ$. In the case of Bravin-Fedorov's model, calculations have been performed at three fixed β values: 0.1, 0.2, and 0.3. The obtained sets of eigenvalues and wave functions have

been used for the study of statistical and dynamical quantum chaos criteria $P(S)$, $W(\Psi_i)$, and $\kappa(\Phi_k)$.

3.2 Behaviour of statistical and dynamical quantum chaos criteria in the case of rigid triaxial rotator models

First, we shall consider the results obtained using Davidov's rigid triaxial rotator model, when theoretical level energies (expressed in $\hbar^2[4B\beta_{eff}^2]^{-1}$ units) depend only on the asymmetry angle γ.

Statistical chaos criteria - the nearest level energy spacing distributions P(S) have been calculated in the case of maximal considered spin value $I = 100$ when the rank of diagonalized matrix is $n = 51$. Although the number of eigenvalues in the unfolded spectrum at this spin value is small, if one compares it with those at $I \geq 1000$ values used in Ref. [53], one can see that our results allow to make similar conclusion: the level spacing distribution of the rigid triaxial rotator does not obey Poissonian statistics, as one could expect for the classically integrable Hamiltonian.

Fig. 3.1 shows the results of $P(S)$ calculations at different asymmetry angle γ values. The obtained distributions have been fitted by Brody formula Eq. (1.24), and the lower part of Fig. 3.1 presents the obtained value of Brody coefficient ζ in dependence on γ. One can see that the chaoticity of the system grows with asymmetry. For $18^\circ \leq \gamma \leq 29^\circ$, eigenvalues of the rigid triaxial rotator obey the Wigner statistics Eq. (1.23) characteristic to GOE. Note that, at $\gamma = 30^\circ$, the chaoticity of the system again is reduced. However, in order to make more confident conclusions, one should perform $P(S)$ distribution studies at higher spin values.

The wave function entropy $W(\Psi_i)$ values have been calculated according to Eq.(1.25) and averaged over the number of states $n_0(I)$ at given spin value I. Fig. 3.2 displays these values in dependence from the asymmetry angle γ at three different I_{even} and I_{odd} values. One can see that the wave function entropy values $W(\Psi_i)_{av}(I)$, averaged over all $\Psi_1, \Psi_2, \ldots, \Psi_i, \ldots, \Psi_{n_0(I)}$ components at particular asymmetry angle γ, demonstrate a stable trend of $W(\Psi_i)_{av}(I)$ growth when γ is increased up to $\gamma = 30^\circ$. The maximal wave function entropy value is attained at $\gamma = 30^\circ$. This trend is observed both for even and odd spin I values, and it is not affected by some value fluc-

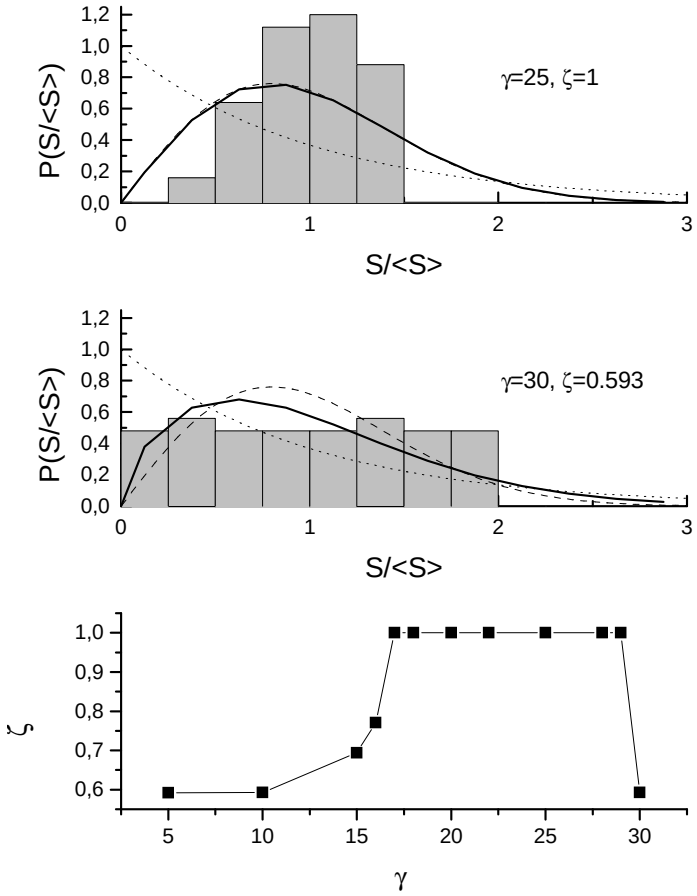

Figure 3.1: Nearest level spacing distributions P(S) in dependence from asymmetry angle γ in the case of rigid triaxial rotator model.

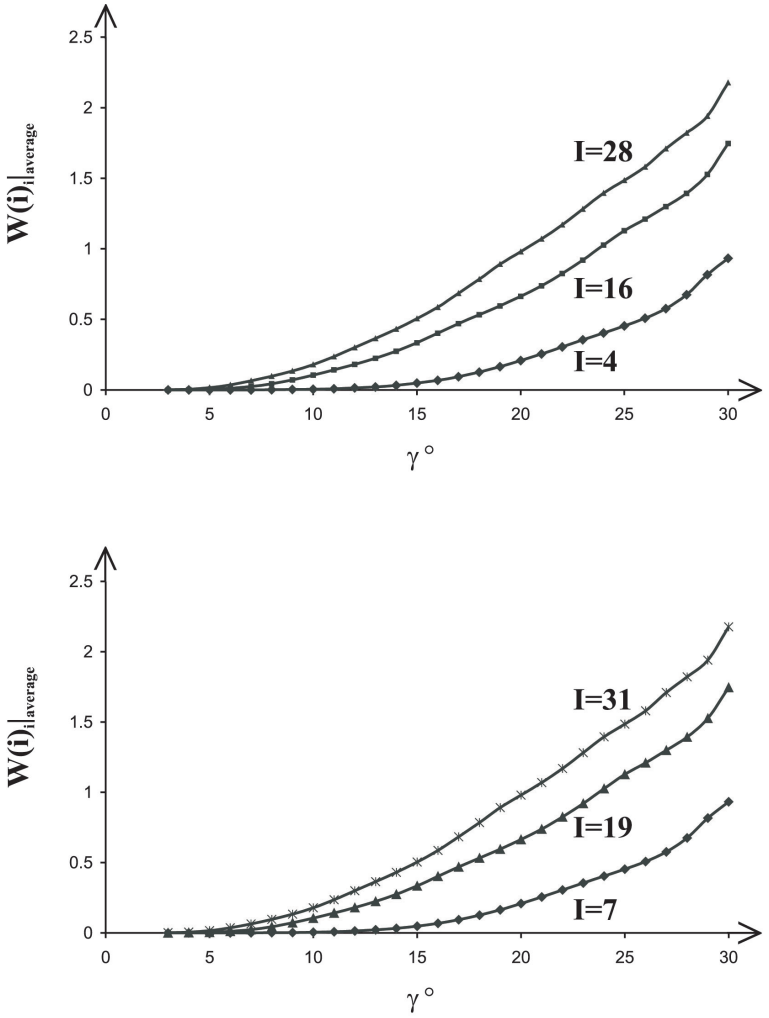

Figure 3.2: Averaged values of the wave function entropy $W(\Psi_i)_{av}(I)$ in dependence from the triaxiality angle γ at even $I = 4, 16, 28$ and odd $I = 7, 19, 31$ spin values (in both cases $n_0 = 3, 9, 15$, correspondingly).

Table 3.1: Comparison of averaged wave function entropy $W(\Psi_i)_{av}(I)$ values with the theoretically possible maximal $W(\Psi_i)_{max}(I)$ values in the case of rigid triaxial rotator model.

I_{even}	I_{odd}	n_0	$W(\Psi_i)_{av}$		$W(\Psi_i)_{max}$	$W(\Psi_i)_{av}/W(\Psi_i)_{max}$	
			I_{even}	I_{odd}		I_{even}	I_{odd}
4	7	3	0.936	0.936	1.099	0.849	0.852
6	9	4	1.047	1.095	1.386	0.755	0.790
8	11	5	1.213	1.254	1.609	0.754	0.779
10	13	6	1.398	1.462	1.792	0.780	0.816
12	15	7	1.508	1.561	1.946	0.775	0.802
14	17	8	1.602	1.659	2.079	0.771	0.798
16	19	9	1.746	1.794	2.197	0.795	0.817
18	21	10	1.811	1.854	2.303	0.786	0.805
20	23	11	1.885	1.926	2.398	0.786	0.803
22	25	12	1.979	2.022	2.485	0.796	0.814
24	27	13	2.033	2.078	2.565	0.793	0.810
26	29	14	2.090	2.143	2.639	0.792	0.812
28	31	15	2.177	2.225	2.708	0.804	0.822

tuations in dependence from γ taking place in the case of separate $W(\Psi_i)$ components.

In Table 3.1, the averaged entropy values $W(\Psi_i)_{av}(I)$, calculated in the case of maximally mixed basis state functions $\Phi_k(I, M, K)$ Eq. (3.4) at $\gamma = 30^\circ$, are compared with the theoretically possible maximal entropy values (see, e.g., [38]) $W(\Psi_i)_{max}(I) = \ln(n_0(I))$, corresponding to the case when mixed perturbed wave functions are uniformly spread over all basis states.

This comparison shows that, even in this case of maximal mixing of model basis states Eq.(3.4), $W(\Psi_i)_{av}(I) = (0.75 \div 0.85)W(\Psi_i)_{max}(I)$. Therefore, the intrinsic structure of the Davidov's rigid triaxial rotator model does not allow to obtain a higher degree of chaoticity with respect to axially-symmetric rotator eigenfunction basis.

Calculation of another dynamical quantum chaos criterion - the fragmentation width of basis states $\kappa(\Phi_k)$, by means of Eqs.(1.26) and (1.27) is a more complicated task. If one adopts as the unperturbed Hamiltonian H_0 the diagonal part of the matrix element expression Eq.(3.2), then the average

distance D_0 between unmixed levels can be evaluated as follows:

$$D_0(I,\gamma) = \begin{cases} IE_0(\gamma), & \text{if } I = I_{even}; \\ \left[I(I-2)-3\right]/(I-3)E_0(\gamma), & \text{if } I = I_{odd}, \end{cases} \tag{3.8}$$

where $E_0(\gamma) = c-(a+b)/2$. The calculation of Γ_{spr} values involves the need to control the fulfillment of the condition (1.28), imposed on mixing amplitudes of involved states. That means that $\kappa(\Phi_k)$ values can be calculated only if the mixing of basis states exceeds certain limit, i.e. in the case of large asymmetry angle values. An example of $\kappa(\Phi_k)$ criterion calculation results at spin $I = 24$ one can find in Table 3.2. At this spin value, the number of basis states $n_0(I = 24) = 13$, and one can start evaluating basis state fragmentation widths at $\gamma = 23^\circ$.

In Table 3.2, one can clearly recognize the trend of $\kappa(\Phi_k)_{av}$ value growth with increasing asymmetry angle γ (see also Fig. 3.3). However, the restriction Eq. (1.28) plays a crucial role in the fluctuations of particular $\kappa(\Phi_k)$ values, preventing the evaluation of fragmentation width in the case of some basis states even within the region of calculated $\kappa(\Phi_k) = f(\gamma)$ dependence (see columns with $k = 5, 6$ in Table 3.2).

It has been found that the theoretically predicted transition from the soft chaos to the hard chaos, in the case of rigid triaxial rotator models, can be studied only starting with a comparatively high spin value ($I = 50$), when the number of basis states $n \geq$26. Analysis of the obtained results shows that, at spin value $I = 24$, there are only two cases of soft quantum chaos [52] when $0 < \kappa(\Phi_k) < 1$ (see $k = 3$ basis state at $\gamma = 25^\circ$ and 29° in Table 3.2). In our calculations, we have not observed a smooth gradual transition from the soft chaos ($\kappa(\Phi_k) < 1$) to hard chaos ($\kappa(\Phi_k) > 1$). In the rigid triaxial rotator model, transition to the hard chaos case is abrupt (see Fig. 3.3), and we can propose two explanations for such situation. The first one is related with the restriction (1.28), which considerably limits a number of states suitable for Γ_{spr} and $\kappa(\Phi_k)$ evaluation. The second one follows from the tridiagonal structure of the model Hamiltonian matrix Eq. (3.2). Due to this the wave function mixing amplitudes in Eq.(3.5) are not smoothly spread over all basis function Eq.(3.4) components: their distribution is approximately Lorentzian, which, in turn, increases the role of restriction Eq.(1.28) for the calculation of $\kappa(\Phi_k)$ values.

In order to check the dependence of quantum chaos in the case of rigid triaxial rotator model from the nuclear quadrupole deformation β, we have

Table 3.2: Basis state fragmentation widths $\kappa(\Phi_k)$ of the rigid triaxial rotator model calculated at spin value $I = 24$ ($n_0(I) = 13$).

γ	$D_0(\gamma)$	$\kappa(\Phi_k)^a$									$\kappa(\Phi_k)_{av}$
		$k=3$	$k=4$	$k=5$	$k=6$	$k=7$	$k=8$	$k=9$	$k=10$	$k=11$	
23°	111.89	X	X	1.71	X	X	X	X	X	X	1.71
24°	98.21	X	X	X	2.15	X	X	X	X	X	2.15
25°	85.81	0.55	1.47	1.98	2.41	X	X	X	X	X	1.60
26°	74.46	1.39	1.69	3.82	X	3.18	X	X	X	X	2.52
27°	63.96	1.45	4.00	5.45	X	2.91	3.13	X	X	X	3.39
28°	54.14	1.48	5.98	7.45	3.97	3.50	3.02	3.15	X	X	4.08
29°	44.87	0.71	2.81	8.57	9.97	2.27	3.16	3.72	X	4.97	4.52
30°	36.00	7.33	3.50	3.50	10.00	6.50	5.33	4.67	5.50	4.50	5.65

^{a} – States for which one cannot evaluate $\kappa(\Phi_k)$ value due to the violation of condition Eq.(1.28) are marked by "X".

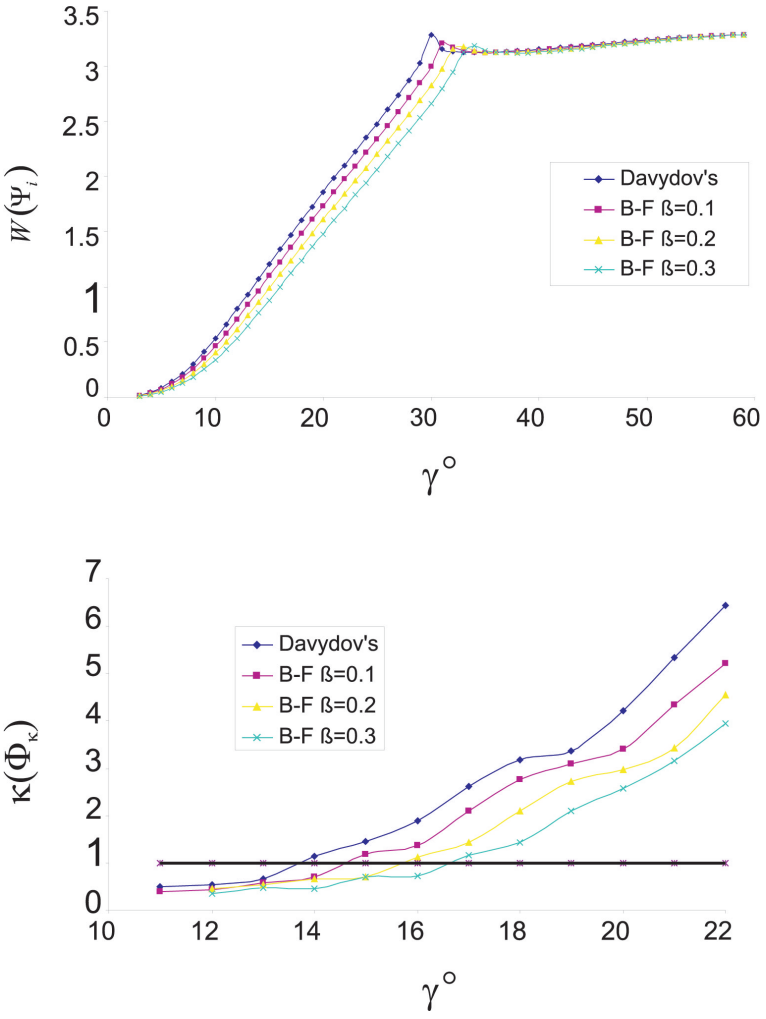

Figure 3.3: Averaged fragmentation width $\kappa(\Phi_k)_{av}$ of rigid triaxial rotator basis states in dependence from asymmetry angle γ for even $I = 4, 16, 28$ and odd $I = 7, 19, 31$ spin values.

performed analogous wave function entropy $W(\Psi_i)$ and basis state fragmentation width $\kappa(\Phi_k)$ calculations also in the case of Bravin-Fedorov's model Eq. (3.6). Calculations were performed at asymmetry angle γ values ranging from 4° to $\sim 60^\circ$, and at three different quadrupole deformation parameter β values: β=0.1, 0.2, and 0.3. The results of quantum chaos dynamical criteria calculations in the case of both rigid triaxial rotator models are compared in Fig. 3.4. One can see that the values of both criteria: $W(\Psi_i)$ and $\kappa(\Phi_k)$, are reduced if quadrupole deformation β is increased, which is as expected since we consider mixing with respect to axially-symmetric rotator basis functions.

In addition, we have performed the analysis of theoretical energy spectra, obtained in the case of both rigid triaxial rotator models, with the aim to search for the transition from the rotational type level sequence to the librational one. Such transition in the frameworks of semi-classical description [13] occurs at the energy value $E_{tr} = (b/2)I^2$, i.e., the quantum statistics of the rigid triaxial rotator model behaves analogously to that of another anomalous quantum system - the one-dimensional harmonic oscillator.

Characteristic maxima of energy level density $\rho(E_i)$ and corresponding wave function entropy $W(\Psi_i)$ have been observed at E_{tr} in dependence from I and γ in the case of Davydov's model (see Fig. 3.5) and in dependence from I, β and γ in the case of Bravin-Fedorov's model. That agrees with the results of [13] obtained in the case of Davydov's rigid triaxial rotator model.

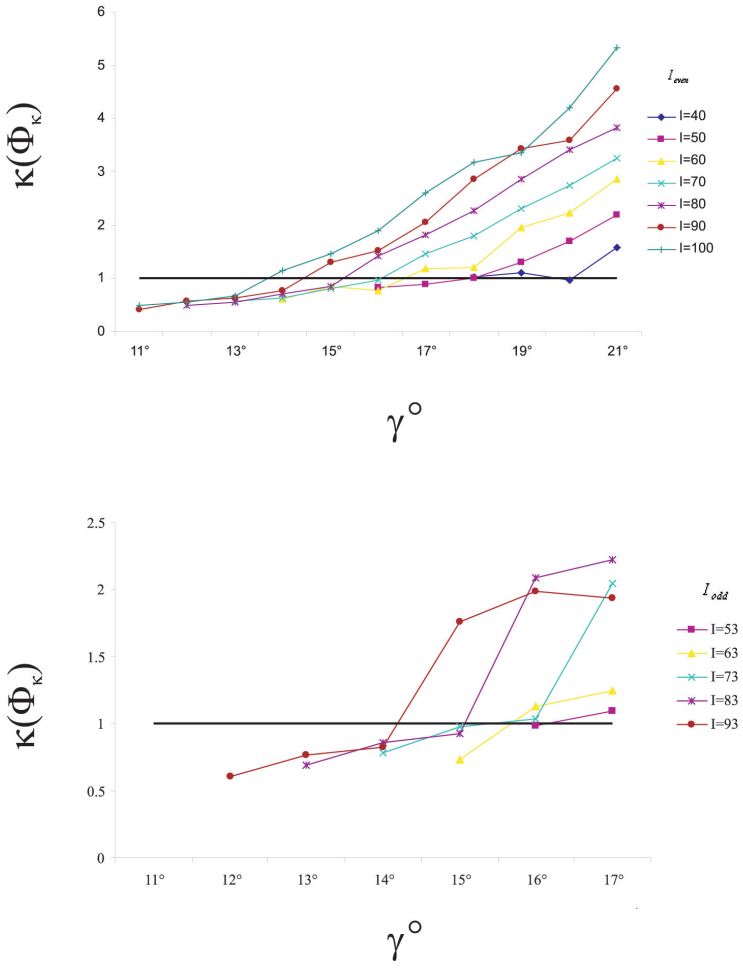

Figure 3.4: Behaviour of averaged dynamical quantum chaos criteria $W(\Psi_i)_{av}$ and $\kappa(\Phi_k)_{av}$ in the frameworks of rigid triaxial rotator models of Davydov and Bravin-Fedorov at $I = 100$ in dependence from the asymmetry angle γ and quadrupole deformation parameter β.

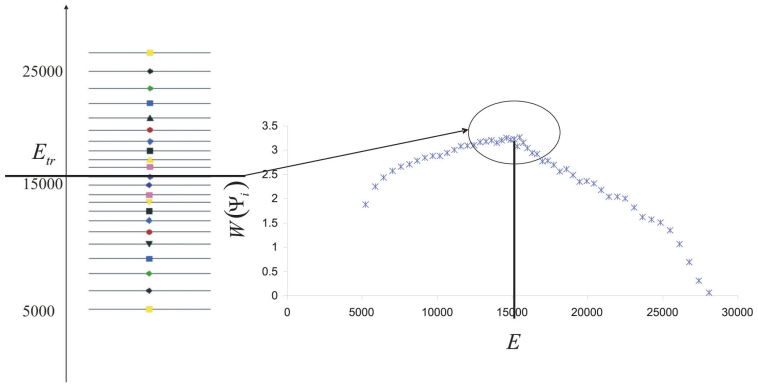

Figure 3.5: Transition from the rotational type spectrum to the librational type spectrum in the case of Davydov's rigid triaxial rotator model at $I = 100$ and $\gamma = 25°$.

Chapter 4

The study of QPT in the case of complete IBM-1 model

It was logical to continue our studies of nuclear shape phase transitions, which were started employing simplified versions of IBM-1 (see Chapter 2), with the use of complete IBM-1 version. Standard IBM-1 Hamiltonian Eq. (1.12), depending on six degrees of freedom of one s-boson and five d-bosons, allows to describe complete dynamics of the even-even nuclear core collective excitations in terms of $U(5)$, $SU(3)$, and $O(6)$ subgroup chains Eq. (1.14) of the total model symmetry group $U(6)$. Complete IBM-1 Hamiltonian and its classical energy limit depend on six model parameters (1.13), therefore, in order to analyze their behaviour in the entire model parameter space, one requires special methods. In [20], the approach based in catastrophe theory has been proposed. Their method allows to reduce the analysis of IBM-1 classical energy functional to the study of its behaviour in the space of just two essential control parameters.

We have used the approach developed in [20] for our study of complete IBM-1 Hamiltonian classical energy E_{cl} surfaces employing the method of precise solution of minima condition equations, applied in Chapter 2 in the case of simplified IBM-1 versions. The results of our studies have been published in a journal paper [R6] and reported at the international scientific conference in 2008 [A7].

4.1 Classical energy limit of complete IBM-1 Hamiltonian in terms of catastrophe theory parameters.

The authors of Ref. [20] have presented classical energy expression of the standard IBM-1 Hamiltonian (1.12) in the following transformed form:

$$E_{cl}(N_b, \varepsilon_s, \varepsilon_d, C_0, C_2, C_4, v_0, v_2, u_0, u_2; \beta, \gamma) = \frac{N_b \varepsilon \beta^2}{1+\beta^2} +$$

$$\frac{N_b(N_b-1)}{(1+\beta^2)^2}\left(a_1\beta^4 + a_2\beta^3\cos 3\gamma + a_3\beta^2 + \frac{u_0}{2}\right), \tag{4.1}$$

where the s-boson contribution is subtracted introducing $\varepsilon \equiv \varepsilon_d - \varepsilon_s$. Since E_{cl} is a rotational scalar and there is no dependence from Euler angles, the initial two-boson interaction parameters $C_0, C_2, C_4, V_2, V_0, u_2$ are replaced by new parameters a_1, a_2, and a_3 defined as:

$$\begin{aligned} a_1 &= C_0/10 + C_2/7 + 9C_4/35; \\ a_2 &= -(2/\sqrt{35})v_2; \\ a_3 &= (1/\sqrt{5})(v_0 + u_2). \end{aligned} \tag{4.2}$$

Then, employing the catastrophe theory formalism (for details see [20]), the following essential control parameters are introduced:

$$r_1 = \frac{a_3 - u_0 + w}{2a_1 + w - a_3}; \qquad r_2 = -\frac{2a_2}{2a_1 + w - a_3}, \tag{4.3}$$

where

$$w = \varepsilon/(N_b - 1). \tag{4.4}$$

Now, if one introduces a quantity

$$\varepsilon_0 = N_b(N_b-1)(2a_1 + w - a_3)/2, \tag{4.5}$$

such that, in the case of $\varepsilon_0 = 0$, E_{cl} assumes constant value independent both from β and from γ, one can rewrite the classical energy Eq. (4.1) as follows:

$$E_0(N_b, r_1, r_2; \beta, \gamma) = \frac{E_{cl}(N_b, \varepsilon, a_1, a_2, a_3, u_0; \beta, \gamma) - N_b(N_b-1)u_0/2}{\varepsilon_0} =$$

$$= \frac{1}{(1+\beta^2)^2}\left[\beta^4 + r_1\beta^2(\beta^2+2) - r_2\beta^3\cos 3\gamma\right], \qquad (4.6)$$

where the dependence from the total boson number N_b enters via the expressions for r_1 and r_2 defined by Eqs.(4.3) and (4.4). Employing Eq. (4.6), one can study all physically interesting cases with $\varepsilon_0 \neq 0$.

It has been shown in [20] that minima of the classical energy expression (4.6) have same depth at any value of asymmetry angle γ: the classical energy minima of complete IBM-1 version are γ-unstable. Therefore, one can study a qualitative picture of the energy surface at $\gamma = 0^\circ$ or $\gamma = 60^\circ$. If one takes $\gamma = 0^\circ$, eliminating in such a way the γ-degree of freedom, one obtains following final expression for the classical energy functional of complete version of IBM-1 in terms of control parameters r_1, r_2:

$$E_0(r_1, r_2; \beta) = \frac{1}{(1+\beta^2)^2}\left[\beta^4 + r_1\beta^2(\beta^2+2) - r_2\beta^3\right]. \qquad (4.7)$$

We shall use this expression for our analysis of nuclear shape phase transitions via precise solution of equations following from classical energy minima conditions.

The classical energy functional $E_0(r_1, r_2; \beta)$ in the space of control parameters (r_1, r_2) has the form of a "swallow tail" diagram [20]. This diagram (see Fig. 4.1) involves all limiting cases of IBM-1 dynamical symmetries ($U(5)$, $O(6)$, $SU(3)$, $\overline{SU(3)}$). The evaluation of (r_1, r_2) coordinates corresponding to the vertexes and the triple point of this diagram would be considered in the next section.

4.2 Precise solution of equations for the minima of complete IBM-1 classical energy functional

Let us consider a solution for the classical energy minimum problem. A corresponding equation one can obtain applying to Eq.(4.7) the extreme condition

$$\frac{\partial E_0(r_1, r_2; \beta)}{\partial \beta} = 0, \qquad (4.8)$$

which gives

$$\frac{\beta\left[4(\beta^2 + r_1) + \beta(\beta^3 - 3)r_2\right]}{(1+\beta^2)^3} = 0 \qquad (4.9)$$

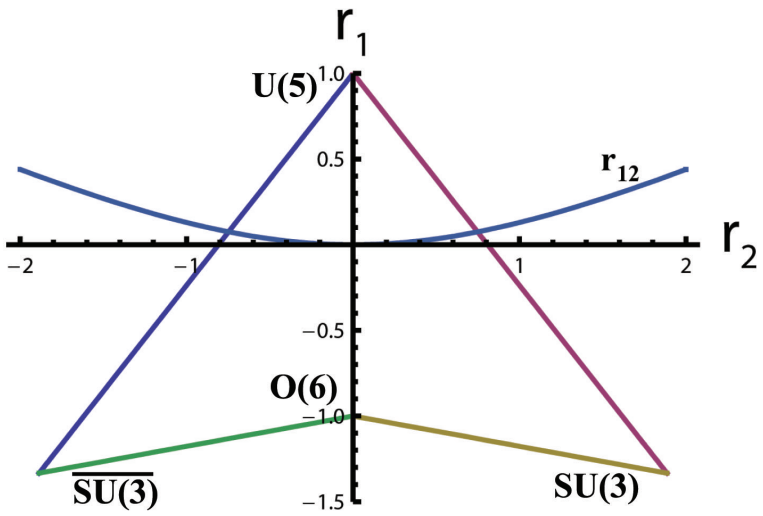

Figure 4.1: Critical lines and points of the classical energy functional Eq. (4.7) in the space of catastrophe theory control parameters r_1 and r_2.

If one excludes trivial solutions by imposing conditions $(1+\beta^2)^3 \neq 0$ and $\beta \neq 0$, one can reduce Eq. (4.9) to a cubic equation

$$A\beta^3 + B\beta^2 + C\beta + D = 0 \tag{4.10}$$

with following coefficients

$$A = r_2; \qquad B = 4; \qquad C = -3r_2; \qquad D = 4r_1. \tag{4.11}$$

The three roots β_{0i} $(i = 1, 2, 3)$ of this cubic equation give deformation parameter β values at which energy functional Eq.(4.7) has minimum. The obtained explicit expressions for these roots are very cumbersome and, in general, complex functions of control parameters r_1 and r_2, so we shall not give them here. The behaviour of these roots within parameter value ranges $-2 \leq r_1 \leq 2$, and $-2 \leq r_2 \leq 2$ is shown in Figs. 4.2-4.4, separately for real and imaginary parts of β_{0i}.

Main features of these roots one can analyze analogously as it has been done in the case of simplified IBM-1 version (see Chapter 2) by considering values of the cubic equation (4.10) discriminant:

$$D_3 = \frac{B^2C^2 - 4B^3D + 18ABCD - A(4C^3 + 27AD^2)}{A^4}. \tag{4.12}$$

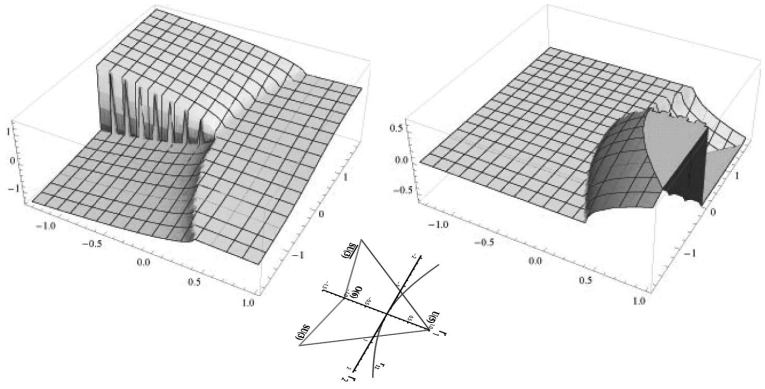

Figure 4.2: Behaviour of the real (left panel) and imaginary (right panel) parts of the first root β_{01} of Eq.(4.10) in the $-2 \leq r_1 \leq 2$ and $-2 \leq r_2 \leq 2$ range of control parameters.

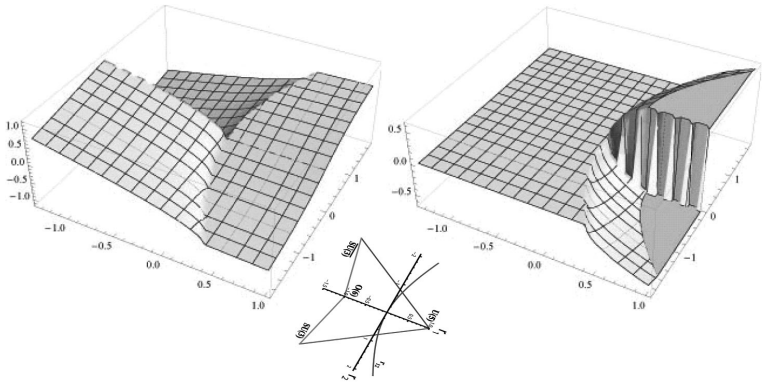

Figure 4.3: Behaviour of the real (left panel) and imaginary (right panel) parts of the third root β_{03} of Eq.(4.10) in the $-2 \leq r_1 \leq 2$ and $-2 \leq r_2 \leq 2$ range of control parameters.

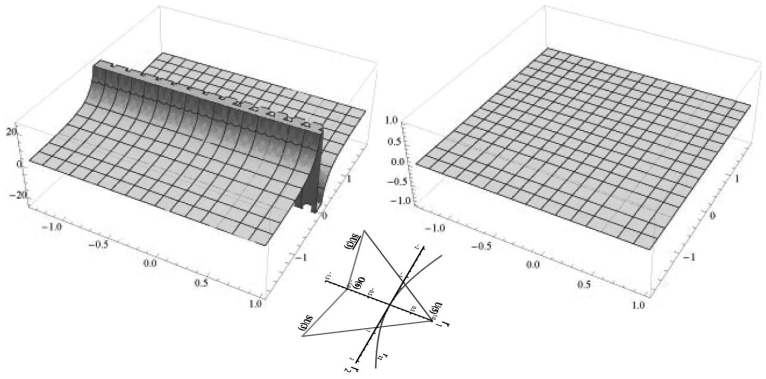

Figure 4.4: Behaviour of the real (left panel) and imaginary (right panel) parts of the second root β_{02} of Eq.(4.10) in the $-2 \leq r_1 \leq 2$ and $-2 \leq r_2 \leq 2$ range of control parameters.

When $D_3 < 0$, one has one real and two complex conjugated roots. If $D_3 > 0$, there are three real, unequal roots, while at $D_3 = 0$ - two real, equal roots.

The $D_3 = 0$ case with two real degenerate roots defines the second order phase transition line between spherical and deformed nuclear shapes. Let us consider this case in detail. If one inserts coefficients Eq.(4.11) into Eq.(4.12), one obtains

$$D_3 = \frac{-1024r_1 + 144r_2^2 - 864r_1r_2^2 - r_2(432r_1^2r_2 - 108r_2^3)}{r_2^4} = 0, \qquad (4.13)$$

which, with the restriction $r_2 \neq 0$, gives two solutions for the dependence $r_1 = r_1(r_2)$:

$$\begin{pmatrix} r_{11} \\ r_{12} \end{pmatrix} = \mp\frac{(9r_2^2 + 16)^{3/2}}{54r_2^2} - \frac{32}{27r_2^2} - 1, \qquad (4.14)$$

These solutions coincide with those given by Eqs.(3.19 a,b) of Ref. [20] where the lines r_{11} and r_{12} define, according to the catastrophe theory, the bifurcation set as the locus of points in the space of control parameters (r_1, r_2) at which a transition occurs from the one local minimum to another. In our case, the r_{12} solution defines the arc line, separating spherical and deformed shape areas (see Fig. 4.1), while the r_{11} solution has no such clear physical interpretation.

The triple point, where spherical and both deformed (prolate and oblate) shapes meet, one can obtain from the critical point condition imposed on the second-order derivative of Eq.(4.7) (see, e.g., [62]):

$$\left.\frac{d^2E_0(r_1,r_2;\beta)}{d\beta^2}\right|_{\beta=0} = 0 \tag{4.15}$$

which gives one the coordinates of this point at $r_1 = r_2 = 0$.

The coordinates of vertexes, and critical points of the classical energy functional Eq.(4.7) in the space of control parameters r_1 and r_2 (see Fig. 4.1) are summarized in Table 4.1.

Table 4.1: Values of control parameters (r_1, r_2) at the dynamical symmetry limits and at the triple point in the case of complete IBM-1 version.

Symmetry type	r_1	r_2
$U(5)$	1	0
$O(6)$	-1	0
$SU(3)$	$-4/3 = -1.333\ldots$	$4\sqrt{2}/3 = 1.88562\ldots$
$\overline{SU(3)}$	$-4/3 = -1.333\ldots$	$-4\sqrt{2}/3 = -1.88562\ldots$
Triple point ($E(5)$)	0	0

In the bottom "deformed shape" part of Fig. 4.1, below the r_{12} arc line defined by Eq.(4.14), we have the $D_3 > 0$ case of Eq.(4.10) with three real and unequal roots. The numerical values for the two of them: (β_{01} and β_{03}), are mirror symmetric (see Figs. 4.2 and 4.3, and have opposite signs with respect to the $r_2 = 0$ line. The second root β_{02} (see Fig. 4.4 has a close to zero value far from the $r_2 = 0$ line in the entire (r_1, r_2) area on both sides of the r_{12} arc line and nonphysically large values $\beta_{02} \to \pm\infty$ with opposite signs along the entire length of the $r_2 = 0$ line when $r_2 \to \pm 0$.

In the top "spherical shape" part of the diagram (Fig. 4.1, above the r_{12} arc line, we have the $D_3 < 0$ case with two complex conjugated roots β_{01}, β_{03}, which are mirror-symmetric with respect to $r_2 = 0$ line. These roots have very small real parts and large imaginary parts with opposite signs. The behaviour of the second real root β_{02} in this area is similar to that in the at $D_3 > 0$ case, described above.

In order to compare the results of our precise solution of the classical energy functional minima problem with the results obtained using the Landau theory approach, let us expand Eq.(4.7) in Taylor series with respect to deformation parameter β. One obtains

$$E_{0T}(r_1, r_2; \beta) = 2r_1\beta^2 - r_2\beta^3 + (1-3r_1)\beta^4 + 2r_2\beta^5 + (4r_1-2)\beta^6 + O(\beta^7). \quad (4.16)$$

Then, applying to this expression the extreme condition Eq.(4.8), one obtains the following equation for the classical energy minimum in the case of complete IBM-1 version:

$$(24r_1 - 12)\beta^5 + 10r_2\beta^4 + (4 - 12r_1)\beta^3 - 3r_2\beta^2 + 4r_1\beta = 0. \quad (4.17)$$

In the frameworks of approach based on the Landau theory of phase transitions, higher order terms in Eq. (4.16), starting with the $\sim \beta^4$ power term, are usually disregarded (see, e.g., [22]). In order to assess the effects due to cut-off of the expansion Eq.(4.16), we have applied extreme condition Eq.(4.8) to corresponding Taylor series including subsequently all terms up to β^4, up to β^5, and up to β^6. It has been found that only the inclusion of power terms up to β^5 allows one to reduce Eq.(4.17) to a cubic equation (with the condition $\beta \neq 0$)

$$10r_2\beta^3 + (4 - 12r_1)\beta^2 - 3r_2\beta + 4r_1 = 0, \quad (4.18)$$

where only two coefficients, those at β^3 and β^2, slightly differ from the corresponding coefficients (see Eq.(4.11)) in the equation obtained via a precise solution method.

Analysis of the three roots of Eq.(4.18) gives a similar picture of phase transition critical points and lines as in the case of precise solution. However, if one cuts off the Taylor expansion Eq.(4.16) at β^4 or β^6 power terms, one obtains non-physical values of corresponding roots β_{0i}.

Chapter 5

The study of prolate-oblate shape phase transition in the case of $A \sim$190 region nuclei

In Chapters 2-4, characteristics of nuclear shape phase transitions and quantum chaos in the frameworks of algebraic and geometric models of even-even nuclei have been studied theoretically, without relation to realistic properties of specific nuclei. Therefore, in order to check how one can apply the developed theoretical methods for the interpretation of experimentally observed spectroscopic data, we have undertaken study of QPT and quantum chaos relationships in the case of even-even nuclei belonging to the well-known deformation transition region at $A \sim$190.

The results of these studies have been included in the journal paper manuscript [R7], submitted for publication in September 2010, and reported at the international nuclear physics conference [A10] in 2010.

5.1 Experimental characteristics of nuclei belonging to the deformation phase transition region at $A \sim$190

For our study of relationships between shape phase transitions and quantum chaos in the case of specific nuclei, we have chosen even-even isotopes of tungsten (W, $Z = 74$), osmium (Os, $Z = 76$) and platinum (Pt, $Z = 78$)

with $184 \leq A \leq 194$. Nuclei of these three elements have shapes ranging from the stable prolate axial-symmetry (^{184}W) to the triaxial γ-unstable (^{194}Pt) form. We have included in our IBM-1 model calculations 15 isotopes with boson numbers ranging from 7 to 12, covering the entire phase transition region. The experimentally known platinum isotopes with smaller boson numbers were not included because: a) one must have a sufficient number of theoretical IBM-1 states for the evaluation of quantum chaos criteria; b) at smaller deformations, the spherical-to-deformed $U(5) - E(5) - O(6)$ phase transition becomes dominant and one cannot recognize the weaker prolate-oblate $SU(3) - O(6) - \overline{SU(3)}$ change of shape.

Experimental data about excited level energies and electromagnetic properties of these nuclei have been taken from the ENSDF data compilation [61]. Unfortunately, the available experimental information about transitional region nuclei not always provides levels with confidently established spins and parities, as well as the interpretation of these levels in terms of rotational bands: in some cases, one cannot even tell whether the level belongs to collective or to particle excitation. So, one must be very careful including experimental level energies for the fit of model parameters, giving attention to the smooth variation of analogous state energies in neighboring nuclei.

The energies of confidently established low-lying collective states of tungsten, osmium and platinum isotopes belonging to the $184 \leq A \leq 194$ region are summarized in Fig. 5.1. These data indicate the transition from the strong axial deformation of ^{184}W, characterized by the energy spectrum with three distinct lowest rotational bands obeying the $\sim I(I+1)$ level sequence: the $K^\pi = 0^+$ ground state band, the $K^\pi = 0^+$ β-vibrational band, and the $K^\pi = 2^+$ γ-vibrational band, to the γ-soft form of $^{190-196}$Pt nuclei with the stretched $K^\pi = 0^+$ ground state band, and the $K^\pi = 2^+$ quasi γ-band. Especially characteristic is the behaviour of the second 0_2^+ level, which indicates the transition from deformed shape nuclei to spherical: this shape transition is well-recognizable in the case of platinum isotopes.

The type of IBM symmetry, which is preferable for the description of specific nucleus, can be characterized, in the first approximation, by the $R_4 = E(4_1)/E(2_1)$ ratio between energies of the first 4^+ and 2^+ spin levels. This ratio assumes value 3.33 in the case of $SU(3)$-limit axially-symmetric deformation, 2.5 - for γ-unstable deformed nuclei in the $O(6)$-limit, and 2 - for spherical nuclei in the $U(5)$-limit (see, e.g., [9]). The experimental R_4 ratios for considered W, Os, and Pt isotopes are displayed in the top part of Fig. 5.2. One can see that, up to $A = 188$, the low-lying levels of W and

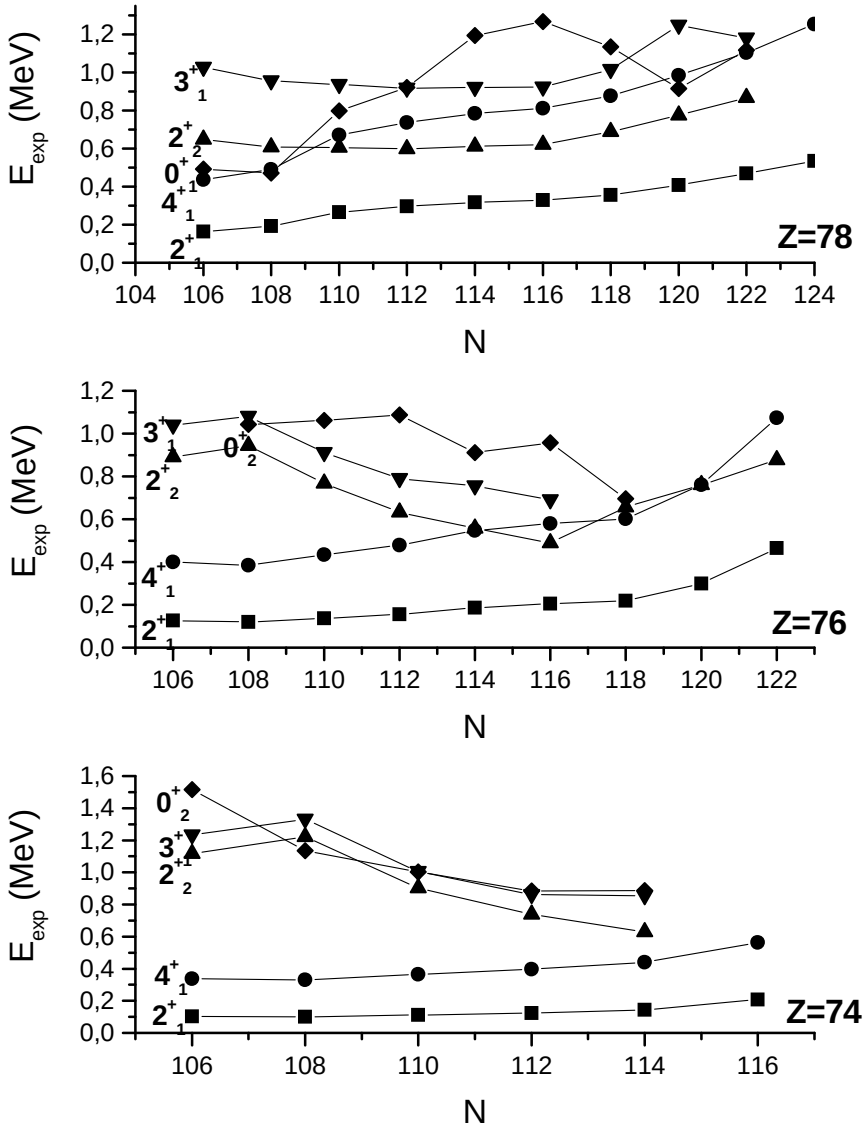

Figure 5.1: Experimental energies (in MeV) of 2_1^+, 4_1^+, 2_2^+, 2_3^+, and 0_2^+ collective levels of even-even W, Os and Pt nuclei with neutron numbers $106 \leq N \leq 124$.

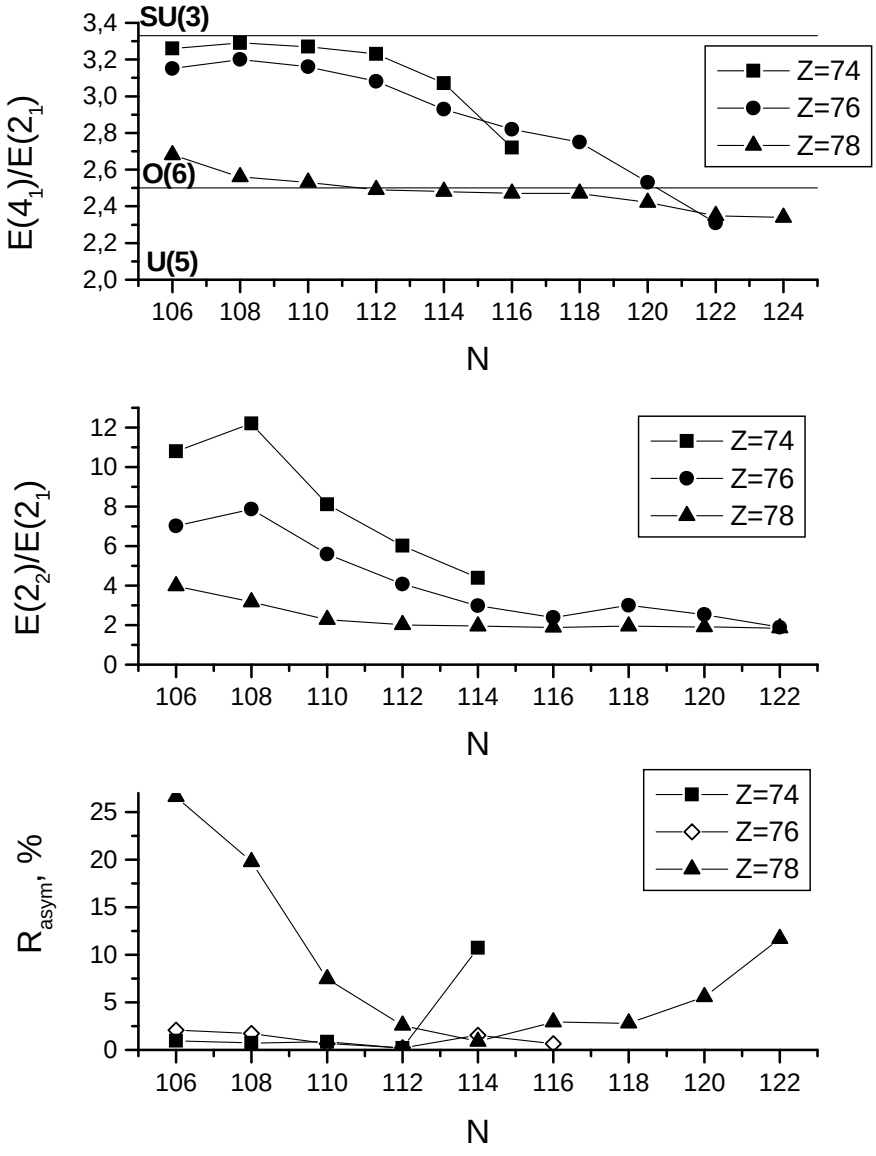

Figure 5.2: The ratios between experimental level energies of W, Os, and Pt isotopes with $106 \leq N \leq 124$ characterizing the change of nuclear shape when neutron number approaches closed shell at $N = 126$.

Os nuclei can be classified using the $SU(3)$-limit scheme of IBM with three lowest collective bands of the axially-symmetric core: the $(\lambda, \mu) = (2N_b, 0)$ irrep $K^\pi = 0^+$ ground state rotational band, and the $(\lambda, \mu) = (2N_b - 2, 2)$ irrep $K^\pi = 0^+$ β-vibrational and $K^\pi = 2^+$ γ-vibrational bands. The low-lying levels of all Pt isotopes with $184 \leq A \leq 194$ are reproduced better if one uses the (σ, n_Δ)-band classification scheme of the γ-unstable $O(6)$-limit of IBM with a gradual transition to spherical $U(5)$-symmetric shape towards magical $N = 126$.

Transition from the stable axial-deformation, characteristic to nuclei in the middle of the rare-earth region $150 < A < 190$, to the spherical shape, observed for nuclei in the vicinity of the doubly-magic ^{208}Pb, occurs via the γ-unstable phase, when nuclear deformation changes from prolate ($\beta > 0$) to oblate ($\beta < 0$). Experimentally this transition is indicated by the change of nuclear quadrupole moment Q sign from $Q < 0$, in the case of prolate deformation, to $Q > 0$, for oblate shaped nuclei. However, nuclear quadrupole moment measurement data are often unavailable. In such a case, one can determine quadrupole deformation parameter β of the nuclear ground state from the experimental value of reduced probability of transition from the first excited 2_1^+ state to the 0_1^+ ground state. It can be done via the well-known expressions (see, e.g., [4, 5]):

$$B(E2; KI_1 \to KI_2) = \frac{5}{16\pi} e^2 Q_0^2 < I_1 K 20 | I_2 K >^2, \tag{5.1}$$

and

$$Q_0 \approx \frac{3}{5\pi} R_0^2 Z \beta, \tag{5.2}$$

where Q_0 is an intrinsic nuclear quadrupole moment, related to the experimentally measured value as

$$Q = \frac{3K^2 - I(I+1)}{(I+1)(2I+3)} Q_0, \tag{5.3}$$

and $R_0 \approx 1.2A^{1/3}$ is the radius of the equivalent volume sphere (see Sect. 1.1).

Fig. 5.3 presents the experimental values of the nuclear electric quadrupole moment Q, and the empirical values of the deformation parameter β, derived from the experimental $B(E2, 2_1^+ \to 0_1^+)$ values, in the case of $184 \leq A \leq 194$ region W, Os, and Pt nuclei. The sign of β is adopted in accordance with the sign of measured Q value. When there is no known Q value, the sign

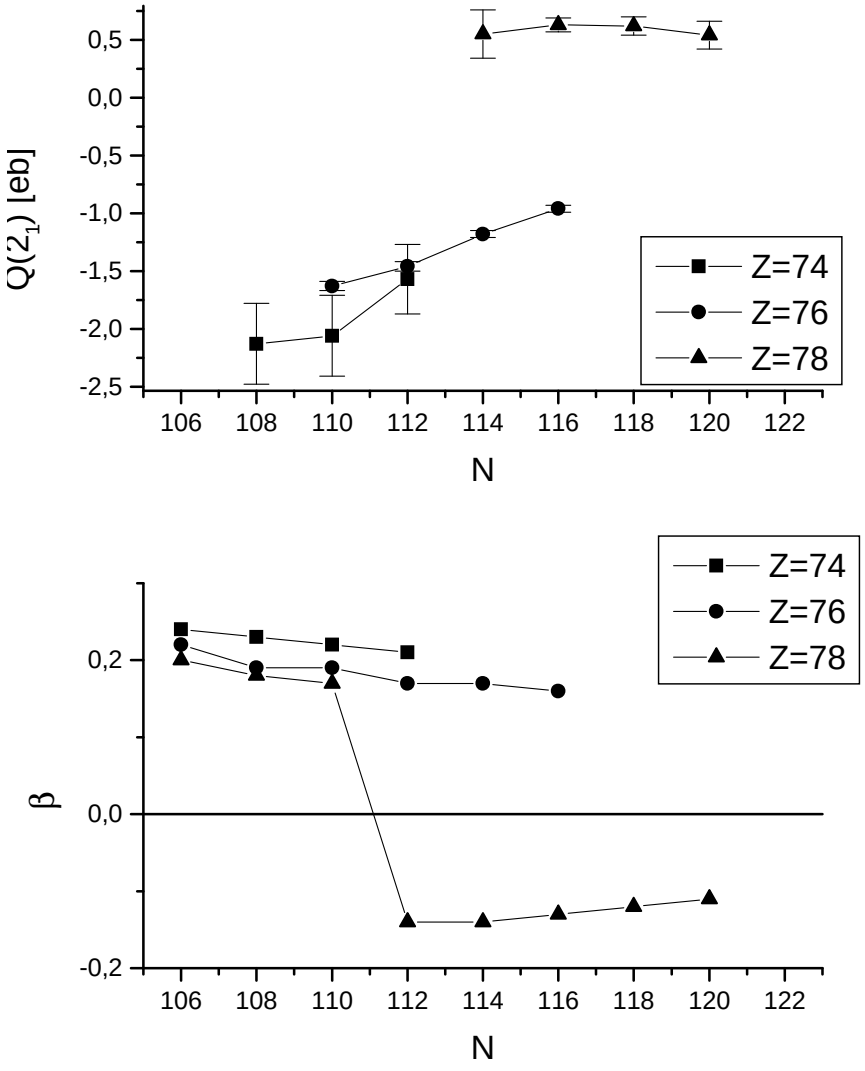

Figure 5.3: Experimental values of the nuclear quadrupole moment Q, and empirical values of the quadrupole deformation parameter β for W, Os, and Pt isotopes with $106 \leq N \leq 122$.

of β is chosen assuming smooth variation of deformation from one isotope to another. Since we have not found in [61] the experimentally measured Q values for ^{184,186,188,190}Pt nuclei, we have presumed, basing on the spectra of low-lying levels, that ^{184,186,188}Pt have prolate shape, at least in the ground state, and transition to oblate deformation for platinum nuclei occurs at $A = 190$.

In [32], on the basis of model calculations performed in the frameworks of simplified Casten's version of IBM-1, it was assumed that the platinum isotope closest to the phase transition critical point $O(6)$ is ^{194}Pt. However, both ^{194}Pt and ^{192}Pt have measured positive Q values. Besides, our complete IBM-1 version model calculations (see Sect. 5.2) indicate that ^{192}Pt has the smallest absolute value of phase transition control parameter χ. It indicates that the prolate-to-oblate shape phase transition in the platinum isotope chain takes place either at $A = 192$, or $A = 190$.

One should note that it is hard to identify the exact prolate-oblate phase transition point for $A \sim$190 region nuclei because of the rapid decrease of $|\beta|$ values towards closed shell at $N = 126$. Another indication of the prolate-oblate phase transition can be the behaviour of the asymmetry parameter γ. Although the IBM-1 $O(6)$-limit classical energy does not allow to obtain a stable collective triaxial shape minimum, one can regard this limit as an analogue of strong γ-vibrations of the axially-deformed nucleus in the frameworks of RV-model (see, e.g., [5]). So, the prolate-oblate shape phase transition may be characterized by the drop of $R_2 = E(2_2)/E(2_1)$ ratio indicating the γ-softness of the nucleus (see the middle part of Fig. 5.2).

In [5], a condition for the levels of asymmetric rotator is given:

$$E(2_1) + E(2_2) = E(3_1), \tag{5.4}$$

which is fulfilled approximately also in the case of RV-model. The lower part of Fig. 5.2 presents the ratio $R_{asym} = (E(2_1)+E(2_2)-E(3_1))/(E(2_1)+E(2_2))$ for W, Os, and Pt isotopes with $106 \leq N \leq 122$. R_{asym} attains minimal value at $N = 112$ for tungsten and osmium, and at $N = 114$ for platinum. Large deviations from the condition Eq. (5.4) in the case of platinum nuclei indicate that this isotope is practically outside the deformation region where one can apply the collective nuclear rotation conception.

5.2 Calculation of low-lying collective levels of W, Os, and Pt nuclei with $184 \leq A \leq 194$ employing complete version of IBM-1

Analysis of experimental data shows that the nuclear shape phase transition in the W-Os-Pt region has a very complex nature. In fact, two parallel transitions take place: the $SU(3) - O(6) - \overline{SU(3)}$ phase transition from the deformed prolate shape to the oblate one, and the deformed-to-spherical $O(6) - E(5) - U(5)$ transition due to the nearness of the $N = 126$ shell closure. Therefore, one must consider the variation of IBM-1 parameters in the entire model parameter space, not just along some selected phase transition critical line. So, in order to obtain a realistic theoretical description for specific nuclei, we have employed the complete IBM-1 Hamiltonian presented in multipole form Eq.(1.15).

Model calculations for each nucleus have been performed at boson number N_b determined by the sum of proton hole pairs with regards to closed $Z = 82$ shell, and neutron hole pairs with regards to closed $N = 126$ shell. The computer code PHINT [17] was used for the diagonalization of the model Hamiltonian in order to obtain corresponding eigenvalues and eigenfunctions in the spherical $U(5)$ basis. The parameters of IBM-1 Hamiltonian (1.15): $\varepsilon', \eta, \chi, \kappa$, and ω, have been varied in order to achieve a best possible agreement with available experimental data in the case of each selected nucleus. These data included the energies of confidently established low-lying levels with spin values $I \leq 8$ (in the case of ground state band), and with $I \leq 6$ (in the case of other collective excitations). In such a way, the entire known low-lying part of the excited level scheme has been involved for the study of nuclear shape phase transition. Usually, only a ground state or a few lowest levels are taken into account (see, e.g., [32]).

Since the IBM-1 Hamiltonian is symmetric with respect to the sign of the prolate-oblate phase transition control parameter χ, we have performed our level energy calculations at $\chi \leq 0$ values, assigning the sign of χ later with regards to the experimentally observed electromagnetic properties (see Fig. 5.3) and taking into account the behaviour of model parameters in neighbouring nuclei.

In order to facilitate the fit of IBM-1 model parameters, their starting values were obtained via the least squares method solution of linear equation systems for experimental and theoretical level energy values either in the

$SU(3)$-limit of axially-symmetric rotator, or in the $O(6)$-limit of γ-unstable nucleus. The hexadecapole deformation term of Eq. (1.15) has been disregarded assuming $\xi = 0$.

In the $SU(3)$-limit, the level energies of IBM-1 are evaluated as [17]:

$$E(N_b, (\lambda, \mu), I) = (k' + \frac{3}{4}k)I(I+1) - kC_2(\lambda, \mu), \tag{5.5}$$

where $k' = \eta/2$, $k = -\kappa/4$, and $C_2(\lambda, \mu) = \lambda^2 + \mu^2 + \lambda\mu + 3(\lambda + \mu)$. The linear equation system for model parameters η and κ included all experimentally known energies of three lowest rotational bands: the $K^\pi = 0^+$ ground state band (up to $I = 8$ level), classified according to quantum numbers of the $SU(3)$ irrep $(\lambda, \mu) = (2N_b, 0)$, and the $K^\pi = 2^+$ γ-vibrational band and the $K^\pi = 0^+$ β-vibrational band (up to $I = 6$ levels), both corresponding to the doubly degenerate band of the $(\lambda, \mu) = (2N_b - 4, 2)$ $SU(3)$ irrep. According to Elliott's classification of $SU(3)$ bands, K and I values assume following values: $K = 0, 2, \ldots, \min(\lambda, \mu)$, and $I = 0, 2, \ldots, \max(\lambda, \mu)$, if $K = 0$; $I = K, K+1, \ldots, \max(\lambda, \mu) + K$, if $K \neq 0$.

Solution of such equation system in the case of each axially-symmetric rotator type nucleus allowed to obtain the starting values for parameters κ and η which give complete IBM-1 Hamiltonian Eq.(1.15) eigenvalues at $\varepsilon' = \omega = \xi = 0$, and $\chi = \pm\sqrt{7}/2$. Further variation of five IBM-1 model parameters allowed to remove a degeneracy of $SU(3)$-bands and to obtain rotational band spectrum typical for deformed even-even nucleus, like that in the case of ^{184}W (see the upper part of Fig. 5.4).

The $O(6)$ classification of states (σ, n_Δ) has been used for nuclei with a non-axial rotator type spectrum. Theoretical level energies in the $O(6)$-limit of IBM-1 are evaluated as [17]:

$$E(N_b, \sigma, \tau, n_\Delta, I) = A(N_b - \sigma)(N_b + \sigma + 4)/4 + B\tau(\tau+3)/6 + CI(I+1), \tag{5.6}$$

where $A = -2\kappa$, $B = 15\omega - 3\kappa$, $C = (\eta - \omega)/2$. Lowest experimental states correspond to (σ, n_Δ) irreps $(N_b, 0)$, $(N_b - 2, 0)$, and $(N_b, 1)$, for which τ assumes values $0, 1, \ldots, 2\sigma$, if $n_\Delta = 0$, and $3n_\Delta, 3n_\Delta + 1, \ldots, \sigma$, if $n_\Delta = 1$. The allowed level spin values are $I = 2\sigma - 3n_\Delta$; $2\sigma - 3n_\Delta - 2$; $2\sigma - 3n_\Delta - 1$; $\ldots$; $\tau - 3n_\Delta$.

For the least squares method solution of the linear equation system, following lowest $O(6)$-limit states have been used (if the corresponding experimental level was established, or surmised from the analogy with neighbouring nuclei): a) the $(\sigma, n_\Delta) = (N_b, 0)$ irrep, describing the stretched

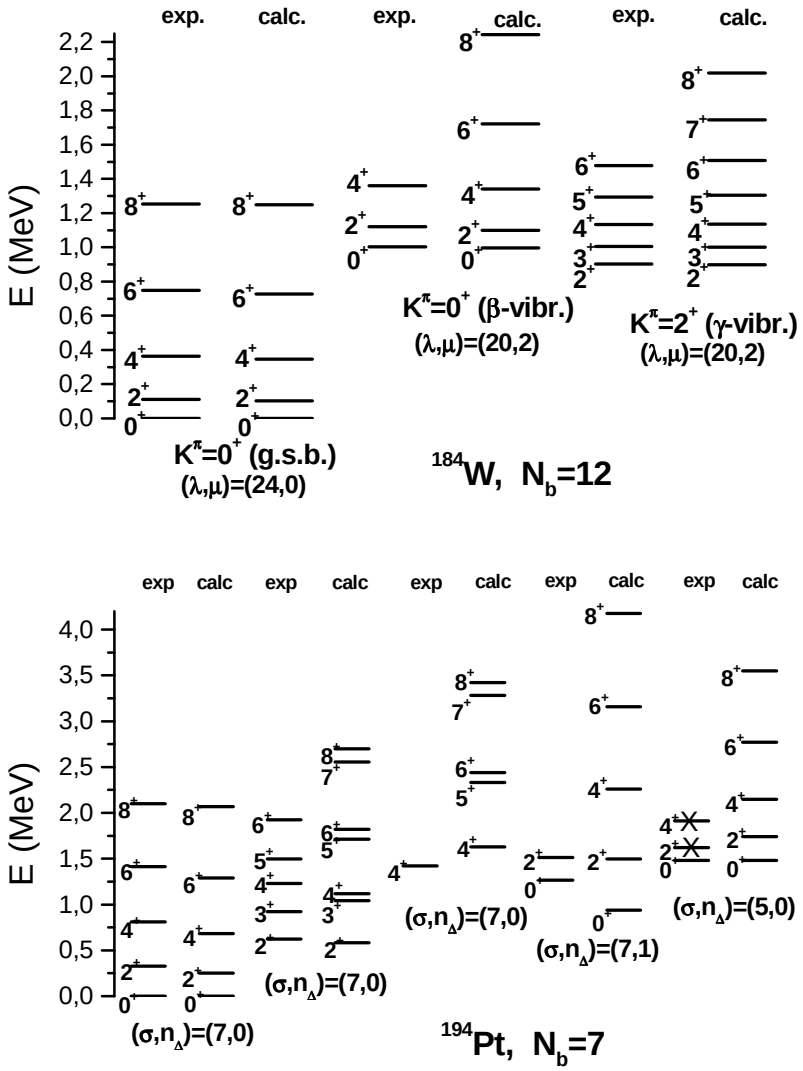

Figure 5.4: Experimental and calculated level energies of low-lying states of ^{184}W, and ^{194}Pt at IBM-1 parameter values given in Table 5.1. Experimental levels marked with crosses have not been used for the fit of model parameters.

$K^\pi = 0^+$ ground state band, the $K^\pi = 2^+$ quasi γ-band, and the $K^\pi = 4^+$ band levels with $\tau = K, 1, \ldots, 2\sigma$; b) the $(\sigma, n_\Delta) = (N_b, 1)$ irrep, describing the second $K^\pi = 0^+$ band, and the third $K^\pi = 2^+$ band levels with $\tau = K + 3n_\Delta, K + 3n_\Delta + 1, \ldots, \sigma$; c) the $(\sigma, n_\Delta) = (N_b - 2, 0)$ irrep, describing the third $K^\pi = 0^+$ band, and the second $K^\pi = 2^+$ band levels with $\tau = K, 1, \ldots, 2\sigma$. In order to resolve the linear equation system, one must include at least one level belonging to the $(\sigma, n_\Delta) = (N_b, 1)$ irrep.

Solution of this linear equation system, in the case of each nucleus having non-axial deformation, allows to obtain the starting approximation for IBM-1 parameters κ, η, and ω, reproducing the complete IBM-1 Hamiltonian Eq. (1.15) eigenvalues at $\varepsilon' = \chi = \xi = 0$. A typical spectrum of the $O(6)$-limit of IBM-1 is presented in the lower half of Fig. 5.4 in the case of ^{194}Pt nucleus.

Then, IBM-1 multipole representation Hamiltonian Eq. (1.15) parameters: ε', η, χ, κ, and ω, were varied in order to achieve a best possible agreement with known experimental low-lying level energies. One should note that the classification of specific levels according to IBM-1 basis states depends on model parameters. So, the IBM-1 band structure, characteristic to initially adopted limiting case, is not conserved when one moves away from the parameter values determined via the solution of corresponding linear equation system. In that sense, the adopted starting approximation is good only for nuclei close either to $SU(3)$- or to $O(6)$-limit. In intermediate positions, which is the case for transitional nuclei when there is a strong mixing of basis states, the notion about regular collective bands has no sense: one has to assign levels according to their spin and energy sequence. This ordering of experimental level energies is most sensitive to the variation of the $SU(3) - O(6) - \overline{SU(3)}$ phase transition control parameter χ.

The obtained values of IBM-1 parameters for all considered tungsten, osmium and platinum isotopes are summarized in Table 5.1. The agreement between experimental and calculated level energies is characterized by the mean square deviation $d = \sqrt{(E_{exp} - E_{calc})^2/m}$, where m is the number of experimental levels included in the fit. One can see that the agreement which can be achieved in the frameworks of IBM-1 improves for nuclei towards the $SU(3)$-limit. In the case of $O(6)$-limit nuclei, the overall quality of the fit for all involved experimental levels is notably worse, and the dependence on χ value is more pronounced. The prolate-oblate phase transition is abrupt, especially for osmium and tungsten nuclei.

It has been found that the employed IBM-1 version does not allow to

describe with good quality all observed low-energy levels of considered nuclei in the vicinity of phase transition critical line $E(5) - O(6)$. If one can successfully reproduce the $K^\pi = 0^+$ ground state band and the $K^\pi = 2^+$ quasi γ-band levels, then, if one includes observed additional collective 0^+ and 4^+ states, they would not fit together. Again, the model parameter values, which improve the description of these additional states, would shift the odd spin levels of the quasi γ-band too far away from their experimental values. Such behaviour can be explained by the complex nature of observed phase transition taking place at different critical parameter χ values in dependence from excitation energy, i.e., one observes a coexistence of prolate and oblate shapes in the same nucleus (see, e.g., [58]).

Farther away from the $O(6)$ critical point, one can successfully describe all experimental levels up to 2.5 MeV with the same IBM-1 parameter set. Moreover, parameter sets for neighbouring nuclei towards the $SU(3)$-limit are similar, which is not the case in the vicinity of the $O(6)$-limit. It means that one should be most careful when adopting for IBM model calculations parameter values used earlier for neighboring nuclei - such approach is not applicable for nuclei belonging to transitional deformation regions.

In the last two columns of Table 5.1, the values of control parameters r_1 and r_2, employed in the catastrophe theory analysis of nuclear shape phase transitions (see Chapter 4), are given. The use of these parameters allows one to associate the complete IBM-1 model parameter set $(\varepsilon', \eta, \kappa, \omega, \xi, \chi)$, obtained for each of considered nuclei, with the point within the "swallow-tail" phase diagram (see Fig. 4.1), characterizing nuclear deformation and its stability. One can evaluate r_1, r_2 values from the ε', η, κ, χ, ω, ξ values via Eqs.(4.3)-(4.4) employing the relationships between parameters of the IBM-1 multipole form Hamiltonian and those of the standard IBM-1 Hamiltonian form (ε, C_0, C_2, C_3, V_2, V_0, u_2, u_0) (see., e.g., [17]). The values of control parameters obtained for $184 \leq A \leq 194$ isotopes of W, Os, and Pt are displayed as points in the (r_1, r_2) parameter space diagram (Fig. 5.5). One can see that all considered nuclei belong to the domain below the r_{12} bifurcation set Eq.(4.14) separating spherical and deformed nuclei.

Now, let us consider the Maxwell sets of points in the (r_1, r_2) parameter space. At these points, the classical energy surface assumes the same value for two or more different critical values of control parameter, i.e., a coexistence of different shapes becomes possible. Maxwell sets, associated with the energy surface minimum (r_{13}^+) and maximum (r_{13}^-) at β_c=0, are given by equation

Table 5.1: IBM-1 parameter values of $184 \leq A \leq 194$ region W, Os, and Pt nuclei

Nucleus	N_b	ε' (MeV)	κ (MeV)	η (MeV)	ω (MeV)	χ	m	d (MeV)	r_1	r_2
^{184}W	12	0.024	-0.03094	0.0263	-0.00420	-1.17170	12	0.0155	-0.87412	1.31552
^{186}W	11	0.017	-0.03096	0.0290	-0.00412	-1.13056	12	0.0451	-0.82056	1.22351
^{188}W	10	0.008	-0.04480	0.0112	0.01080	-0.19230	9	0.0455	-0.57963	0.16004
^{184}Os	12	0.028	-0.03300	0.0272	-0.00340	-1.11133	12	0.0253	-0.82736	1.20022
^{186}Os	11	0.025	-0.04400	0.0276	-0.00420	-0.67082	12	0.0280	-0.74747	0.65199
^{188}Os	10	0.026	-0.07900	0.0170	-0.00700	-0.31305	11	0.0775	-0.79163	0.30385
^{190}Os	9	0.010	-0.07500	0.0142	0.00100	-0.10733	13	0.0907	-0.70298	0.09769
^{192}Os	8	0.005	-0.06650	0.0185	0.00160	-0.11180	13	0.1069	-0.63925	0.09788
^{194}Os	7	0.005	-0.09500	0.0150	-0.00200	0.12969	7	0.0657	-0.67312	-0.11630
^{184}Pt	12	0.015	-0.02440	0.0175	0.01360	-0.55902	12	0.0970	-0.43119	0.42030
^{186}Pt	11	0.015	-0.02450	0.0195	0.01100	-0.55902	12	0.0631	-0.42336	0.42120
^{188}Pt	10	0.012	-0.04000	0.0255	0.00900	-0.15652	11	0.0977	-0.50327	0.12400
^{190}Pt	9	0.009	-0.08100	0.0190	0.00235	-0.06261	13	0.0891	-0.68075	0.05615
^{192}Pt	8	0.013	-0.08400	0.0195	0.00300	0.00894	12	0.1471	-0.63467	-0.00780
^{194}Pt	7	0.005	-0.09200	0.0195	0.00210	0.08050	13	0.1445	-0.61535	-0.06942

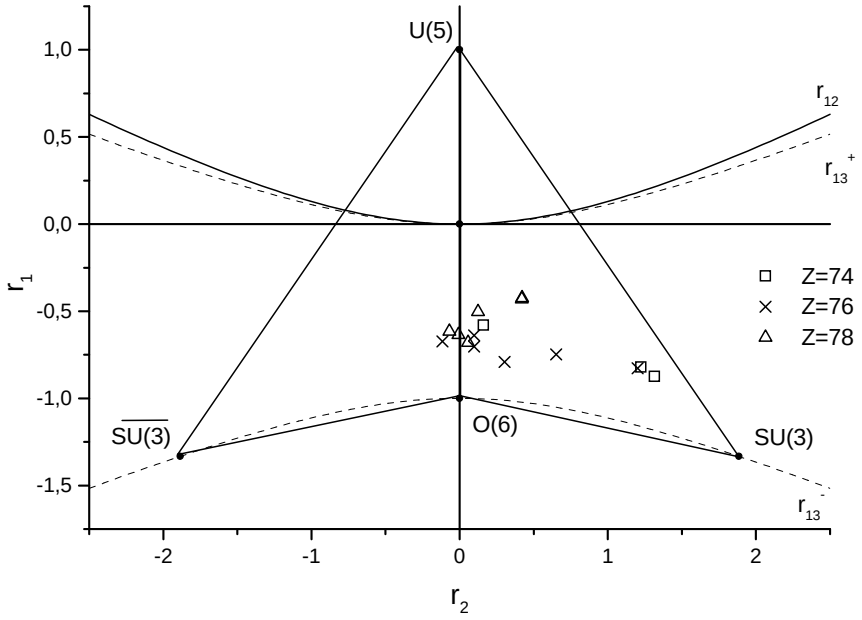

Figure 5.5: The values of catastrophe theory control parameters r_1, r_2 obtained for W, Os, and Pt nuclei with $184 \leq A \leq 194$.

[20]:

$$r_{13}^{\pm} = -\frac{1}{2} \pm \frac{1}{2}\sqrt{1+\frac{r_2^2}{2}}. \tag{5.7}$$

Another Maxwell set - for $\beta_c = \sqrt{r_1}$, forms a locus of points on the negative r_1 semi-axis at r_2=0; this set of points coincides with the $E(5)-O(6)$ critical line between prolate $r_2 > 0$, and oblate $r_2 < 0$ deformed shapes.

The study of the minima of complete IBM-1 version classical energy functional (see Sect. 4.2) shows that it has a well defined prolate minimum ($\beta > 0$) in the region $r_{13}^{-} < r_1 < 0$ in which the values of control parameters for all considered $184 \leq A \leq 194$ nuclei are located. An additional oblate minimum is a saddle point, unstable with respect to nuclear asymmetry parameter γ. It means that at higher excitations both prolate and oblate structures are allowed, and a possibility of such coexistence grows when r_1 value approaches zero. When $\beta < 0$, the picture is mirror symmetric with respect to r_1 negative semi-axis: one has a stable oblate minimum with a γ-unstable prolate saddle point.

As one can expect, the ^{184,186}W nuclei are close to the stable axially-deformed $SU(3)$-limit. Those of considered nuclei which have $|r_2| \leq 0.2$ (see Table 5.1) are situated in the region where nuclear shape changes from prolate to oblate. It has been shown in [45] that χ is the control parameter of a prolate-oblate phase transition with critical point at $\chi = 0$ corresponding to $O(6)$-limit. In reality, this phase transition can occur at any point on the line connecting the $E(5)$ triple point of the Casten's triangle with the $O(6)$-symmetry point in the middle of the line connecting maximal quadrupole deformation points $SU(3)$ and $\overline{SU(3)}$. We have assigned plus sign to χ values of ^{192,194}Pt nuclei with regard to their experimental electric quadrupole moment Q values (see Sect. 5.1). The plus sign for χ value of ^{194}Os, for which there are no Q measurement data, is predicted from the observed dependence of r_2 values in neighboring osmium nuclei. The obtained location of (r_1, r_2) points for ^{184,186}Pt indicate that these nuclei have prolate ground state band and oblate excited bands. With high probability, similar shape coexistence is present also in the case of ^{188}W.

Fig. 5.6 presents the $SU(3) - O(6) - \overline{SU(3)}$ phase transition control parameter χ values in dependence from the neutron number N for each of three isotope chains. For comparison, the corresponding parameter values used for the analysis of prolate-oblate phase transition in Ref.[32] are given as well. The authors of [32] employed the two-parametric Casten's version of IBM-1

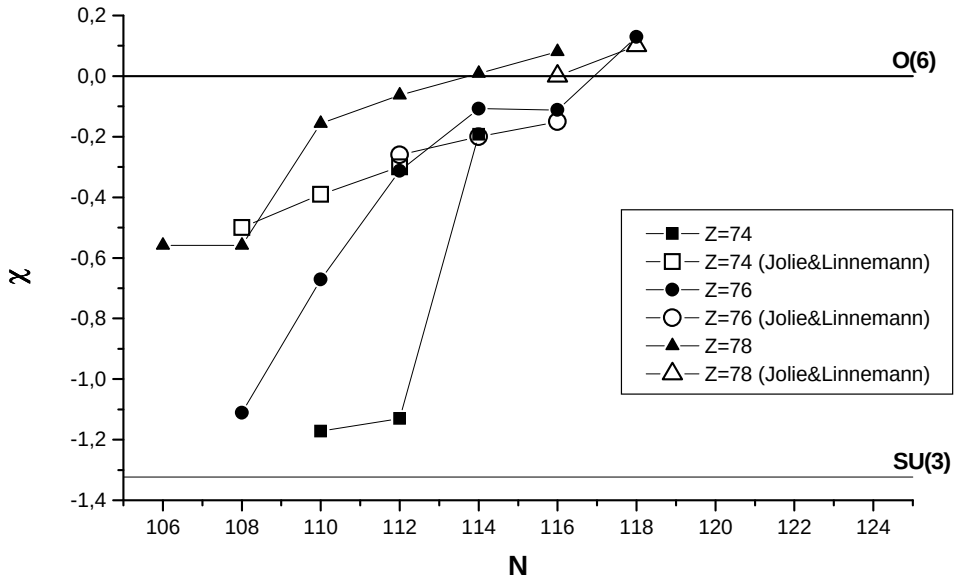

Figure 5.6: Behaviour of control parameter χ in dependence from N for W, Os, and Pt nuclei with $184 \leq A \leq 194$.

with model parameter η fixed at $\eta = 0$. Greatest difference between the results of both approaches is observed for tungsten nuclei with $N \leq 112$ which are farther away from the critical line $E(5) - O(6)$, and which display properties inherent to axially-symmetric rotators. Also, the authors of [32] have not considered the lighter isotopes of platinum and assumed that the nucleus most close to the $O(6)$ phase transition point is ^{194}Pt. Our results, obtained via the fit of complete IBM-1 Hamiltonian eigenvalues to the experimental energies of all low-lying experimental levels, indicate that phase transition occurs already in the case of ^{192}Pt.

The quality of obtained description of the prolate-oblate phase transition can be assessed via a comparison of experimental (see Sect. 5.1) and calculated R_4, R_2, and R_{asym} ratios in dependence from the value of control parameter χ (see Fig. 5.7). One can see that, in most cases, the calculated R_4

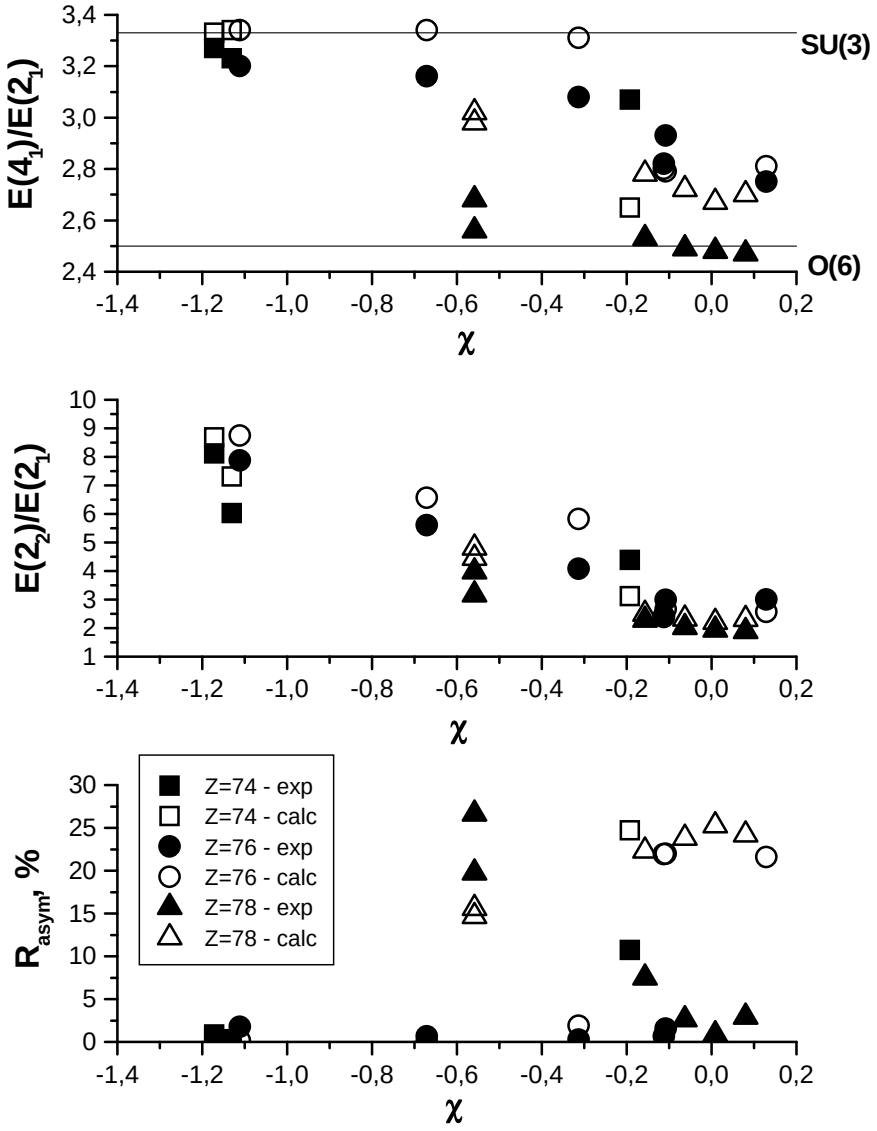

Figure 5.7: Comparison of experimental and calculated values of R_4, R_2, and R_{asym} ratios in dependence from the $SU(3) - O(6) - \overline{SU(3)}$ phase transition control parameter χ for W, Os, and Pt nuclei with $184 \leq A \leq 194$.

ratio exceeds the experimental one. This difference grows when one transits from the axially-symmetric $SU(3)$-limit to the $O(6)$-limit, where, as it has been already noted above, ground state band and excited bands can have different deformations - nuclear shape is soft. Such shape coexistence prevents one to describe successfully all levels with the same set of IBM-1 Hamiltonian parameters. The agreement between experimental and calculated R_2 ratios is much better, while the triaxiality criterion R_{asym} agrees with its experimental value only for W and lighter Os nuclei. In the vicinity of $E(5)-O(6)$ phase transition critical line, large values of R_{asym} ratio indicate a considerable influence of the concurrent deformed-to-spherical phase transition when N approaches the $N = 126$ shell closure. Obviously, although IBM-1 allows one to establish the fact of shape phase transition, it fails to provide a satisfactory description of the structure of specific nucleus belonging to the critical region. For that purpose, one must employ more refined mean-field based calculation methods (see, e.g., [58]).

5.3 Behaviour of quantum chaos criteria in the nuclear shape phase transition region at $A \sim$190

In order to study relationships between nuclear shape phase transition and quantum chaos in the $A \sim$190 region, we have performed the analysis of statistical and dynamical quantum chaos criteria in dependence from the $SU(3) - O(6) - \overline{SU(3)}$ phase transition control parameter χ, as well as in terms of catastrophe theory essential control parameters r_1, r_2 (see Table 5.1).

At first, let us consider the statistical criteria of quantum chaos - the nearest level spacing distribution $P(S)$. For this purpose, we have taken all obtained IBM-1 eigenvalues with spins ranging from 0 to 8 and created the unfolded theoretical energy spectrum for each nucleus. We have not included all allowed theoretical IBM-1 states for the sake of comparison and in order to minimize the effect due to model basis cutoff, which becomes notable at higher spins for nuclei with relatively small N_b values. The assessment of the effect due to inclusion of higher spin states has shown that, e.g., in the case of $N_b = 12$ when the number of additional levels (up to $I_{max} = 24$) is maximal, one obtains the same form $P(S)$ distribution with less than 7% change of its maximum value.

Table 5.2: Results of the fit of nearest level spacing distributions $P(S)$ for $184 \leq A \leq 194$ W, Os, and Pt nuclei.

Nucleus	N_b	m'	$< S >$	σ_S^2	ζ	d'
^{184}W	12	205	0.0252	0.0017	0.000	0.041
^{186}W	11	169	0.0267	0.0020	0.000	0.050
^{188}W	10	137	0.0476	0.0183	0.000	0.623
^{184}Os	12	205	0.0265	0.0020	0.000	0.041
^{186}Os	11	169	0.0306	0.0023	0.000	0.052
^{188}Os	10	137	0.0453	0.0028	0.000	0.052
^{190}Os	9	108	0.0452	0.0024	0.056	0.046
^{192}Os	8	83	0.0474	0.0022	0.081	0.024
^{194}Os	7	61	0.0636	0.0034	0.606	0.028
^{184}Pt	12	205	0.0427	0.0096	0.000	0.169
^{186}Pt	11	169	0.0396	0.0042	0.120	0.010
^{188}Pt	10	137	0.0454	0.0029	0.000	0.033
^{190}Pt	9	108	0.0525	0.0029	0.169	0.011
^{192}Pt	8	83	0.0604	0.0036	0.307	0.025
^{194}Pt	7	61	0.0696	0.0044	0.112	0.025

It is well known (see, e.g., [34]), that for regular (integrable) systems $P(S)$ values should obey the Poisson distribution, while in the case of totally chaotic system - the GOE Wigner distribution is expected. In order to trace the deviation from the integrable IBM-1 limiting case, we have performed for each nucleus the least-squares fit of obtained $P(S)$ values employing the well-known Brody distribution Eq. (1.24). For comparison between different nuclei, we have normalized S by its mean value $< S >$ and $P(S/ < S >)$ normalized to 1. The results of the fit of Brody parameter ζ in the case of all 15 considered nuclei are presented in Table 5.2. Quality of the least-squares fit is characterized by $d' = \sum_{i=1}^{m'}(P(S/ < S >) - P_B(S/ < S >))^2$, where m' is the number of level spacings. Additional characteristics of the $P(S)$ distribution are the mean value of S and its variance σ_S^2. Increased mixing is indicated by the growth of mean level spacings when one moves away from the $SU(3)$-limit.

One can see that the form of $P(S)$ distribution changes very slowly from the $SU(3)$-limit side: in the case of W and Os nuclei with $A \leq 188$, one

cannot practically distinguish $P(S)$ from the Poisson form. On the contrary, in the vicinity of the $E(5) - O(6)$ critical line, a drastic change of chaoticity between neighboring isotopes is observed reflecting instability of nuclear shape and complex nature of observed phase transition. Fig. 5.8 presents histograms of normalized theoretical level spacings $< S >$ for three osmium nuclei: ^{184}Os, ^{190}Os, and ^{194}Os. One can see the transition from Poisson distribution in the case of axially-symmetric ^{184}Os to the almost Wigner-type distribution in the case of ^{194}Os, characterized by considerable mixing of IBM-1 basis states. Dependence of the fitted Brody parameter ζ values from the $SU(3) - O(6) - \overline{SU(3)}$ phase transition critical parameter χ for W, Os, and Pt is shown on Fig. 5.9.

In addition, we have studied the dependence of IBM-1 nearest level spacings from the nuclear spin I. Table 5.3 presents the results obtained for spin values $I = 0, 2, 4$: energy ratios of levels with these spin values characterize the type of nuclear deformation (see Sect. 5.1). Because of the small number of involved eigenvalues, we have not performed the fit of Brody parameter ζ for individual spin values: $P(S)$ distributions are characterized by $< S >$, and σ_S^2 values.

When I value increases, the mean level spacing value $< S >$ becomes smaller. The greatest mixing is observed in the case of IBM-1 states with $I = 0$. If one considers $< S >$ values of $I = 0$ states in different nuclei, one can see the increase of mean level spacings when χ decreases from $-\sqrt{7}/2$ at $SU(3)$-limit to 0 at $O(6)$-limit. These spacings increase again when one observes the oblate-to-spherical nuclear shape change (see Sect. 5.2). This effect is most pronounced in the case of osmium nuclei. The least chaotic of platinum isotopes are ^{186,188}Pt, which is indicated also by their Brody distribution coefficients (see Table 5.2). The growth of mixing for ^{190,192,194}Pt coincides with the approach to the deformed-to-spherical phase transition along the $E(5) - O(6)$ critical line.

Statistical quantum chaos criterion $P(S)$ characterizes the distribution of Hamiltonian eigenvalues and, therefore, it is independent from the model diagonalization basis. Behaviour of system's dynamical quantum chaos criteria characterizes its deviation from the symmetry properties inherent to the Hamiltonian of the chosen regular system. Wave function entropy $W(\Psi_i)$, just like fragmentation width of basis states $\kappa(\Phi_k)$, or any other dynamical quantum chaos criterion, evaluated using wave functions of considered states, depends on the choice of Hamiltonian diagonalization basis. Complete IBM-1 Hamiltonian is usually diagonalized in the $U(5)$-symmetric basis of

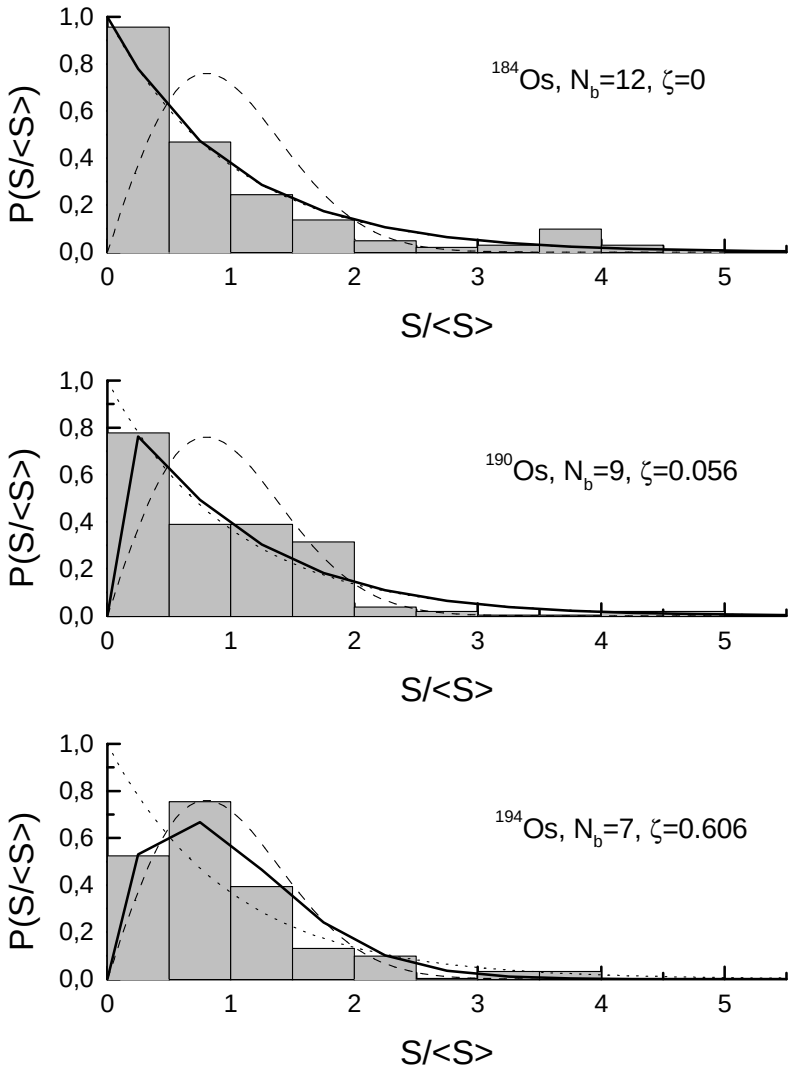

Figure 5.8: Nearest level energy spacing distributions $P(S/ < S >)$ for Os nuclei in the $184 \leq A \leq 194$ transitional deformation region. Solid line represents the fitted Brody distribution curve, while dotted line corresponds to Poisson distribution and dashed line to Wigner distribution.

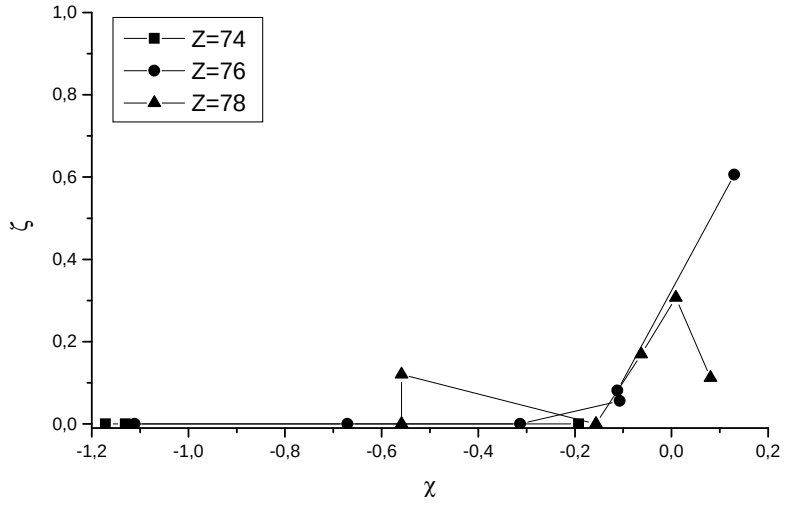

Figure 5.9: Values of Brody distribution parameter ζ in dependence from the phase transition control parameter χ for tungsten, osmium, and platinum nuclei with $184 \leq A \leq 194$.

Table 5.3: Characteristics of IBM-1 nearest level spacing distributions at spin values $I = 0, 2, 4$

Nucl.	N_b	I	m'	$< S >$	σ_S^2	Nucl.	N_b	I	m'	$< S >$	σ_S^2
^{184}W	12	0	18	0.2521	0.0474	^{184}Pt	12	0	18	0.4801	0.3784
		2	29	0.1528	0.0260			2	29	0.2515	0.0425
		4	35	0.1217	0.0215			4	35	0.2350	0.0558
^{186}W	11	0	15	0.2527	0.0430	^{186}Pt	11	0	15	0.3415	0.0804
		2	25	0.1465	0.0234			2	25	0.2514	0.0715
		4	29	0.1220	0.0178			4	29	0.2085	0.0394
^{188}W	10	0	13	0.4172	0.0937	^{188}Pt	10	0	13	0.3599	0.0706
		2	21	0.3016	0.0811			2	21	0.2602	0.0598
		4	24	0.2515	0.0783			4	24	0.2169	0.0502
^{184}Os	12	0	18	0.2603	0.0549	^{190}Pt	9	0	11	0.4608	0.0878
		2	29	0.1588	0.0313			2	17	0.2791	0.0645
		4	35	0.1270	0.0258			4	19	0.2425	0.0254
^{186}Os	11	0	15	0.2953	0.0509	^{192}Pt	8	0	9	0.4720	0.1263
		2	25	0.1727	0.0189			2	14	0.3014	0.0762
		4	29	0.1443	0.0170			4	15	0.2612	0.0344
^{188}Os	10	0	13	0.4583	0.0807	^{194}Pt	7	0	7	0.5046	0.1039
		2	21	0.2729	0.0184			2	11	0.3109	0.0752
		4	24	0.2311	0.0186			4	11	0.2827	0.0340
^{190}Os	9	0	11	0.4009	0.0796						
		2	17	0.2516	0.0442						
		4	19	0.2115	0.0183						
^{192}Os	8	0	9	0.3616	0.0688						
		2	14	0.2275	0.0341						
		4	15	0.1973	0.0179						
^{194}Os	7	0	7	0.5037	0.0850						
		2	11	0.3153	0.0548						
		4	11	0.2780	0.0174						

the five-dimensional spherical harmonic oscillator eigenfunctions, while the prolate-to-oblate shape phase transition is mostly analyzed in the $SU(3)$-symmetric axial-rotator wave function basis (see, e.g., [45]).

However, we have already noted that, for nuclei belonging to the $A \sim 190$ region, the $O(6)$ critical point should be considered rather as the $E(5) - O(6)$ critical line with a considerable influence from the deformed-to-spherical transition. Therefore, we believe that it is justified to perform the IBM-1 Hamiltonian diagonalization in the spherical $U(5)$-limit basis and consider the critical behaviour of dynamical quantum chaos criteria from that point of view.

At first, let us analyze the evaluated $W^{U(5)}(\Psi_i)$ values in dependence from the $SU(3)-O(6)-\overline{SU(3)}$ phase transition control parameter χ (see Fig. 5.10). For comparison, we display also the $W^{U(5)}(\Psi_i)$ values evaluated at χ ranging from $-\sqrt{7}/2$ to 0: for $N_b = 12$, at fixed $SU(3)$-limit parameter values derived for ^{184}W via the solution of linear equation system (5.5) (ε'=0; η=0.023921; κ=-0.025448; ω=0; ξ=0), and for $N_b = 7$, at fixed $O(6)$-limit parameter values derived for ^{194}Pt via the solution of linear equation system (5.6) (ε'=0; η=0.021142; κ=-0.082184; ω=0.004875; ξ=0). One can see that $W^{U(5)}(\Psi_i)$ attains its maximal value in the $SU(3)$-limit and gradually decreases towards the $O(6)$ critical point. The slope of this dependence increases with the boson number N_b, which corresponds to experimentally observed picture that the phase transition in the case of tungsten isotopes is more abrupt than in the case of platinum [58].

Let us consider the $W^{U(5)}(\Psi_i)$ values for 5 lowest states (0_1^+, 2_1^+, 4_1^+, 2_2^+, 3_1^+) listed in Table 5.4. Besides the calculated IBM-1 wave function entropy value, we give its ratio (in %) to the maximal possible entropy value for the given number n of diagonalized matrix basis states $W_{max} = \ln(n)$. This maximal value corresponds to the theoretical case when mixed wave function components are uniformly spread over all n basis states [38].

The analysis of obtained data allows to make following conclusions:

a) maximal dynamical quantum chaos criteria values, for all $184 \leq A \leq 194$ W, Os, and Pt nuclei, except ^{192}Pt, are obtained for states with spin values $I = 2$. That differs from the case of statistical chaos (see Table 5.3), when maximal chaoticity in all cases was observed for $I = 0$ states. Though, if one considers dynamical chaos relative to corresponding $W_{max}(n)$ value, then one obtains maximal ratio in the case of $I^+ = 0_1^+$ ground state for nuclei in the vicinity of critical line $E(5) - O(6)$;

b) the values of dynamical chaos criteria decrease towards $E(5) - O(6)$

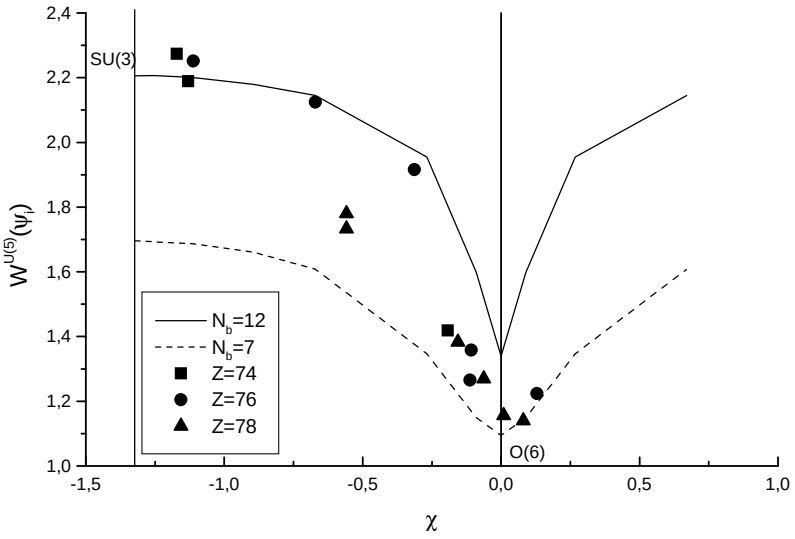

Figure 5.10: Values of the $I = 0^+$ ground state wave function entropy $W^{U(5)}(\Psi_i)$ in dependence from phase transition control parameter χ for $184 \leq A \leq 194$ W, Os, and Pt nuclei. Solid line shows the theoretical χ-dependence for $N_b = 12$ (at ^{184}W $SU(3)$-limit parameters), while dashed line – for $N_b = 7$ (at ^{194}Pt $O(6)$-limit parameters).

Table 5.4: Wave function entropy values for low-lying states of $184 \leq A \leq 194$ W, Os, and Pt nuclei.

Nucleus	N_b	$I^\pi = 0_1^+$			$I^\pi = 2_1^+$			$I^\pi = 4_1^+$			$I^\pi = 2_2^+$			$I^\pi = 3_1^+$		
		W	n	%	W	n	%	W	n	%	W	n	%	W	n	%
^{184}W	12	2.274	19	77.2	2.744	30	80.7	2.741	36	76.5	2.821	30	82.9	2.014	12	81.0
^{186}W	11	2.189	16	79.0	2.646	26	81.2	2.628	30	77.3	2.713	26	83.3	1.891	10	82.1
^{188}W	10	1.419	14	53.8	1.615	22	52.2	1.521	25	47.3	1.549	22	50.1	1.094	8	52.6
^{184}Os	12	2.251	19	76.5	2.711	30	79.7	2.699	36	75.3	2.805	30	82.5	1.982	12	79.8
^{186}Os	11	2.124	16	76.6	2.553	26	77.6	2.484	30	73.0	2.639	26	81.0	1.754	10	76.2
^{188}Os	10	1.916	14	72.6	2.237	22	72.4	2.143	25	66.6	2.362	22	76.4	1.363	8	65.6
^{190}Os	9	1.358	12	54.6	1.536	18	53.2	1.426	20	47.6	1.458	18	50.5	0.993	7	51.0
^{192}Os	8	1.265	10	54.9	1.399	15	51.7	1.271	16	45.8	1.300	15	48.0	0.869	5	54.0
^{194}Os	7	1.224	8	58.9	1.372	12	55.2	1.209	12	48.7	1.249	12	50.3	0.721	4	52.0
^{184}Pt	12	1.780	19	60.4	2.067	30	60.4	1.999	36	55.8	2.079	30	61.1	1.331	12	53.6
^{186}Pt	11	1.733	16	62.5	2.014	26	61.8	1.939	30	57.0	2.010	26	61.7	1.257	10	54.6
^{188}Pt	10	1.383	14	52.4	1.546	22	50.0	1.453	25	45.1	1.477	22	47.8	1.084	8	52.1
^{190}Pt	9	1.269	12	51.1	1.346	18	46.6	1.246	20	41.6	1.264	18	43.7	0.981	7	50.4
^{192}Pt	8	1.156	10	50.2	1.100	15	40.6	1.001	16	36.1	1.002	15	37.0	0.855	5	53.1
^{194}Pt	7	1.140	8	54.8	1.169	12	47.0	1.022	12	41.1	1.042	12	41.9	0.712	4	51.4

critical line, along with the value of the prolate-oblate phase transition control parameter χ, and towards the r_{12} bifurcation set, along with the value of control parameter $|r_1|$ (see Table 5.1). Such behaviour is characteristic to IBM-1 wave functions evaluated in the spherical $U(5)$ basis;

c) in the case of nuclei with $SU(3)$-type spectrum, maximal wave function entropy values are obtained for $I = 2_2$ states, i.e., the $K^\pi = 2^+$ γ-vibration band-heads, while in the case of nuclei with $O(6)$-type spectrum, maximal wave function entropy values are inherent to levels of the $K^\pi = 0^+$ ground state band;

d) in each isotope chain, the least dynamical chaos level is obtained for nuclei which are closest to the prolate-oblate shape phase transition critical line $E(5) - O(6)$: the ^{188}W, ^{190}Os, and ^{192}Pt, correspondingly.

Finally, let us compare the behaviour of quantum chaos criteria calculated using algebraic complete IBM-1 version with those obtained in the frameworks of geometric rigid triaxial rotator models (see Sect. 3.2). The dependence of the wave function entropy from the nuclear quadrupole deformation parameters β and γ is shown on Fig. 3.4. One can note that the entropy in the case of rigid triaxial rotator model rapidly increases towards $\gamma = 30^\circ$. The dependence from the quadrupole deformation parameter β is weaker, displaying the decrease of wave function entropy for greater β values.

Now, one should take into account that minima of the classical energy of IBM-1 Hamiltonian Eq.(4.6) do not depend on the nuclear asymmetry angle γ value, i.e., the obtained energy saddle-points are γ-unstable [20]. However, it is generally assumed that $\gamma = 0^\circ$ in the $SU(3)$-limit of prolate deformation, $\gamma = 30^\circ$ in the γ-unstable $O(6)$-limit, and $\gamma = 60^\circ$ in the case of oblate $\overline{SU(3)}$-symmetric rotator. The $O(6)$-limit is the critical point both for β- and γ-deformations. Experimental data do not provide a distinction between static and dynamic nuclear triaxiality (see Sect. 5.1). Therefore, such comparison between IBM-1 and rigid triaxial rotator results can take place.

However, in order to perform quantitative comparison of dynamical quantum chaos criteria evaluated in the frameworks of both model approaches, one should use IBM-1 wave functions obtained via the diagonalization of model Hamiltonian in the axially-symmetric $SU(3)$-limit wave function basis, employed also for the diagonalization of geometrical rigid triaxial rotator model Hamiltonians.

Values of quadrupole deformation parameter β for considered nuclei can be evaluated from corresponding r_1, r_2 values via the expressions for the cubic

equation (4.10) roots. The effective asymmetry angle γ_{eff} one can derive from the theoretical level energies of 2_1, and 2_2 levels. Another possibility is to associate nuclear effective triaxiality directly with the fitted value of control parameter χ. Such detailed comparison is a theme for future studies.

Chapter 6

Conclusions

6.1 Summary of main results

Let us characterize the fulfillment of aims set for this dissertation work (see Sect. 1.3) by summarizing the results obtained in our studies of nuclear shape phase transitions and quantum chaos in the frameworks of geometrical and algebraic models of even-even nuclei.

1. Precise analytical expressions for the classical energy functional E_{cl} minima conditions in terms of nuclear quadrupole deformation parameter β have been obtained in the case of several algebraic interacting boson model versions:

a) the simplified two-parameter Casten's version of IBM-1;

b) the $O(6)$-limit Hamiltonian with included cubic d-boson interaction;

c) the $O(6)$-limit Hamiltonian with included cubic quadrupole operator term $[\mathbf{QQQ}]^{(0)}$ in two variants - the $O(6)$-symmetry conserving, and the $O(6)$-symmetry non-conserving;

d) the complete IBM-1 version depending on six model parameters.

Corresponding classical energy surfaces have been analyzed in terms of spherical-to-deformed and prolate-to-oblate nuclear shape phase transitions in dependence on IBM-1 model parameter values. It has been found that:

a) the results of our approach to the minimum problem of the classical energy functional in the case of simplified Casten's version of IBM-1 allow one to obtain precise values of deformation parameter β at each (η, χ) point of Casten's triangle. The obtained roots β_{0i} $(i = 1, 2, 3)$ of the cubic equation for the E_{cl} minima condition are complicated and, in general, complex functions

from the total boson number N_b and IBM-1 model parameters, that are well suited for the analysis of phase transition lines and critical points, as well as for other studies involving the considered model;

b) in the case of $O(6)$-limit IBM-1 Hamiltonian with cubic d-boson interaction term, one can obtain the minimum of E_{cl} expression corresponding to stable triaxial deformation only if one takes into account the sum of all three-boson interaction terms with moments $L' = 0, 3, 4, 6$, and not just the $L' = 3$ term, as it has been supposed earlier. Also, it has been shown that this triaxial shape minimum is an effect due to finite number of bosons, disappearing at $N_b \to \infty$;

c) in the case of $O(6)$-limit Hamiltonians with attached cubic $[\mathbf{QQQ}]^{(0)}$ term, the main attention has been given to the study of regions where E_{cl} expression minima condition equations have only complex roots. The boundaries of these regions define phase transition from the spherical shape to the deformed ones. Also, the conditions for the prolate-oblate phase transition, as well as for the triple point of deformations have been analyzed. Analysis has been performed in the case of two versions of the model Hamiltonian - the $O(6)$-symmetric and the $O(6)$-non-symmetric.

In the case of $O(6)$-symmetric model version, our results, obtained employing a precise solution method, have shown that the spherical shape region forms a closed ellipsoid like figure, contrary to the earlier results obtained in Ref. [30]. The analysis of shape phase transition conditions in the case of $O(6)$-non-symmetric Hamiltonian version was not given previously by other authors;

d) the detailed analysis of minima conditions for the classical energy functional $E_{cl}(r_1, r_2; \beta)$ of complete IBM-1, performed using precise expressions for three roots β_{0i} $(i = 1, 2, 3)$ of the cubic equation, similar to that in the case of simplified Casten's version, allowed to obtain coordinates for phase transition critical lines and points in the space of catastrophe theory essential control parameters r_1 and r_2. The properties of real and imaginary parts of roots β_{0i} have been analyzed in the "spherical" and "deformed" parts of the control space diagram;

e) the classical energy E_{cl} minima conditions obtained using the precise solution method have been compared with the ones obtained employing the approach of the Landau theory of phase transitions, in which the higher order terms of E_{cl} expansion are disregarded. In the case of simplified Casten's version of IBM-1, the qualitative conclusions drawn in our analysis of phase transition critical lines and points are similar to those obtained employing the

Landau theory approach. However, the results of the analytical solution of the classical energy minimum problem allow to obtain more precise numerical values of β_0 and $E_{cl}(N_b, \eta, \chi; \beta_0)$.

In the case of complete IBM-1 version, the effects due to accounting of higher order terms of E_{cl} expansion have been assessed. It has been found that, in order to obtain the classical energy minima condition similar to that obtained via a precise solution method, one should take into account in such E_{cl} expansion all power terms up to β^5. The usual practice to consider just $\sim \beta^2$ and $\sim \beta^3$ terms can give distorted results. Therefore, if one can obtain precise analytical solutions of equations for the classical energy functional minimum conditions, then such approach to the study of nuclear shape phase transitions is preferable to the use of approximate Landau theory method.

2. Statistical - the nearest level energy spacing distribution $P(S)$, and dynamical - the wave function entropy $W(\Psi_i)$ and fragmentation of basis states $\kappa(\Phi_k)$, quantum chaos criteria have been evaluated in the frameworks of algebraic simplified Casten's version of IBM-1, and in the case of two geometric rigid triaxial rotator models of even-even nuclei - Davydov's model, depending on asymmetry angle γ only, and Bravin-Fedorov's model, depending on both quadrupole deformation parameters γ and β. Behaviour of quantum chaos criteria has been analyzed both in terms of nuclear quadrupole deformation parameters and in terms of shape phase transition control parameters in the space of Casten's triangle. Dependence from nuclear spin and rank of diagonalized model Hamiltonian matrix has been studied as well.

In the case of simplified Casten's version of IBM-1, values of statistical and dynamical quantum chaos criteria have been calculated at $N_b = 8$ in selected points within the (η, χ) parameter space represented by Casten's triangle. Values of model parameters have been chosen in the range from below the $X(5) - E(5) - \overline{X(5)}$ phase transition line separating spherical and deformed shapes to the $SU(3) - O(6) - \overline{SU(3)}$ line corresponding to the maximal deformation.

The results of quantum chaos statistical criterion calculations show that the simplified Casten's version of IBM-1 at $N_b = 8$ is quite regular. The deviation of nearest level spacings distributions $P(S)$ from the Poisson form is very slight even in the case of maximal mixing farther away from the vertexes of Casten's triangle. At such relatively low boson numbers, $P(S)$ distribution is strongly influenced by the model basis cut-off which affects the energies of higher spin states.

The results of dynamical quantum chaos criteria calculations show that,

on the $U(5)-SU(3)$ line and in the area near it (with $\chi = 0.75 \cdot \chi_{max}$), the behaviour of $\kappa(\Phi_k)_{av}$ and $W(\Psi_i)_{av}$ values is correlated: increasing from the middle part (with $0.75 \cdot \eta_{E(5)} = 0.5625$) to the bottom line ($\eta = 0$). The correlation between $\kappa(\Phi_k)_{av}$ and $W(\Psi_i)_{av}$ values with respect to parameter χ value, when it changes in the direction from the $X(5)-SU(3)$ line towards the first order phase transition line $E(5)-O(6)$, is lost when mixing increases.

The results of quantum chaos calculations in the case of Davydov's model and in the case of Bravin-Fedorov's model, performed at three different β values, have shown that the behaviour of quantum chaos criteria in the case of rigid triaxial rotator depends mostly on the triaxiality angle γ, the dependence on β is negligible. Maximal values of dynamical quantum chaos criteria are attained at $\gamma = 30^\circ$ both for even and odd spin I values. Statistical chaoticity of the rigid triaxal rotator is maximal ($\zeta = 1$) at $18^\circ \leq \gamma \leq 29^\circ$; system's regularity increases again at $\gamma = 30^\circ$.

In the case of geometrical rigid triaxial rotator models, it has been shown that the averaged wave function entropy values $W(\Psi_i)_{av}$, even at maximal mixing of basis states (at $\gamma = 30^\circ$), reach only about 75-85 % of the theoretically possible maximal $W(\Psi_i)_{max}$ values. It indicates that the intrinsic structure of the rigid triaxial rotator model does not allow a higher degree of chaoticity with respect to axially-symmetric rotator eigenfunction basis. Due to the need to control the fulfillment of the condition (1.28), imposed on mixing amplitudes of involved states, one can evaluate another dynamical quantum chaos criterion $\kappa(\Phi_k)$ only if the mixing of basis states exceeds certain limit, i.e. in the case of large asymmetry angle values.

The results of quantum chaos dynamical criteria calculations in the case of Davydov's and Bravin-Fedorov's models show that the values of both criteria: $W(\Psi_i)$ and $\kappa(\Phi_k)$, become smaller when the value of quadrupole deformation parameter β is increased, which is as expected since the unperturbed system is an axially-symmetric rotator.

The analysis of obtained theoretical energy spectra of rigid triaxial rotator models allowed to obtain characteristic maxima of energy level density and wave function entropy at $E_{tr} \approx (b/2)I^2$, corresponding to the transition from the rotational type level sequence to the librational one. Such transition demonstrates [13] that the quantum statistics of the rigid triaxial rotator model behaves analogously to that of another anomalous quantum system - the one-dimensional harmonic oscillator. This transition has been studied in dependence from I and γ in the case of Davydov's model and in dependence from I, β, and γ in the case of Bravin-Fedorov's model.

3. A possibility to use the basis state fragmentation $\kappa(\Phi_k)$ as the dynamical quantum chaos criterion has been studied in the case of algebraic Casten's version of IBM-1, and in the case of geometrical rigid triaxial rotator models. It has been shown that $\kappa(\Phi_k)$ can be successfully applied for characterization of quantum chaos inherent to model Hamiltonian with respect to chosen eigenfunction basis of unperturbed quantum system, just like the generally used wave function entropy $W(\Psi_i)$. The correlation between both criteria has been observed in the inner regions of Casten's triangle below the $X(5) - E(5) - \overline{X(5)}$ first order phase transition line between spherical and deformed shapes in the direction of the $SU(3) - O(6) - \overline{SU(3)}$ basis line.

The use of basis state fragmentation width criterion allows one to apply additional grouping of model Hamiltonian states according to their $\kappa(\Phi_k)$ value: separating soft quantum chaos states with $\kappa(\Phi_k) < 1$, and hard quantum chaos states with $\kappa(\Phi_k) > 1$. The averaged $\kappa(\Phi_k)_{av}$ values then characterize the dynamical chaoticity of the perturbed system as a whole. It has been found that the theoretically predicted transition from the soft chaos to the hard chaos, in the case of rigid triaxial rotator models, can be studied only starting with a comparatively high spin value ($I = 50$), when the number of basis states $n \geq$26.

In our calculations, we have not observed a smooth gradual transition from the soft chaos ($\kappa(\Phi_k) < 1$) to hard chaos ($\kappa(\Phi_k) > 1$), i.e., in the rigid triaxial rotator model, transition to the hard chaos case is abrupt, which can be explained by the tridiagonal structure of the model Hamiltonian matrix, which increases the role of restriction Eq.(1.28) for the calculation of $\kappa(\Phi_k)$ values.

4. The developed theoretical methods of quantum phase transition and quantum chaos studies have been applied for the analysis of prolate-oblate shape phase transition in the tungsten, osmium, and platinum isotope chains belonging to the transitional $A \sim$190 region. Nuclei of these three elements have shapes ranging from the stable prolate axial-symmetry to the asymmetric γ-unstable form.

The energies and wave functions of low-lying collective states in the case of 15 even-even nuclei with $184 \leq A \leq 194$ have been calculated employing complete version of IBM-1. Model parameter values for each nucleus have been determined via the fit to all experimentally observed level energies with $I \leq 8$, in the case of ground state band, and $I \leq 6$, in the case of other collective excitations. The relationships between shape phase transitions and quantum chaos criteria: $P(S)$, and $W(\Psi_i)$, have been analyzed: a) in depen-

dence on the $SU(3) - O(6) - \overline{SU(3)}$ prolate-oblate shape phase transition control parameter χ; b) in dependence on catastrophe theory control parameters r_1 and r_2; c) in dependence on proton and neutron numbers Z and N; d) in dependence on level spin I.

A good agreement has been obtained in the case of nuclei with stable prolate deformation, while, in the phase transition region close to the $E(5) - O(6)$ critical line, one cannot successfully describe employing the same IBM-1 model parameter set the levels of stretched ground state band and quasi γ-band with those of excited collective 0^+ and 4^+ bands. It indicates the coexistence of different shapes for the ground and excited levels in the γ-unstable deformation region due to the nearness of the deformed-to-spherical phase transition.

It was found that the transition from prolate to oblate deformation, in the case of low-lying collective states, occurs at $A = 194$ for even-even osmium nuclei and at $A = 192$ for even-even platinum nuclei. A coexistence of prolate ground state and oblate excited states is predicted in the case of ^{184,186}Pt and ^{188}W.

In the case of statistical chaos criteria - the nearest level spacing distribution $P(S)$, it has been found that the chaoticity slowly increases from the $SU(3)$-limit side, where $P(S)$ has a Poisson form. However, in the vicinity of the $E(5) - O(6)$ critical line, the chaoticity within isotope chain changes drastically reflecting a complex nature of observed phase transition.

The results of dynamical quantum chaos criteria - the wave function entropy $W^{U(5)}(\Psi_i)$, calculations for the $184 \leq A \leq 194$ region W, Os, and Pt nuclei have shown that the chaoticity with respect to spherical $U(5)$-symmetric basis diminishes towards $E(5) - O(6)$ critical line for each isotope chain. The change is more abrupt in the case of tungsten nuclei, which is explained by the greater stability of prolate axial deformation in the case of $Z = 74$ tungsten than in the case of $Z = 78$ platinum.

The obtained results have been compared with the results of other authors obtained in the frameworks of different theoretical approaches. A possibility to compare the results of calculations performed in the frameworks of algebraic complete IBM-1 model with the ones obtained using geometrical rigid triaxial rotator model has been considered and a method for such comparison has been proposed.

The studies of nuclear shape phase transitions and their relationship with quantum chaos could be continued also in other directions, e.g.:

a) the study in the frameworks of complete IBM-1 of different shape

phase coexistence phenomena, observed in transitional region nuclei at higher excitation energies;

b) the study of phase transitions and quantum chaos employing IBM-2 model, when the isospin dependence of nucleons is taken into account;

c) the study of phase transitions in the case of odd and odd-odd nuclei when one observes additional polarization of the nuclear core due to interaction with unpaired nucleons.

6.2 Approbation of obtained results

The results of present doctor studies, have been published in 3 refereed journal papers [R1,R3,R6] and 1 paper in international conference proceedings [R5]. One journal paper [R2] has been published in the local scientific journal.

One journal article manuscript [R4], submitted to refereed journal in 2007, presently is revised and extended, including additional calculation results. A journal article manuscript [R7] about results of phase transition and quantum chaos studies for A 190 region nuclei is submitted to journal in July 2010.

The results of studies have been reported both at international and local scientific conferences: 8 oral presentations - 4 international [A1,A3,A5,A7,A10] and 3 local [A2,A4,A6], and 2 poster presentations - 1 international [A8] and 1 local [A9].

Author's list of publications

Journal papers

R1 J. Proskurins, A. Andrejevs, T. Krasta, J. Tambergs. Studies of Phase Transitions and Quantum Chaos Relationships in Extended Casten Triangle of IBM-1. Physics of Atomic Nuclei, 2006, vol.69, p.1248-1253.

R2 A. Andrejevs, T. Krasta, J. Proskurins, J. Tambergs. Precise Solution of the Classical Energy Functional for the Extended Casten Triangle of IBM-1. Latvian J.Phys.Tech.Sci., 2006, No.3, p.58-65.

R3 J. Proskurins, A. Andrejevs, T. Krasta, L. Neiburgs, J. Tambergs. Studies of the Classical Energy Limit of the Interacting Boson Model in the Case of Three-Body Interactions. Bulletin of the Russian Academy of Sciences: Physics, 2007, vol.71, No.6, p.894-900.

R4 J. Proskurins, K. Bavrins, A. Andrejevs, T. Krasta, J. Tambergs. Study of Quantum Chaos in the Framework of Triaxial Rotator Model. Manuscript (10 pages) has been submitted to Physics of Atomic Nuclei in 2007 and presently is in the process of revision.

R5 J. Proskurins, K. Bavrins, A. Andrejevs, T. Krasta, J. Tambergs. Study of quantum chaos in the framework of triaxial rotator models. In: Proc.13th Int. Conf. on Capture Gamma-Ray Spectroscopy and Related Topics. Eds. A. Blazhev, J. Jolie, N. Warr, A. Zilges, AIP Conference Proceedings Vol.1090 (2009), pp.635-636.

R6 J. Proskurins, A. Andrejevs, T. Krasta, J. Tambergs. Phase transitions in the framework of complete version of IBM-1. Bulletin of the Russian Academy of Sciences: Physics, Vol.73, No.2 (2009), pp. 241-244.

R7 J. Proskurins, T. Krasta, K. Bavrins. Study of the onset of chaos in the A 190 nuclear deformation phase transition region. Manuscript (12 pages, September, 2010) submitted for publication in the Bulletin of the Russian Academy of Sciences: Physics.

Conference abstracts

A1 J. Proskurins, A. Andrejevs, T. Krasta, J. Tambergs. Studies of Phase Transitions and Quantum Chaos Relationships in Extended Casten Triangle of IBM-1. In: LV National Conference on Nuclear Physics "Frontiers in the Physics of Nucleus". June 28-July 1, 2005, St.-Petersburg, Russia. Book of Abstracts. St.-Petersburg, 2005, p.95.

A2 J. Proskurins, A. Andrejevs, T. Krasta, L. Neiburgs, J. Tambergs. Studies of Classical Energy Limit of Interacting Boson Model in the Case of Triaxial Deformations. In: LU ISSP 22nd scientific conference, Riga, 29-30 March, 2006. Book of abstracts. Riga, ISSP, 2006, p.27.

A3 J. Proskurins, A. Andrejevs, T. Krasta, L. Neiburgs, J. Tambergs. Studies of Classical Energy Limit of Interacting Boson Model in the Case of Three-Body Interactions. In: 56 International Conference "Nucleus-2006" on Problems of Nuclear Spectroscopy and Structure of Atomic Nucleus, September 4-8, 2006, Sarov, Russia. Abstracts, Sarov 2006, pp.111-112.

A4 J. Proskurins, K. Bavrins, A. Andrejevs, T. Krasta, J. Tambergs. Study of Quantum Chaos in the Framework of Triaxial Rotator Model. In: LU ISSP 23rd scientific conference devoted to the 75th anniversary of LU professor Ilmārs Vītols, Riga, 13-15 February, 2007. Book of abstracts. Riga, ISSP, 2007, p.12.

A5 J. Proskurins, K. Bavrins, A. Andrejevs, T. Krasta, J. Tambergs. Study of Quantum Chaos in the Framework of Triaxial Rotator Model. In: 57 International Conference on Nuclear Physics Nucleus-2007, Fundamental Problems of Nuclear Physics, Atomic Power Engineering and Nuclear Technologies. June 25-29, 2007, Voronezh, Russia. Book of Abstracts, St.-Petersburg, 2007, p.191.

A6 J. Proskurins, K. Bavrins, A. Andrejevs, J. Tambergs. Studies of Phase Transitions and Quantum Chaos in the Framework of Interacting Boson and Geometrical Nuclear Models. In: LU ISSP 24th scientific conference, Riga, 20-22 February, 2008. Book of abstracts. Riga, ISSP, 2008, p.38.

A7 J. Proskurins, A. Andrejevs, T. Krasta, J. Tambergs. Phase Transitions in the Framework of Complete Version of IBM-1. In: 58 International Meeting on Nuclear Spectroscopy and Nuclear Structure "Nucleus-2008". Fundamental Problems of Nuclear Physics, Nuclear Methods in Nanotechnology, Medicine and Nuclear Power Engineering. June 23-27, 2008, Moscow, Russia. Book of Abstracts. St.-Petersburg, 2008, p.165.

A8 J. Proskurins, K. Bavrins, A. Andrejevs, T. Krasta, J. Tambergs. Study of quantum chaos in the framework of triaxial rotator models. In: 13th International Symposium on Capture Gamma-Ray Spectroscopy and Related Topics, Cologne, Germany, August 25-29, 2008. Book of Abstracts, pp.174-175.

A9 J. Proskurins, A. Andrejevs, K. Bavrins, T. Krasta, J. Tambergs. Use of Peres lattice method for the study of nuclear phase transitions. In: LU ISSP 25th scientific conference, Riga, 11-13 February, 2009. Book of abstracts. Riga, ISSP, 2009, p.38.

A10 J. Proskurins, T. Krasta, K. Bavrins. Study of the onset of chaos in the $A \sim$190 nuclear deformation phase transition region. In: "Nucleus 2010. Methods of Nuclear Physics for Femto- and Nanotechnologies (LX Meeting on Nuclear Spectroscopy and Nuclear Structure)", 6-9 July 2010, St.-Petersburg, Russia. Book of Abstracts, St.-Petersburg, 2010, p.214.

Bibliography

[1] P.Cejnar and J.Jolie, Phys.Rev.C. (2009).

[2] V.E.Bunakov, Neutron resonances and quantum chaos. In: ISINN-2 Proceedings. Dubna 1994. (JINR, E3-94-419, Dubna, 1994), p.76-85.

[3] B.R. Barrett et al., *Nuclear Physics News* **13** (2003) 17-23.

[4] A. Bohr and B.R. Mottelson. Nuclear Structure, Vol. 2, Benjamin, New York, 1974.

[5] J.M. Eisenberg and W. Greiner. Nuclear Theory. Vol. 1. Nuclear Models, North-Holland, Amsterdam-London, 1970.

[6] A.Arima and F.Iachello. Collective Nuclear States as Representations of a SU(6) Group. *Phys.Rev.Lett.* Vol.35, No.16 (1975) 1069-1072.

[7] F.Iachello and A.Arima, *The Interacting Boson Model* (Cambridge University Press, Cambridge, 1987).

[8] F.Iachello and P.van Isacker. The Interacting Boson-Fermion Model. (Cambridge University Press, Cambridge, 1991).

[9] D.Bonatsos, *Interacting Boson Models of Nuclear Structure* (Clarendon Press, Oxford, 1988).

[10] A.Bohr and B.Mottelson. Collective and Individual-Particle Aspects of Nuclear Structure. *Kgl.Danske Videnskab Selskab. Mat.-Fys. Medd.* Vol.27, No.16 (1953) 1-174.

[11] A.S. Davydov and G.E. Filippov, Nucl.Phys. **8**, 237 (1958).

[12] v.R. Manfredi and L. Salasnich, Phys.Rev. E **64**, 066201 (2001).

[13] V.R. Manfredi, V. Penna and L. Salasnich, Mod.Phys.Lett. B **17**, 803-812 (2003).

[14] A.S.Davydov, *Excited states of atomic nuclei* (Atomizdat, Moscow, 1967).

[15] A.V.Bravin and A.D.Fedorov, Izv.AN SSSR, Ser.Fiz. **34**, 454 (1970).

[16] A.D.Fedorov, Yadernaya fizika (Sov.Journal of Nucl.Phys.) **15**, 36 (1972).

[17] O.Scholten, in *Computational Nuclear Physics 1, Nuclear Structure.* Eds. K.Langanke, J.A.Maruhn, S.E.Koonin (Springer, Berlin-Heidelberg, 1991), p.88.

[18] R.F. Casten and D.D. Warner, Rev.Mod.Phys. **60**, 389 (1988).

[19] Jolie,J., Heinze,S., Linnemann,A., Werner,V., Cejnar,P. and Casten, R.F. in: Proceedings of the 11th International Symposium on Capture Gamma Ray Spectroscopy and Related Topics. Ed. by J.Kvasil, P.Cejnar, M.Krtička (World Scientific, Singapore, 2003), p.36.

[20] Lopez-Moreno,E. and Castanos,O. Phys.Rev.C., 1996, vol.54, p.2374.

[21] L.D. Landau and E.M. Lifshitz, *Course of Theoretical Physics. Vol.5, Statistical Physics. Part 1.* (Nauka, Moscow, 1976).

[22] Jolie,J., Cejnar,P., Casten, R.F., Heinze,S., Linnemann,A. and Werner,V. Phys.Rev.Lett., 2002, vol.89, p.182502.

[23] R.F. Casten et al., Nucl.Phys.A **439**, 289 (1985).

[24] Y. Alhassid and N. Whelan, Phys.Rev.Lett. **67**, 816 (1991).

[25] Y. Alhassid and N. Whelan, Phys.Rev.C **43**, 2637 (1991).

[26] R.Gilmore, J.Math.Phys. **20**, 891 (1979).

[27] A.E.L. Dieperink, O.Scholten and F. Iachello, Phys.Rev.Lett. **44**, 1747 (1980).

[28] P. Van Isacker and J.-Q. Chen, Phys.Rev.C **24**, 684 (1981).

[29] K.Heyde et al., Phys.Rev.C **29**, 1420 (1984).

[30] G.Thiamova and P.Cejnar, Nucl.Phys.A **765**, 97 (2006).

[31] H.-J.Stöckmann, *Quantum Chaos. An Introduction.* (Cambridge Univ. Press, 2000).

[32] J. Jolie and A. Linnemann, Phys.Rev. C, **68** (2003) 031301.

[33] M.V.Berry and M.Tabor, *Proc. Roy. Soc.* **A356**, 375 (1977).

[34] O.Bohigas, M.J.Giannoni and C.Schmidt, *Phys. Rev. Lett.* **52**, 1 (1984).

[35] T.A. Brody, J. Flores, J.B. French, P.A. Mello, A. Pandey, S.S.M. Wong, Rev.Mod.Phys. **53** (1981) 385-479.

[36] Y.Alhassid, A.Novoselsky, and N.Whelan, Phys.Rev.Lett. **65**, 2971 (1990).

[37] Y.Alhassid and A.Novoselsky, Phys.Rev.C **45**, 1677 (1992).

[38] P.Cejnar and J.Jolie, Phys.Rev.E. **58**, 387 (1998); P. Cejnar and J. Jolie, Phys.Lett. B **420** (1998) 241.

[39] V.E.Bunakov, F.F.Valiev and J.M.Chuvilsky, *Izv.RAN, ser.fiz.* **62**, 41 (1998).

[40] W.D. Heiss, R.G. Nazmitdinov and S. Radu, Phys.Rev.Lett. **72**, 2351 (1994).

[41] S. Aberg, Phys.Rev.Lett. **64**, 3119 (1990).

[42] P. Stránský, M. Kurian, and P. Cejnar, Phys.Rev.C **74**, 014306 (2006).

[43] T. Mizusaki, N. Yoshinaga, T. Shigehara and T.Cheon, Phys.Lett.B **269** 6-12 (1991).

[44] P. Cejnar and J. Jolie, Phys.Rev.E **61**, 6237 (2000).

[45] Jolie,J., Casten,R.F., von Brentano,P. and Werner,V. Phys.Rev.Lett., 2001, vol.87, p.162501.

[46] V. Werner et al., Phys.Rev.C **61**, 021301 (2000).

[47] V. Werner, P. von Brentano, R.F. Casten, and J. Jolie, Phys.Lett.B **527**, 55 (2002).

[48] F.Iachello, Phys.Rev.Lett. **85**, 3580 (2000).

[49] F.Iachello, Phys.Rev.Lett. **87**, 052502 (2001).

[50] Liao Ji-zhi and Wang Huang-sheng, Phys.Rev.C **49**, 2465 (1994).

[51] P. Van Isacker, Phys.Rev.Lett. **83**, 4269 (1999).

[52] J.Tambergs et al., *Proceedings of the 11th International Symposium on Capture Gamma-Ray Spectroscopy and Related Topics. Eds. J.Kvasil, P.Cejnar and M.Krtička* (World Scientific, Singapore, 2003), p.417.

[53] V.R. Manfredi and V. Salasnich, Int.J.Mod.Phys.E **4**, 625 (1995).

[54] V.R. Manfredi and L. Salasnich, arXiv:nucl-th/9707030v1

[55] Iachello,F., Zamfir,N.V. and Casten,R.F. Phys.Rev.Lett., 1998, vol.81, p.1191.

[56] J. Jolie et al., Phys.Rev.Lett. **93** 132501 (2004).

[57] A. Ansari, Phys.Rev.C **33**, 321 (1986).

[58] P.D. Stevenson *et al.*, Phys.Rev. C **72** (2005) 047303.

[59] C. Wheldon et al., Phys.Rev.C **63**, 011304 (2000).

[60] Zs. Podolyak et al., *Phys.Rev. C*, 2009, vol.79, p.031305.

[61] NNDC On-Line Data Service from ENSDF database, http://www.nndc.bnl.gov/ensdf/.

[62] Arias,J.M. *et al.*, Phys.Rev.C. **68**, 041302, (2003).

[63] E.L.Rees, American Mathematical Monthly **29**, 51 (1922).